ALCAM Dynamically Regulates Tumor Cell Adhesion Through Differential Proteolysis and a Novel Binding Partner, Tetraspanin CD151

By

Katie E. Hebron

Dissertation

Submitted to the Faculty of the

Graduate School of Vanderbilt University

in partial fulfillment of the requirements

for the degree of

DOCTOR OF PHILOSOPHY

in

Cancer Biology

May 11, 2018

Nashville, Tennessee

Approved:

Barbara M. Fingleton, Ph.D.

Andries Zijlstra, Ph.D.

Simon W. Hayward, Ph.D.

Deborah A. Lannigan, Ph.D.

To my family, for nurturing the fiery and inquisitive personality that
led me to a career in science.

To my husband, without your endless love, support, and encouragement,
none of this would be possible.

Finally, to those, including family and friends, who bear the burden of cancer,
you inspire this work.

AKNOWLEDGEMENTS

The work presented here was made possible because of the generous support, encouragement, and guidance from countless individuals over the past six years. I would like to highlight a few of those individuals here.

I am especially thankful for my mentor, Dr. Andries Zijlstra, or affectionately, “Z”. My time in your lab has allowed me to grow, both as a scientist and a person. Your guidance has significantly improved my critical thinking and communication skills, and for that, I am forever grateful. Your love of science is contagious. I hope to spark the same passion for science in my future mentees, as you have sparked in me. I would also like to thank my dissertation committee, Barbara Fingleton, Simon Hayward, and Deborah Lannigan, for your support. Your guidance and constructive criticism have immeasurably improved the work presented here. I am thankful for your time and dedication to my training.

I am grateful for the people within the Zijlstra lab who made my time here all the more enjoyable. To the past members, Will, Amanda, Trenis, Celeste, and Tatiana K., I cannot thank you enough for the support you gave me in those early days. You all set me on the right track as a doctoral candidate. To the more recent members, Holli, Chase, Tatiana N., and Adel, thank you for putting up with all of my quirks and for supporting me, nonetheless. To Ariana, the fresh, new student, I wish you the best of luck in your scientific endeavors; enjoy the new bench and the best set of pipets the lab has to offer. To Shanna, your continued guidance, in science and in life, throughout my time in the Zijlstra lab has been priceless. I am truly grateful for the time and energy you have invested into my training. To Elizabeth, my never-ending mentee, my work with you has solidified my choice to pursue a career in academic research. If I have even one more mentee as talented, driven, and special as you, I will be lucky. Good luck with the rest of your training and your undoubtedly successful future career.

This work would not be possible without the support of several groups within Vanderbilt. Thank you to the Bone Center, especially Dr. Julie Sterling, for your assistance. To Dave Flaherty, of the Flow Cytometry Shared Resource, thank you for taking my crazy requests and making them a reality. I am grateful for your help in improving my science, and for the friendship that has spurred from our collaboration.

Thomas Stricker has been a great resource for all things DNA and RNA-related. Thanks also goes to the administrative staff of the program in Cancer Biology and the Department of Pathology, Microbiology, and Immunology Your hard work does not go unnoticed. This work was financially supported by National Institutes of Health grants R01CA143081 (AZ), T32CA009592 (KEH), and F31CA189764 (KEH), and the Department of Veterans Affairs grant IK2BX002498 (SAE).

Finally, achieving this strenuous goal would not have been possible without the support of my family and friends. Thank you for enduring years of missed holidays, births, and birthdays; for being understanding of last minute cancelations because I have to tend to lab work, and for being empathetic as I sit here in the corner during Christmas “vacation” ironing out my dissertation. To my mom, Ruth, you are always my inspiration. From you, I have learned hard work, dedication, sacrifice, and curiosity; I am so fortunate to be able to call you Mom. To my dad, Dave, thank you for stepping in to our crazy family and loving us all as your own. And for passing me your genes, we all know I got my smarts from you. To my siblings, growing up with you gave me the grit and perseverance to tackle graduate school, thank you. Your continued support means the world to me. To the Hebrons, you have accepted me into your family without question, and that means more to me than you will ever know. To my dad, Ron, thank you for your continued support and genuine curiosity in my work. Thank you to the friends, old and new, that have supported me through this journey. Brandon, Elizabeth, Ryan, Nicole, Henry, and Aiden, you are and always will be our Nashville family. I look forward to a lifetime of memories with you.

I am forever grateful for my husband, Ryan. Your love for and dedication to our family is a constant source of motivation for me. I am so lucky to have your unconditional support. You will never know how much it meant to me for you to pack up your life, leave your family and stable job, and move to a new city that you’d never visited and where you didn’t have a job waiting. Thank you for choosing me, and for taking on this adventure with me.

TABLE OF CONTENTS

Page

Appendix

LIST OF TABLES

Table **Page**

LIST OF FIGURES

Figure **Page**

LIST OF PUBLICATIONS

Palmer, TD., Martínez, CH., Vasquez, C., Jones-Paris, CR., Hebron, KE., Chan, SM., Chalasani, V., Gomez-Lemus, JA., Williams, AK., Chin, JL., Ketova, T., Lewis JD., and Zijlstra, A. Integrin-free tetraspanin CD151 can inhibit tumor cell motility upon clustering and is a clinical indicator of prostate cancer progression. Can Res, Jan 2014 vol. 74 (1) pp. 173-87

Babaev, VR., Hebron, KE., Ding, L., Zhang, Y., May, JM., Fazio, S., and Linton, MF. Macrophage deficiency of Akt2 but not Akt1 reduces atherosclerosis in LDLR null mice. J Lipid Res, 2014 vol. 55 pp. 2296-2308

Stoletov, K., Bond, D., Hebron, KE., Raha, S., Zijlstra, A., and Lewis JD., Metastasis as a therapeutic target: a conceptual framework. Am J Clin Exp Urol 2014 vol. 2 (1) pp. 45-56.

Campbell, P., Mulcrone, P., Masood, SK., Karolak, M., Merkel, A., Hebron, KE., Zijlstra, A., Sterling, J., Elefteriou, F., TRIzol and Alu qPCR-based quantification of metastasis seeding within the skeleton. Sci Rep. 2105 vol. 5 article: 12635

Enyindah-Asonye, G., Li, Y., Ruth, JH., Spassov, DS., Hebron, KE., Zijlstra, A., Moasser, MM., Wang, B., Singer, NG., Cui, H., Ohara, RA., Rasmussen, SM., Fox, DA., Lin, F., CD318 is a ligand for CD6. Proc Natl Acad Sci USA, 2017 vol. 114 (33) pp. E6912-E6921. *Epub ahead of print.*

Loomans, HA., Arnold Egloff, SA., Hebron, KE., Taylor, CJ., Zijlstra, A., Andl, CD., Loss of ACVRIB leads to increased squamous cell carcinoma aggressiveness through alterations in cell-cell and cell-matrix adhesion proteins. Am J Cancer Res. 2017 vol. 7 (12) pp. 2422-2437. eCollection 2017.

Hebron, KE., Li, E., Wang, J., Taylor, C., Eskaros, A., Flaherty, DK., Arnold Egloff, SA., Houkes, J., Stricker, T., and Zijlstra, A. Alternative splicing of ALCAM controls metastasis through differential proteolysis of its extracellular domain. *In press.* Sci Rep*.* **Chapter 2 of this dissertation.**

Fröse, J., Chen, MB., Hebron, KE., Reinhardt, F., Zijlstra, A., Kamm, RD., Weinberg, RA. Epithelial-Mesenchymal Transition Induces Podocalyxin to Promote Extravasation via Ezrin Signaling. *Submitted*. Can Res.

Hebron, KE., Ketova, T., Flaherty, D., Arnold Egloff, SA., Manning, HC., Sterling, J., Elefteriou, F., Zijlstra, A. Fluorescent Barcoding Offers Increased Dimensionality in Tracking Tumor Cells in vitro and in vivo. *In preparation.* Clin Exp Met. **Appendix A of this dissertation.**

Hebron, KE., Palmer, TD., von Lersner, AK., Li, EY., Mazzocca, A., Hansen, AG., Ishida, H., Hyndman, ME., Vogel, HJ., and Zijlstra, A. Integrin-free CD151 controls tumor cell adhesion, migration, and metastasis via a trimeric complex with ALCAM and syntenin-1. *In preparation*. J Cell Sci. **Chapter 3 of this dissertation.**

ABBREVIATIONS

ADAM17	A disintegrin and metalloprotease-17
ALCAM	Activated leukocyte cell adhesion molecule
ALCAM-Iso1	Canonical isoform of ALCAM (Isoform 1)
ALCAM-Iso2	Alternatively spliced isoform of ALCAM (Isoform 2)
AP-1	Activator protein-1
Bcl-2	B-cell lymphoma-2
CAM	Chorioallantoic membrane
CADM1	Cell adhesion molecule-1
CD6	Cluster of differentiation 6
CD151	Cluster of differentiation 151
$CD151^{free}$	Integrin-free CD151
CD166	Cluster of differentiation 166 (ALCAM)
E-cadherin	Epithelial-cadherin
ECD	Extracellular Domain
ECM	Extracellular matrix
ELISA	Enzyme-linked immunosorbent assay
EMT	Epithelial to mesenchymal transition
FACS	Fluorescence-activated cell sorting
GATA-1	GATA binding factor-1
GFP	Green fluorescent protein
GSI	ɣ-secretase inhibitor
GTEx	Genotype-Tissue Expression
IACUC	Institutional animal care and use committee
ICD	Intracellular domain
Ig-CAM	Immunoglobulin superfamily of cell adhesion molecules
IgSF	Immunoglobulin superfamily
IP	Immunoprecipitation
IV	Intravenous
KO	Knockout

KD	Knockdown
LC-MS-MS	Liquid chromatography tandem mass spectrometry
mAB	Mouse monoclonal antibody
miR	MicroRNA
MMP	Matrix metalloprotease
NCAM	Neural cell adhesion molecule
NFκB	Nuclear factor kappa-light-chain-enhancer of activated B cells
NMR	Nuclear magnetic resonance
ns	not significant
OE	Overexpression
PBS	Phosphate-buffered saline
PBSt	Phosphate-buffered saline with 0.05% tween-20
PKCα	Protein kinase C alpha
PSA	Prostate-specific antigen
PVDF	Polyvinylidene fluoride
RPKM	Reads per kilobase of transcript per million mapped reads
RUNX-2	Runt-related transcription factor-2
SDS-PAGE	Sodium dodecyl sulphate polyacrylamide gel electrophoresis
TCGA	The Cancer Genome Atlas
TERM	Tetraspanin-enriched microdomain
TSPAN	Tetraspanin
VE-cadherin	Vascular endothelial-cadherin
VEGF	Vascular endothelial growth factor

CHAPTER 1:
INTRODUCTION

Metastasis and Cell Adhesion

Metastasis is generally considered the deadliest aspect of cancer. As such, significant effort has been dedicated to early detection and prevention of disease progression. However, it is becoming apparent that prevention and early detection are only one piece of the puzzle that is cancer treatment. Understanding the mechanisms by which tumor cells spread from the primary tumor, or metastasize, will continue to reveal more therapeutic targets to be investigated in the fight against cancer. This dissertation examines the relationship between the dynamic regulation of cell adhesion and the progression to metastasis. In this chapter, I will define metastasis, outline the major classes of cell adhesion molecules, and summarize their known contributions to cancer progression.

Definition and clinical concerns

Metastasis is the process by which tumor cells disseminate from their site of origin to a distant location (1). This dissemination takes place as a sequential series of steps in which the cell escapes the primary tumor, evades cell death and immune-mediated clearance in circulation, and arrives in a distant organ to survive in an environment distinct from its origin. Fundamentally, investigations of this highly inefficient process consider the dissemination of even a single cell to a distant organ a metastatic event. Clinically, however, metastasis is less about the behavior of individual cells and more about the disease state and its presentation in the patient. Metastatic disease is clinically recognized when the secondary tumor is detectable by diagnostic tools such as imaging and biopsy. For most cancers, only a small proportion of patients progress to metastatic disease; for example, only 4% of prostate and bladder cancer patients ultimately progress to this terminal state (2). Nevertheless, metastatic disease accounts for more than 90% of cancer-related deaths (3). Despite significant advances in detection and treatment of early disease, very few therapies effectively target

metastases. Indeed, while an increasing portion of patients are diagnosed with and successfully treated for early stage disease, survival and prognosis for patients with aggressive metastatic disease remains poor (2). In prostate and bladder cancer, respectively, five-year survival rates fall from >99% and 70% for patients with localized disease to 29% and 5% for patients with disseminated disease (2). Consequently, the detection and treatment of metastatic disease remains an unsolved clinical challenge.

Alterations to, and dysregulation of, the mechanisms that control tumor cell adhesion and migration commonly promote disease progression and metastasis (4). However, the regulation of these mechanisms is still poorly understood and not easily targeted for therapeutic interventions (5). Because of the limited options in treating metastatic disease, current treatment plans for patients presenting with early, localized disease often focus on assessing and reducing the patient's risk of future disease progression. For example, prostate cancer patients with localized disease can undergo one of two treatment plans: 1) Active surveillance or watchful waiting observation with continuous monitoring of the patient's symptoms and prostate-specific antigen (PSA) levels, or 2) Active treatment that could include radiation therapy, hormone therapy, and/or radical prostatectomy, each of which carries significant potential for complication and morbidities (6). However, it has been difficult to find reliable predictive markers of progression, especially ones that stratify patients with indolent disease from those with aggressive disease. Even PSA, often touted as the gold standard of biomarkers, is only 60-80% accurate, in sensitivity and specificity, as a diagnostic marker (7). A more complete understanding of mechanisms controlling a tumor cell's progression to metastasis will provide a knowledge base from which better therapeutics for and biomarkers of metastatic disease can evolve.

The metastatic cascade

The steps a tumor cell has to undertake in order to metastasize are referred to as the metastatic cascade (Fig. 1). The steps are defined as (I.) escape from the primary tumor, (II.) intravasation into local vasculature, (III.) circulation through the vasculature and dissemination to a distant site, (IV.) arrest within and extravasation from the

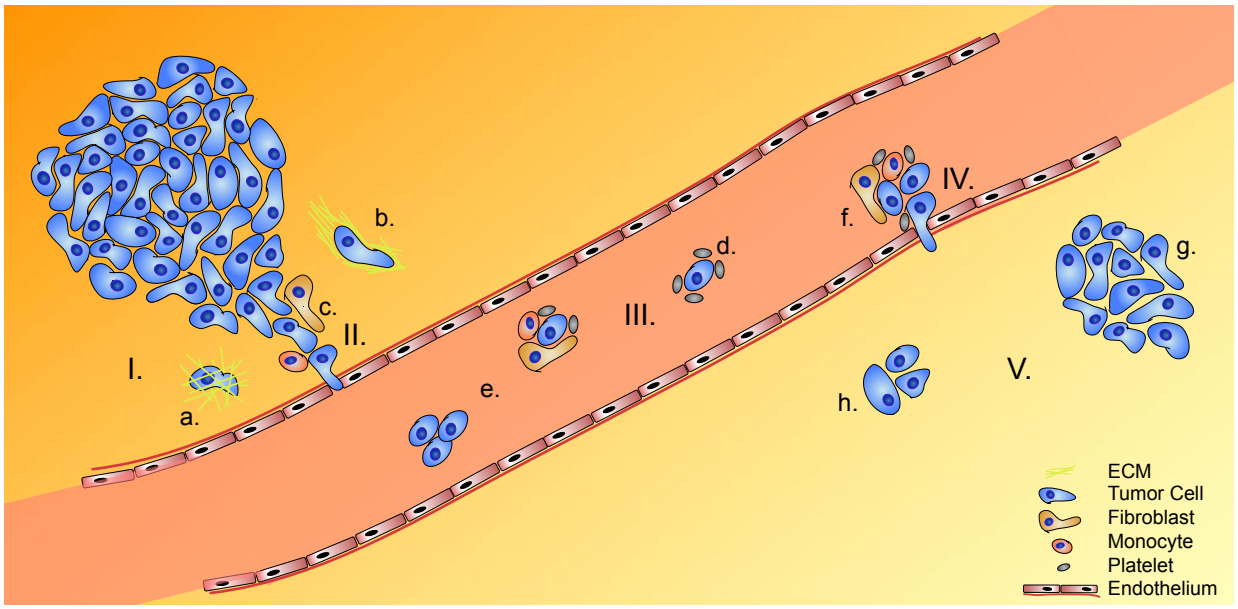

Figure 1. The metastatic cascade. The metastatic cascade consists of five sequential steps: I.) escape from the primary tumor, II.) intravasation into local vasculature, III.) systemic circulation IV.) extravasation from the vasculature, V.) colonization of the secondary site. (a) amoeboid-like migration from the primary site, (b) mesenchymal, single cell migration from the primary site, (c) collective cell migration from the primary site, (d) platelet shielding of circulating tumor cells, (e) circulation of tumor cell aggregates, with and without microenvironmental "passengers", (f) extravasation aided by microenvironmental "passengers", (g) overt metastasis at secondary site, (h) dormant tumor cells at secondary site.

vasculature, and, finally, (V.) colonization at a secondary site (1). Moreover, each of these steps must occur in sequence in order for a cell to metastasize, making this an inefficient process (8,9). These broad steps each encompass several different biological processes in order to occur, and not everything is known about the mechanisms regulating each of these steps. This chapter will summarize the contribution of cell adhesion to each step of the metastatic cascade.

Escape from the primary tumor

The “linear progression model” of cancer considers metastasis the final step in disease progression, but a growing body of evidence suggests that metastasis can occur even from tumors that are considered early stage, reflected by the “parallel progression model” (10,11). The latter model has proven to be especially true for the first step of the metastatic cascade. As primary tumors grow, neovascularization is induced in order to prevent hypoxia and provide growth factors to the entirety of the tumor. Vessels formed during tumor-induced neovascularization are often disorganized and leaky (12). The increased permeability of these new vessels provides a doorway for tumor cells into the host vasculature.

In order for tumor cells to escape the primary tumor into the new tumor-induced vasculature, they must both migrate and remodel the surrounding extracellular matrix (ECM) (4). There are conflicting hypotheses regarding the reasons for departure from the primary tumor mass. It is unknown whether tumor cells begin to migrate away from the primary tumor using intrinsic migratory mechanisms stimulated by external cues such as hypoxia, or paracrine, cytokine, or growth factor signaling, or because genomic instability results in gain-of-function mutations that confer the ability to migrate on normally immotile epithelial cells (10,13).

Beyond the stimulus for tumor cell migration, there is existing controversy regarding the method of cell migration away from the primary tumor. The classical dogma of metastasis depicts a single tumor cell breaking cell adhesions with neighboring cells and navigating the surrounding ECM with ameboid-like migration mechanisms; this type of migration requires little to no remodeling of the ECM (4,14,15). Alternatively, these single cancer cells may undergo epithelial-to-mesenchymal

transition (EMT), which is the process of epithelial cells losing the expression of key cell adhesion molecules such as epithelial-cadherin (E-cadherin) to adopt a more mesenchymal-like phenotype with polarized migration assisted by remodeling of the ECM by matrix metalloproteases (MMPs) (4,14,16,17). Conversely, a growing body of evidence suggests that tumor cells escape from the primary tumor most effectively when they undergo collective migration, often in a follow-the-leader process similar to that seen in angiogenesis or mammary gland development. This method of migration often requires significant remodeling of the ECM by the leader cells or by co-migrating tumor-associated fibroblasts (18-20). Regardless, there is general agreement that alterations in both cell adhesion and migration mechanisms must occur for cells to escape the primary tumor (21,22).

Intravasation

After escape from the primary tumor, cells can disseminate through both the lymphatic and blood vessels. Although hematopoietic dissemination is often considered the dominant mode of tumor cell dissemination, growing evidence suggests that the cancer type and location of metastasis strongly influence the dominant mode of dissemination (23,24). In order for this dissemination to occur, tumor cells must migrate into the vessels, a process called transendothelial migration. It is still a matter of debate whether tumor cells passively or actively undergo transendothelial migration (25). The disorganized, immature vessel growth induced in the primary tumor lends support to passive transendothelial migration (26). However, differences in response of metastatic and non-metastatic cells to paracrine signaling from tumor vessels lend support to the model of active transendothelial migration (13,27,28).

Circulation

Even in models of early disease progression, millions of tumor cells can be detected in circulation (9). Very few of these circulating tumor cells survive long enough to extravasate and form secondary tumors. Circulating tumor cells are subjected to an onslaught of challenges, from the mechanical stresses of blood flow and high-pressure capillaries, to the environmental stresses of anoikis induced by detachment from the

ECM, to immune detection and subsequent lysis (29). Several factors have been shown to improve tumor cell survival in circulation. For example, platelet aggregation on circulating tumor cells shields the surface of these tumor cells, protecting them from the shear forces of blood flow and from immune detection by natural killer cells (30-32). Additionally, several groups have shown that circulating aggregates of tumor cells are far more likely to survive circulation and successfully extravasate than single circulating tumor cells (33,34). Moreover, the number of tumor cell aggregates detected in patient circulation is a better prognostic marker of progression than single circulating tumor cells, indicating that tumor cell aggregation indeed promotes survival in circulation (33,35).

Extravasation

Cells that survive circulation must ultimately leave the vasculature to form a secondary tumor in a process called extravasation (36). Extravasating cells must first arrest within the vasculature either through activation of rolling adhesion mechanisms (often aided by circulating “passengers” such as platelets and tumor-associated stromal cells) or by embolization within capillary beds (37,38). Similar to intravasation, extravasation requires transendothelial migration (39). Again, aggregates composed of multiple tumor cells, tumor cells and platelets, or tumor cells and tumor-associated stromal cells have been shown to be more efficient at extravasation than single circulating tumor cells (33,40).

Colonization at secondary site

The final step of metastasis is colonization at the secondary site. Clinically, this is the most important step because disseminated tumor cells rarely cause life-threatening complications. Overt metastases are most commonly associated with complications that cause cancer-related deaths. This is also considered the rate-limiting step in metastasis, as not all cells that extravasate are able to colonize the secondary site (41,42).

In 1889, Stephen Paget made a pivotal discovery suggesting that the site of metastasis is determined by “seeds” (tumor cells) reaching their favorable “soil” (the

host microenvironment) (43). Forty years later, James Ewing challenged this discovery by suggesting that the site of metastasis was a random event influenced only by the path of blood flow from the tumor (44). However, it is now well established that the sites of metastasis can typically be predicted from the primary tumor type, a phenomenon referred to as organotropism (43,45). The mechanisms directing organotropism are still being unraveled. One model suggests that the exchange of systemic cues from the primary tumor to the secondary site “prime” the tumor cells for that site and create a favorable environment or “pre-metastastic niche” at the secondary site (46). These systemic cues can come in the form of exosomes or other vesicles, cytokines, or “resident” immune cells (47,48). Another model suggests that the physics of the secondary site affect organotropism. For example, many groups hypothesize that the pliability or stiffness of the tissue at the secondary site directs mechanotransduction signals that support survival, migration, and proliferation of metastases (49-51). Yet another model suggests that tumor cells “carry along” supportive stromal cells from the primary microenvironment to the secondary site in order to quickly establish a favorable environment for metastatic outgrowth (52). After arrival at the secondary site, some tumor cells will immediately begin proliferating and form overt metastases quickly, while others will remain dormant for months, years, or decades before growing into clinically detectable tumors.

Dormancy at the secondary site has complicated the treatment of cancer. In some cancers, such as hormone-dependent breast cancer, patients will survive for ten to fifteen years after the successful resection and treatment of what appears to be localized disease, only to succumb to metastatic disease following outgrowth of a previously dormant metastasis (53). Because dormancy at the secondary site occurs before metastases become clinically detectable, it is difficult to predict which patients have dormant metastases and when those tumor cells will escape dormancy. Tumor cell dormancy is a growing field of cancer biology in which many proponents suggest that understanding how to induce or maintain dormancy will significantly advance the treatment of metastatic disease (54).

Cell adhesion in metastasis

As summarized previously, each step of the metastatic cascade involves alterations in cell-cell and cell-matrix adhesions. Changes in cell adhesion are common in the normal physiological processes of embryonic development and tissue maintenance and repair, such as regeneration of neurons and mammary gland alveologenesis during pregnancy and lactation (55,56). Thus, mechanisms regulating the dynamic control of cell adhesion are intrinsic to normal cells, but are altered in tumor cells. It is more common to see epigenetic and post-translational modifications to cell adhesion pathways than it is to see genomic alterations. These alterations shift the regulation of cell adhesion mechanisms to favor that of a pro-migratory state that is essential for metastasis.

The field has made significant progress in understanding the different mechanisms of cell adhesion. The investigation of EMT, collective versus single cell migration, and the interplay of cell adhesion and proliferation have all greatly expanded our knowledge of the importance of cell adhesion in cancer progression. However, these advances in knowledge have not been met with equal advances in patient care. We hypothesize that understanding the mechanisms regulating the dynamic control of cell adhesion, rather than the mechanisms of cell adhesion themselves, will provide the largest benefit to improvement of patient care. This dissertation explores such regulatory mechanisms and identifies two tunable mechanisms of adhesion that exist in normal physiological contexts, but are disproportionately activated in malignant cancers.

Families of Cell Adhesion Molecules

Cell adhesion is a critical mechanism by which cells communicate with each other and their microenvironment. It is critical to cell cycle regulation, proliferation, tissue morphogenesis and maintenance, immunological response, and wound healing, among many other biological processes. As essential as cell adhesion is to normal physiology, it is often dysregulated in disease states, especially in cancer. In this section, I will discuss three of the major classes of cell adhesion molecules: the cadherins, the integrins, and the immunoglobulin super family of cell adhesion molecules. I will briefly

review their structure and basic mechanism of adhesion and highlight some of the mechanisms by which they contribute to cancer progression.

Cadherins

Structure and function

The cadherins refer to a large family of calcium-dependent cell adhesion molecules (57,58). They are the main cell adhesion molecules associated with the formation of adherens junctions (59). In normal physiology, the cadherins play an important role in the development of tissue layers (60). The differential expression of the over 100 cadherins helps define specific tissue structures during development (61). There are eight different classes of cell adhesion molecules, but the “classical” cadherins are most closely associated with the changes in cell adhesion observed during cancer.

Cadherins are a type I transmembrane protein defined by extracellular cadherin domains. These domains are each around 110 amino acids long and adopt a Greek key motif composed of seven β-strands (62,63). The classical cadherins, including epithelial (E-) and neuronal-cadherin, have six extracellular cadherin domains. The short connecting amino acid sequences between each domain house the Ca^{2+} binding sites, which are integral to establishing the active binding conformation (64).

Upon binding of the Ca^{2+} ions, the N-terminal cadherin domain is primed for *trans* interaction with cadherin from an adjacent cell. *Trans* interaction leads to lateral *cis* clustering and the formation of a zipper-like structure (65,66). The cytoplasmic domain interacts with adaptor and signaling proteins, like the catenins and vinculin, anchoring the adherens junction to the actin cytoskeleton (67).

Cadherins in cancer

The dysfunction of classical cadherins has been a known driver of epithelial cancer progression for several decades (68). These early studies showed that loss (by somatic or germline mutation, or by transcriptional silencing) or mislocalization of E-cadherin in human disease correlates with disease progression and that experimental models of E-cadherin loss promote invasion and metastasis (65,69-71). Conversely, early animal

and cell model studies showed that re-expression of E-cadherin in invasive cells decreased invasion and metastasis (72). Furthermore, loss of E-cadherin is a hallmark of EMT (73,74).

The effect of dysregulated cadherin function on cancer goes beyond the loss of adhesion associated with its down regulation or mislocalization. The loss of cadherin also has significant effects on oncogenic signaling pathways, namely Wnt/β-catenin and growth factor signaling. Independent of its activity with E-cadherin, β-catenin is essential for canonical Wnt pathway activation (75). Additionally, aberrant Wnt pathway activation is a common oncogenic driver (76-78). In environments of high E-cadherin expression, β-catenin is sequestered away from the Wnt pathway (79), while loss of E-cadherin, although not alone sufficient to cause aberrant activation of Wnt signaling, potentiates the activation of the Wnt pathway in several cancer types (80,81). Finally, association of E-cadherin and VE-cadherin with ErbB and VEGF family receptors, respectively, has been shown to inhibit mitogenic signaling of these receptors, indicating another role for the cadherins in down-regulating oncogenic signaling (82,83).

Integrins

Structure and function

The integrins are a family of transmembrane adhesion receptors regulating ECM adhesion (84). They are obligate dimers of α- and β-subunits (85). In mammals, there are twenty-four α-subunits and nine β-subunits. Different combinations of these subunits confer selectivity of the integrin for its ligand, including fibronectin, collagen, laminin, and vitronectin. Expression of the subunits, and their combinations, is tissue specific (86).

Inactive integrins are present on the cell surface in an “unprimed” or bent shape. They can be primed either by binding of Talin to the cytoplasmic domain of the β-subunit, in so-called “inside-out” signaling (87,88), or by binding of divalent cations (Ca^{2+} or Mg^{2+}) to the extracellular domain, in so-called “outside-in” signaling (86). Some integrins can also be primed “outside-in” by cytokines (89). Both “outside-in” and “inside-out” activation of integrins result in an extended or “unbent” conformation of the extracellular domains of the subunits that allow for ligand binding (88). This activation

leads to the assembly of focal adhesions, which serve to link the network of the ECM surrounding the cell to the network of the actin cytoskeleton within the cells. Focal adhesions also contain a plethora of signaling molecules, including receptor tyrosine kinases, that, upon integrin activation and focal adhesion assembly, instruct the cell on what biological processes to initiate: proliferation, migration, adhesion, differentiation, or death (90).

Integrins in cancer

Changes in integrin expression are commonly associated with transformation (91). Altered integrin expression can mediate changes to matrix adhesion as well as to signaling pathways influencing biological processes such as proliferation, differentiation, and migration. For example, expression of αVβ3 in melanoma is associated with increased invasion and is considered a marker of disease progression in melanoma (92). In breast cancer, expression of α3β1 has been shown to promote metastasis through up-regulation of MMP2 and 9, while loss of α2β1 is also associated with progression (93,94). Finally, loss of α3β1 and α6β1 promotes loss of polarity and increase in invasiveness in prostate cancer (95).

Immunoglobulin superfamily

Structure and function

The immunoglobulin superfamily (IgSF) is a large superfamily of proteins that each contain an immunoglobulin-like domain (96). These proteins are mostly transmembrane molecules, but some IgSF members are secreted. The transmembrane IgSF members are mostly type-1 molecules, with a single α-helix traversing the membrane (97). IgSF members fall into a wide range of different protein classes such as antigen receptors, cell adhesion molecules, cytokine receptors, and growth factor receptors (96). Many IgSF members play significant roles in immunological processes such as antigen detection and presentation, immune co-stimulation or inhibition, and Ig binding (98). However, many IgSF members such as Izumo, a protein essential for sperm and egg fusion, and Titin, a 4200 kDa protein important for muscle contraction, function outside of the immune system (99,100). The diversity of the IgSF is linked by the

immunoglobulin-like domain. This ~100 aa domain adopts a Greek key motif similar to the cadherin domain (98). Often, protein-protein interactions occur at the Ig-like domains of IgSF proteins. This is especially true for the IgSF cells adhesion molecules (Ig-CAMs), the focus of this thesis.

Ig-CAMs

Ig-CAMs are cell surface glycoproteins that contribute to cell-cell adhesion at the points of cell-cell contact. Ig-CAM-mediated adhesion is Ca^{2+} independent. Many Ig-CAMs engage in both homophilic and heterophilic interactions, in *cis* and *trans*. Most *trans* interactions occur at the most N-terminal Ig-like domain and, similar to cadherins, result in *cis* clustering to form a zipper-like structure (101). *Cis* clustering of Ig-CAMs strengthens *trans* interactions and often anchors the cytoplasmic domain to the actin cytoskeleton. Alternatively, as in the case for neuronal cell adhesion molecule (NCAM), *trans* interactions may potentiate intracellular signaling through cytoplasmic binding partners (102). It is not necessary for Ig-CAMs to localize to specific adhesion complexes such as tight junctions and adherens junctions. Instead, they are able regulate adhesion across the intercellular boundary (101).

Ig-CAMs in cancer

Because of the diversity of this superfamily, Ig-CAMs have been implicated in nearly every step of cancer progression. At the primary site, ALCAM and NCAM promote apoptotic evasion, and PECAM-1 and ICAM-1 promote angiogenesis. During metastasis, MCAM, L1-CAM, ALCAM, and NCAM enhance local invasion and potentiate effective intravasation and extravasation. Moreover, MCAM, NCAM, and ALCAM are all likely to affect immune evasion (reviewed in detail in (22)).

This group of Ig-CAMs have been known to control proliferation, migration, matrix degradation, angiogenesis, and cell polarity. This makes them attractive targets for therapy; however, few Ig-CAMs are themselves considered targetable because they lack traditional signaling motifs and are rarely genetically altered in cancer (5,103). Nevertheless, many Ig-CAMs are differentially regulated in cancer through epigenetic and post-translational processing (104). Therefore, understanding how the function of

these molecules is dynamically regulated, and how that regulation is appropriated by tumor cells, may reveal new therapeutic targets for cancer progression and metastasis.

Activated Leukocyte Cell Adhesion Molecule

ALCAM, also commonly known as Cluster of Differentiation 166 (CD166), is an Ig-CAM known to participate in both homophilic and heterophilic (namely with CD6) interactions (105,106). ALCAM is critical to several biological processes including neuron development, T-cell activation, and certain types of transendothelial migration (Fig. 2) (107-110). Pathologically, ALCAM expression and function have been associated with invasiveness and progression in several cancers including melanoma, liver, colorectal, and urogenital cancers (111-114). In this section, I will provide a comprehensive review of ALCAM structure, function, regulation, and known interactions. This information will lay a foundation that highlights the importance of understanding the dynamic, and often context-dependent, regulation of ALCAM-mediated adhesion in the context of both normal and pathological processes.

Structure

Gene structure and expression

ALCAM is a large gene, spanning nearly 150 kilobases, located on the 3q13.1-3q13.2 locus in humans. The gene contains 16 exons, 15 of which are coding. *ALCAM* has been cloned in several vertebrate organisms and shows high sequence similarity across organisms, with greater than 90% identity between mouse, chicken, and human (115).

The promotor region lacks a canonical TATA box, but is instead enriched with several GC boxes (116). Functional binding sites for p65/NFκB, GATA-1, and AP-1 have been identified in the promoter region of *ALCAM* (116-118). Transcription of the gene is also regulated epigenetically by hypermethylation in some breast cancer cells (116). Post-transcriptionally, *ALCAM* is regulated by alternative splicing. Four splice isoforms of *ALCAM* have been identified and validated at the mRNA level. Two of these splice isoforms have been verified on the protein level: isoform 1, the canonical isoform,

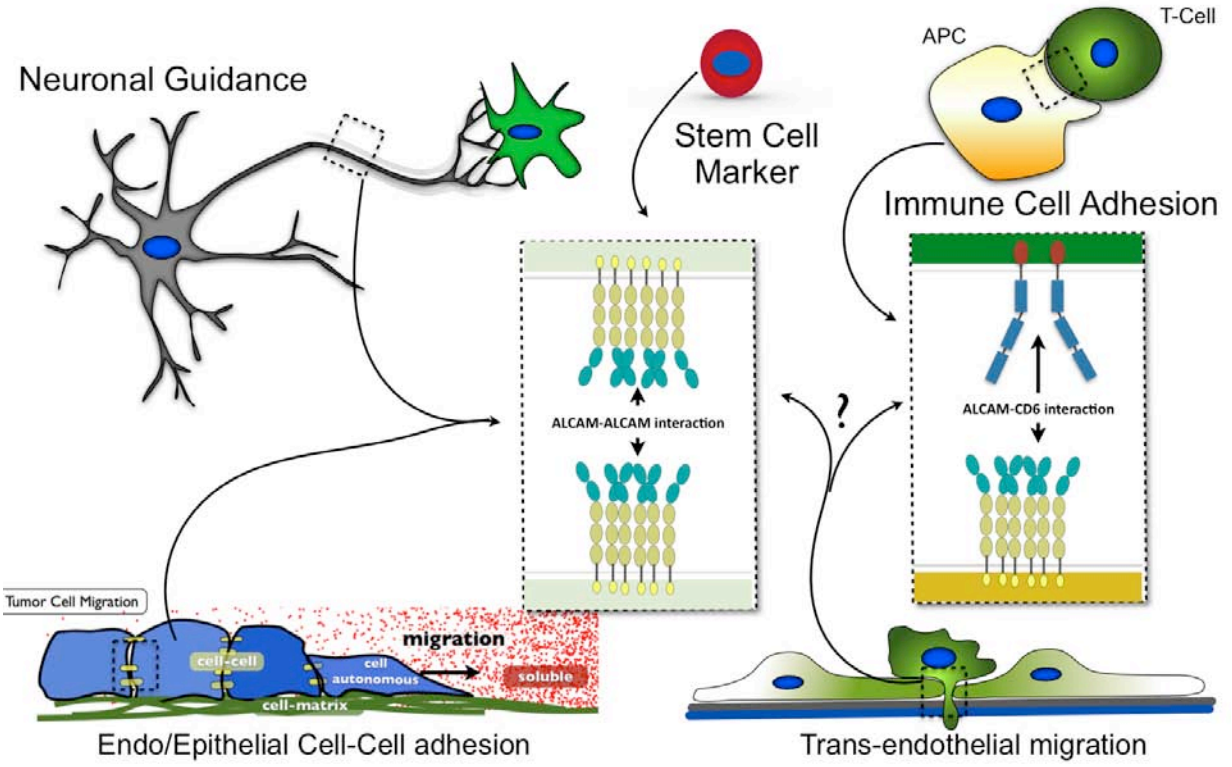

Figure 2. Known biological functions of ALCAM. Schematic depicting known functions of ALCAM and their attribution to either homotypic or heterotypic ALCAM interactions.

and isoform 2, which lacks exon 13. Functional and biochemical differences between the canonical isoform and the understudied ALCAM-Iso2 are examined in Chapter II of this dissertation. Further post-transcriptional regulation occurs by microRNAs. Exon 16, a 3' untranslated region (UTR) contains a binding site for miR-215, which down-regulates ALCAM expression by destabilizing *ALCAM* mRNA (119). Additionally, miR-9 inhibits ALCAM translation, and because miR-9 expression is also positively regulated by p65/NFκB, this indicates an auto regulatory loop in *ALCAM* expression (118).

ALCAM is expressed in most epithelial and endothelial cells. It is also expressed in several highly specialized cell types. ALCAM expression is a considered a marker of several stem cell niches, including those in bone marrow and colonic crypts (120,121). Additionally, expression of ALCAM is essential to the proper function of several cell populations, such as antigen presenting dendritic cells and retinal neurons (109,110).

Protein structure and mechanisms of adhesion

ALCAM is a type I transmembrane molecule with single transmembrane α-helix. The extracellular domain is composed of five Ig domains (Fig. 3). The two most N-terminal Ig domains are variable and the remaining three are type-2 constant domains, resulting in a VVC2C2C2 configuration (115). The small intracellular domain is composed of 32 amino acids predicted to take a coiled-coil conformation by *in silico* models. Both homophilic and heterophilic ALCAM interactions are mediated in *trans* by the V1 domain (105,122). Similar to other Ig-CAMs, *trans* ALCAM interactions are strengthened by lateral *cis* clustering, which is thought to be mediated by the membrane proximal C2 domain (105). The intracellular domain of ALCAM has been shown to anchor ALCAM to the actin cytoskeleton through scaffolding proteins such as syntenin-1 to further stabilize and strengthen *trans* ALCAM interactions (123). Moreover, both ALCAM heterophilic and homophilic interactions are also stabilized through intramembrane binding partners, namely the tetraspanins (124). Association with CD9 mediates *cis* clustering of ALCAM and down-regulates post-translational modification of ALCAM by ADAM17, a process discussed later in this chapter (125). Chapter III of this thesis also examines CD151 as a novel tetraspanin binding partner of ALCAM.

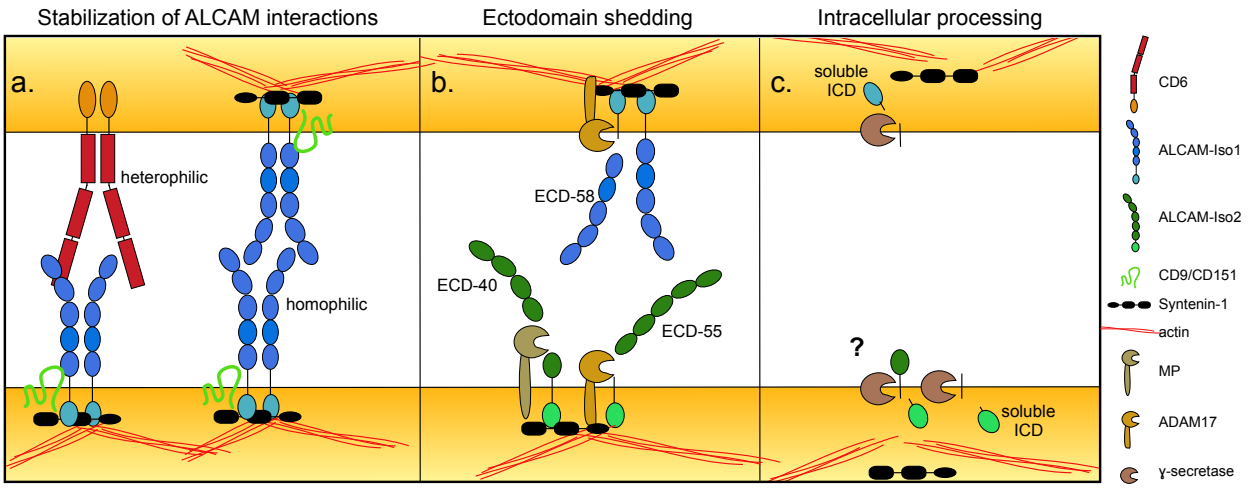

Figure 3. Molecular interactions of ALCAM. (**a**) Interaction with tetraspanin CD9 and scaffolding protein syntenin-1 stabilize ALCAM hemophilic and heterphilic interactions by anchoring ALCAM to the actin cytoskeleton. In Chapter III, we show that tetraspanin CD151 also interacts with ALCAM. (**b**) The ectodomain of ALCAM is shed by ADAM17. In Chapter II, we demonstrate that an alternatively spliced isoform of ALCAM (ALCAM-Iso2) is also shed in an MMP14-dependent manner. (**c**) In Chapter III we show that ALCAM is processed by ɣ-secretase to release soluble intracellular domain (ICD). This process disrupts CD151/syntenin-1/ALCAM interactions. It is unknown if ɣ-secretase also processes ALCAM-Iso2.

Known biological functions

ALCAM has been shown to function in a broad array of biological and pathological processes. ALCAM was originally identified in humans as the only known ligand of CD6 (106). ALCAM-CD6 interactions are essential for T-cell activation. Moreover, prolongation of this interaction is vital to activated T-cell proliferation (109). Anchoring ALCAM to the actin cytoskeleton through scaffolding proteins ezrin and syntenin-1 stabilizes ALCAM-CD6 interactions and promotes T-cell activation and proliferation (123). Reinforcing its importance in the immune system, ALCAM is expressed on both pulmonary endothelial cells and monocytes. ALCAM in pulmonary endothelial cells localizes to adherens junctions at points of cell to cell contact (107). Inhibition of ALCAM activity with either soluble recombinant ALCAM or function-blocking antibodies specifically decreased monocyte transendothelial migration without affecting monocyte migration or adhesion to the endothelium.

In addition to its role in transendothelial migration, ALCAM has also been implicated in angiogenesis and lymphangiogenesis. Cell surface interactions with the lectin, gal-8 promote vascular endothelial cell migration and tube formation in both microvascular endothelial cells and aortic endothelial cells (126). Additionally, ALCAM expression mediates cell-cell adhesion, migration, and tube formation in lymphatic endothelial cells as well as lymphatic transendothelial migration in dendritic cells (127).

In development, ALCAM is expressed in several stem cell populations and has been implicated in hematopoiesis and osteogenesis. Studies with whole-organism ALCAM-knockout in mice show that ALCAM is required for the proper outgrowth, organization, and termination of retinal ganglion cells and motor neurons (110). Furthermore, the zebrafish ortholog of ALCAM, *alcama* is important for neural crest differentiation (128).

ALCAM in disease

Both increased and absent ALCAM expression has been associated with disease pathologies. ALCAM-knockout mice are more susceptible to experimentally induced autoimmune encephalomyelitis due to increased permeability in the blood brain barrier (108), enforcing the importance of ALCAM in maintaining endothelial cell-cell

adhesions. Given the role of ALCAM and CD6 in the transendothelial migration of leukocytes, ALCAM has also been examined in the context of multiple sclerosis, and individuals harboring an ALCAM polymorphism (rs6437585C>T) have more than 2-fold greater risk of disease and experience disease onset around two years sooner than other individuals (129).

ALCAM has been shown to positively mediate cancer hallmarks such as survival, invasion, and angiogenesis in several different tumor types (22). Expression of ALCAM in breast cancer cell lines is associated with increased survival and decreased apoptosis through positive regulation of the anti-apoptotic protein Bcl-2 (130). Additionally, ALCAM expression positively correlates with tamoxifen resistance in breast cancer cells, and this resistance can be overcome through down-regulation of ALCAM expression by miR-148a and -152 (131). ALCAM expression in melanoma is associated with increased invasion through positive regulation of matrix metalloprotease-2 and -14 expression (111). In multiple myeloma, ALCAM expression promotes tumor growth and osteolysis by suppressing RUNX-2 expression and promoting osteoclastogenesis (132). Finally, in several models of lung metastasis, stromal ALCAM-knockout is associated with decreased tumor neovascularization which leads to decreased dissemination to and growth within the lung (133).

ALCAM has emerged as a significant and well-studied biomarker of disease progression in several different cancers; however, there is little consensus on whether ALCAM positively or negatively predicts progression. Mislocalization of ALCAM to the cytoplasm is predictive of invasive disease in breast cancer patients (134). While the loss of ALCAM protein in both bladder and prostate cancer tissue is indicative of advanced disease, down regulation of ALCAM expression is not reflected on the mRNA level (114,135). Conversely, high expression of ALCAM in liver and pancreatic cancer is associated with aggressive disease (112,136). ALCAM expression in early endometrial cancer positively predicts recurrence (137). Discrepancies between mRNA and protein levels, as well as across the field regarding the correlation of ALCAM expression and disease progression, may be explained by examining the post-translational regulation of ALCAM.

Post-translational regulation of ALCAM

Subcellular localization

As with most cell surface receptors, subcellular localization of ALCAM is critical to proper activity. The signal peptide coded by exon 1 facilitates the translocation of ALCAM from the golgi to the cell surface. Once at the cell surface, ALCAM can be internalized through endocytosis (138). This process is clathrin-mediated and has been shown to negatively impact axon fasciculation. Finally, surface biotinylation studies show that endocytosed ALCAM can be recycled back to the cell surface (139).

Furthermore, interactions with other cell surface proteins have been shown to stabilize ALCAM-mediated adhesion. In breast cancer cells, glycosylation-dependent interactions with the lectin gal-8 segregate ALCAM at the cell surface and promote cell adhesion (140). Several studies show that ALCAM, when localized to adherens junctions, functionally supports members of the cadherin family. In prostate cancer cells, this association is dependent on the cadherin-binding molecule α-catenin and promotes an epithelial morphology (141). In endothelial cells, ALCAM is localized to the adherens junctions through interaction with VE-cadherin and β-catenin to promote endothelial cell-cell adhesion (142).

Ubiquitin-mediated degradation

ALCAM has been shown to mediate stem cell-like properties in several cancer types including head and neck cancer. Targeting ALCAM to proteasomal degradation with the E3 ubiquitin ligase, CHIP, significantly decreases stem cell-like phenotypes in head and neck cancers (143). ALCAM is targeted by a viral RING ubiquitin ligase to prevent T-cell activation during Kaposi sarcoma-related herpesvirus infection (144). Although the specific ubiquitin ligase was not identified, other studies also indicated that increased ubiquitination of the intracellular domain of ALCAM decreases surface ALCAM expression in retinal ganglion cells and negatively impacts axon navigation (145).

Proteolytic processing

As previously mentioned, the extracellular domain (ECD) of ALCAM is essential for

mediating cell adhesion. The ECD can be cleaved from the cell surface by the protease a disintegrin and metalloprotease-17 (ADAM17, (146)). This process, also referred to as ectodomain shedding, is an important and well-known method of regulating ALCAM function. It serves both as a mechanism of recycling ALCAM from the cell surface and as a process to interrupt both homophilic and heterophilic interactions (105). Several groups have hypothesized that proteolytic release of the ECD, creating soluble ALCAM-ECD, also serves as mechanism to antagonize ALCAM interactions (122,147,148). Studies with recombinant soluble ALCAM, comprised of only the most N-terminal Ig domain, support this hypothesis and show antagonism of homophilic ALCAM interactions in melanoma and vascular endothelial cells (122,148). Shed ALCAM also functions as a biomarker of disease progression in several cancers. The generation of soluble ALCAM-ECD by ADAM17 was first identified in ovarian cancer cell lines (146). In ovarian cancer, ALCAM shedding positively correlates with disease progression (149). Direct quantification of shed ALCAM in the urine of bladder cancer patients shows that increased ALCAM shedding correlates with poor prognosis (114). Finally, ALCAM shedding detected in the tumor tissue of colorectal cancer patients also correlates with reduced survival (113). Importantly, in all of these studies, expression of ALCAM measured at the mRNA level did not correlate with disease progression. This process of ectodomain shedding is a likely explanation for discrepancies between ALCAM mRNA and protein expression that were highlighted previously.

Purpose of this study

As outlined here, ALCAM is involved in a diverse set of biological and pathological functions. Its functional contribution to cell adhesion is heavily context dependent and is strongly mediated by the proteins with which it is associated. In cancer, ALCAM's contribution as both a functional mediator and biomarker of disease progression is still contested. Similarly, the previously held dogma that lowered cell adhesion equates to increased tumor cell migration and invasion is now known to be a gross oversimplification of dynamic interplay between cell adhesion and metastasis. Discrepancies within the ALCAM literature regarding its contribution to disease

progression are better understood in the context of the dynamic regulation of cell adhesion during metastasis.

This dissertation outlines two novel mechanisms of ALCAM regulation. In Chapter II, we examine the biochemical and functional consequences arising from the alternative splicing of exon 13 in ALCAM through a structure-function analysis of ALCAM isoforms 1 and 2. Here, we find that ALCAM-mediated adhesion is tunably regulated through differential proteolysis of these splice isoforms. This differential regulation specifies ALCAM-Iso2 as a metastasis-promoting isoform. In Chapter III, we identify ALCAM as a novel binding partner of CD151. ALCAM-CD151 interactions can be stabilized using the anti-CD151 antibody 1A5, leading to increased cell adhesion and decreased metastasis. Furthermore, by disrupting the intracellular mechanisms anchoring ALCAM to the actin cytoskeleton, the effect of 1A5 can be disrupted.

The studies presented herein define two mechanisms of dynamic regulation of ALCAM-mediated cell adhesion. They are presented in the context of cancer progression and metastasis; however, because ALCAM is known to contribute to several dynamic adhesion processes, such as axon fasciculation and transendothelial migration, these findings have much further reaching implications. These data also reinforce the notion that the function and regulation of ALCAM (and many other cell adhesion molecules) cannot be studied in isolation, but must be considered in the context of extracellular, intramembrane, and intracellular binding partners. Moreover, considering the structural commonalities across the IgG superfamily, understanding the regulation of ALCAM function not only clarifies this molecule-specific mechanism, but also informs more globally regarding the tunable regulatory mechanisms available to control cell-cell adhesion in both normal physiology as well as pathology.

CHAPTER II:

ALTERNATIVE SPLICING OF *ALCAM* ENABLES TUNABLE REGULATION OF CELL-CELL ADHESION THROUGH DIFFERENTIAL PROTEOLYSIS

Contributing Authors: Katie E. Hebron, Elizabeth Y. Li, Shanna A. Arnold Egloff, Ariana K. von Lersner, Chase Taylor, Joep Houkes, David K. Flaherty, Adel Eskaros, Thomas P. Stricker, Andries Zijlstra

This work is presented as submitted to *Scientific Reports* 2017.

Summary

While many adhesion receptors are known to influence tumor progression, the mechanisms by which they dynamically regulate cell-cell adhesion remain elusive. We previously identified Activated Leukocyte Cell Adhesion Molecule (ALCAM) as a clinically relevant driver of metastasis and hypothesized that a tunable mechanism of ectodomain shedding regulates its contribution to dissemination. To test this hypothesis, we examined an under-explored *ALCAM* splice variant (ALCAM-Iso2) and demonstrated that loss of the membrane-proximal region of ALCAM (exon 13) increased metastasis four-fold. Mechanistic studies identify a novel MMP14-dependent membrane distal cleavage site in ALCAM-Iso2 which mediates a ten-fold increase in shedding, thereby decreasing cellular cohesion and promoting metastatic dissemination. Importantly, the loss of cohesion is not limited to the cell capable of shedding because the released extracellular domain diminishes cohesion of non-shedding cells through disruption of ALCAM-ALCAM interactions. ALCAM-Iso2-dominated expression in bladder cancer tissue, compared to normal bladder, further emphasizes that *ALCAM* alternative splicing can contribute to clinical disease progression. The requirement for both the loss of exon 13 and the gain of metalloprotease activity suggests that ALCAM shedding and concomitant regulation of dissemination is a locally tunable process.

Introduction

Dynamic control of cell-cell adhesion is central to many normal biological processes, including neuronal guidance, cell differentiation, tissue morphogenesis, and immune cell activation and function (reviewed in (21)). Dysregulation of cell-cell adhesion can lead to pathologies of the muscle, skin, and kidney, as well as the nervous and immune systems (reviewed in (150)). In other diseases, such as cancer, the dysregulation of adhesion is a central mediator of malignant progression that can support not only invasion and dissemination but also cell survival and proliferation.

All major classes of adhesion molecules have all been shown to contribute to cancer progression. For example, loss of epithelial cadherin (E-cadherin) expression is a canonical indication of changing cell-cell adhesions that facilitate motility during oncogenic transformation (151), while changes in integrin expression correlate with tumor progression, metastasis, and chemoresistance (152-155). Additionally, following the loss of E-cadherin, the immunoglobulin superfamily of cell adhesion molecules (Ig-CAMs) is upregulated in tumor cells where they modulate cellular proliferation and survival, while promoting disease progression through modulation of matrix metalloprotease (MMP) expression, collective cell migration, and tumor cell-endothelial cell interactions (22,122,131,156). While changes in the expression of these adhesion receptors have been associated with tumor progression, the mechanisms underlying dynamic regulation of their activity remain poorly understood.

The Ig-CAM, Activated Leukocyte Cell Adhesion Molecule (ALCAM), has been shown to modulate cell-cell adhesion in two distinct fashions, through homophilic ALCAM-ALCAM interactions and through heterophilic ALCAM-CD6 interactions. In normal physiology, homophilic ALCAM interactions modulate cell-cell interactions of epithelial and endothelial cells and mediate neuronal guidance, while ALCAM-CD6 interactions are essential for antigen presentation in immune cell adhesion (107,109,157,158). ALCAM is also essential for monocyte transendothelial cell migration specifically in the brain, but it is currently unknown whether this function can be attributed to homophilic or heterophilic ALCAM interactions (159).

In cancer, ALCAM has emerged as a significant factor in disease progression, however the relationship between the expression of ALCAM and its correlation with aggressive disease have been debated. Changes in ALCAM subcellular localization from the cell surface to the cytoplasm in breast cancer correlate with poor prognosis (134). However, loss of ALCAM by immunohistochemistry correlates with advanced stage in prostate and bladder cancer, but the loss of ALCAM protein in the tumor tissue is inconsistent with the persistent and sometimes elevated expression of ALCAM mRNA (114,160). Finally, ALCAM expression positively correlates with increased tumorigenicity and invasiveness in melanoma, pancreatic cancer, and liver cancer (112,161,162). Additional mechanistic studies support the role of ALCAM in promoting tumor progression. It has been shown to promote survival in breast cancer cells through the anti-apoptotic protein B-cell lymphoma 2 (Bcl-2), modulate invasion of melanoma through expression of MMP2 and MMP14, and promote metastasis through collective cell invasion (22,111,163). Despite this large body of evidence indicating that ALCAM is important to cancer progression, the mechanism by which ALCAM contributes to tumor progression remains unclear.

In the absence of evidence for an activation mechanism, such as phosphorylation, the regulation of ALCAM-mediated adhesion is thought to be achieved by controlling ALCAM binding availability. Regulation of ALCAM-ALCAM interactions can occur through changes in expression and membrane localization, proteolytic release of the ALCAM ectodomain, or antagonistic competition by this shed ectodomain and/or a soluble ALCAM isoform (22,122,134,164). ALCAM, like many other Ig-CAMs, can be cleaved from the cell surface by the protease ADAM17, a process referred to as ectodomain shedding (22,165). However, the regulation of this process is not well characterized. Work from our laboratory and others has demonstrated that the level of shed ALCAM in biofluids is elevated in a variety of cancer patients, suggesting that ALCAM shedding increases during oncogenesis and malignant progression (114,149,165). As previously noted, changes in total mRNA expression rarely correlate with the changes in protein expression in tumor tissues, therefore suggesting that ALCAM shedding is the likely cause for these discrepancies reported in the literature.

Thus, we aimed to elucidate the intrinsic regulatory mechanisms controlling ALCAM shedding in cancer progression.

A review of the gene structure of *ALCAM* revealed the existence of a splice variant missing the membrane proximal region stalk, a region targeted by ADAM17 cleavage. This led us to hypothesize that dynamic changes in ectodomain shedding might be achieved through changes in protease susceptibility between ALCAM splice isoforms. *ALCAM* has nine recognized splice variants, four of which have open reading frames (Ensembl, (166)). However, only two isoforms have been confirmed on both mRNA and protein levels (Table 1). Full length ALCAM (ALCAM-Iso1) is composed of all 15 coding exons. ALCAM-Iso2 lacks exon 13, which corresponds to 13 amino acids in the stalk region of the protein (Fig. 4, Ensembl, (166)). Despite the fact that both isoforms are expressed in normal human tissues (Fig. 4), biochemical and functional differences between the two isoforms have never been explored.

In this chapter, we examined the functional and biochemical differences between ALCAM-Iso1 and ALCAM-Iso2 in the context of tumor progression. We investigated the effect of ALCAM-Iso1 and ALCAM-Iso2 expression on metastasis, tumor cell aggregation, and ALCAM homophilic interactions. We defined differences in proteolytic susceptibility between ALCAM-Iso1 and ALCAM-Iso2, as well as the impact of isoform-dependent proteolytic susceptibility on cell-cell adhesion. Finally, we conclude that differential expression of ALCAM-Iso1 and ALCAM-Iso2 correlates with malignancy in bladder tissue.

Materials and Methods

Cell culture, plasmids, transfections, and inhibitors

HT1080 (fibrosarcoma) and UMUC-3 (transitional cell carcinoma) cells were obtained from the ATCC (CCL-121 and CRL-1749, respectively). Cell lines were maintained in RPMI (HT1080) or DMEM (UMUC-3) supplemented with penicillin/streptomycin, sodium pyruvate, nonessential amino acids and 10% fetal bovine serum and cultured at 37°C with 5% CO_2. Knockout cell lines were generated

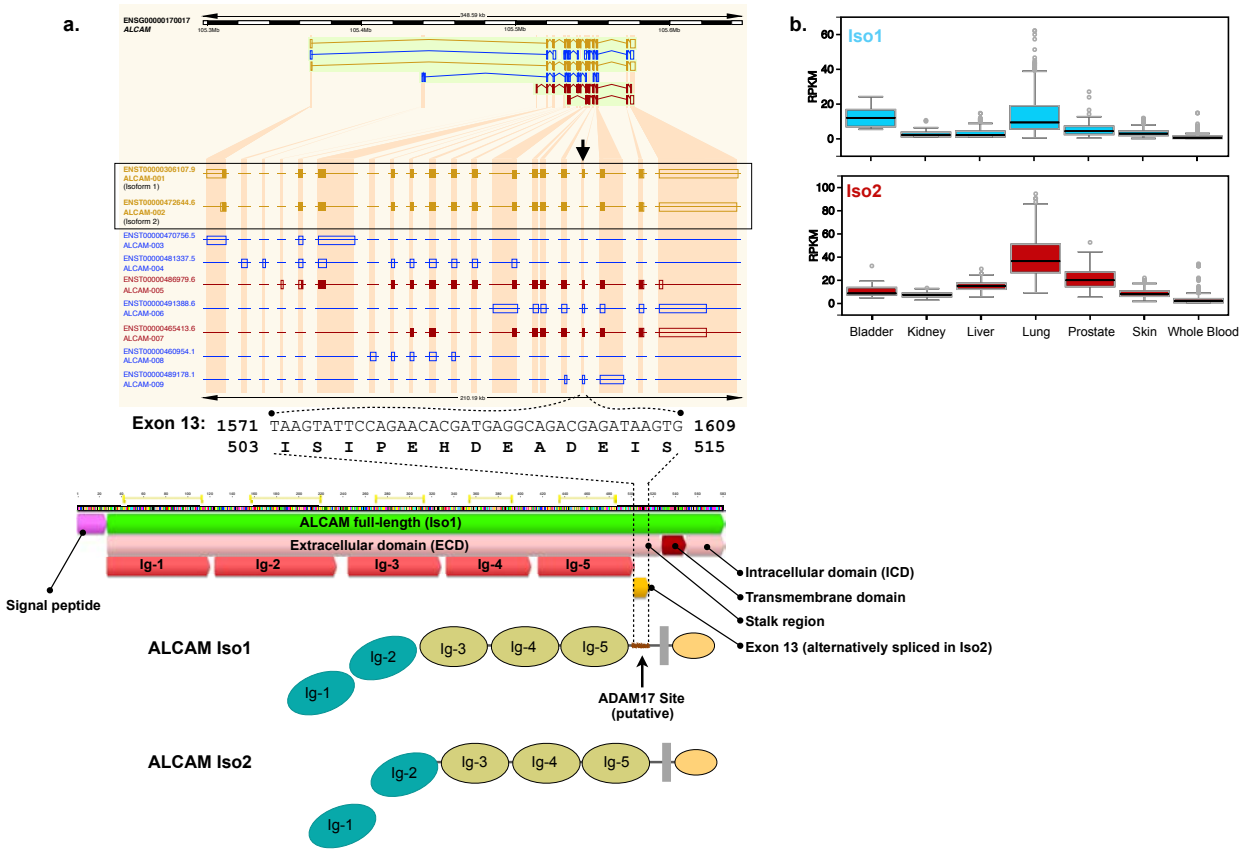

Figure 4. ALCAM is expressed as two distinct splice isoforms in normal human tissue. (**a**) Reported potential splice isoforms of ALCAM. Black arrow indicates exon 13. Gold indicates protein coding transcripts with identical annotations in both Ensembl and HAVANA systems. Red indicates protein coding transcripts with non-identical annotations in Ensembl and HAVANA systems. Blue indicates non-coding transcript. Schematic depicts protein structure of ALCAM-Iso1 and ALCAM-Iso2. (**b**) Isoform expression in indicated normal human tissue. Data extracted from GTEx Portal.

Name	Transcript ID	bp	Protein	Biotype	CCDS	UniProt	RefSeq	Flags
ALCAM-001	ENST00000306107.9	4701	583aa	Protein coding	CCDS33810	Q13740	NM_001243281 NM_001627 NP_001230210 NP_001618	TSL:1, GENCODE basic, APPRIS P1
ALCAM-002	ENST00000472644.6	4189	570aa	Protein coding	CCDS58841	Q13740	NM_001243280 NP_001230209	TSL:1, GENCODE basic
ALCAM-007	ENST00000465413.6	2496	344aa	Protein coding	-	H7C543	-	CDS 5' incomplete, TSL:2
ALCAM-005	ENST00000486979.6	1818	532aa	Protein coding	-	F5GXJ9	-	TSL:5, GENCODE basic
ALCAM-004	ENST00000481337.5	1242	No protein	Processed transcript	-	-	-	TSL:2
ALCAM-008	ENST00000460954.1	564	No protein	Processed transcript	-	-	-	TSL:4
ALCAM-006	ENST00000491388.6	2845	No protein	Retained intron	-	-	-	TSL:2
ALCAM-003	ENST00000470756.5	1770	No protein	Retained intron	-	-	NM_001243283	TSL:1
ALCAM-009	ENST00000489178.1	783	No protein	Retained intron	-	-	-	TSL:2

Table 1. ALCAM predicted splice isoform information. CCDS=consensus coding sequence project identification number, TSL=transcript support level, APPRIS P1=APPRIS principal isoform (Ensembl).

using a CRISPR/Cas9 gRNA targeting the signal peptide of ALCAM (AGACGGTGGCGGAGATCAAG, Horizon Discovery, St. Louis, Missouri). The level of protein expression was verified by flow cytometry for cell surface ALCAM and by immunoblot for total ALCAM expression in whole cell lysates. HT1080 isoform variants were stably transduced with lentiviral particles to express the ALCAM isoform indicated as well as a labeling vector containing firefly luciferase with either Cerulean or TagRFP2 fluorescent protein (Fig. 6). Viral plasmids were constructed using MultiSite Gateway (ThermoFisher Scientific, Waltham, Massachusetts) on the pLenti6.2/V5-DEST backbone. Viral particles were produced in LentiX 293T cells (Clontech, Mountain View, California). Transductions were performed with 5 μg/mL polybrene. Transient transfections were performed using X-tremeGENE HP (Sigma Aldrich, St. Louis, Missouri) with 2 μg plasmid DNA, or 800 ng siRNA (Mission esiRNA human MMP14, Sigma Aldrich), as indicated. Protease inhibitors are listed in Table 2.

Fluorescence activated cell sorting (FACS) and flow cytometry

Following transduction described above, cell populations were purified by FACS. Cells were stained for cell surface ALCAM for 30 min (0.8 μg/10^6 cells, anti-ALCAM (extracellular domain), MAB6561, R&D Systems, Minneapolis, Minnesota). Primary antibody binding was detected with Alexa647-conjugated anti-mouse IgG (0.25 μg/10^6 cells, A28181, ThermoFisher Scientific). Cells were sorted for either the RFP+/GFP+/ALCAM+ or the Cerulean+/GFP+/ALCAM+ population, as appropriate. To quantify the amount of cell surface ALCAM and verify success of FACS, cells were stained as described above and analyzed by flow cytometry.

Avian embryo metastasis models

Spontaneous and experimental metastasis experiments were performed as described previously (167,168). In accordance with the Public Health Services policy on Humane Care and Use of Laboratory Animals, Vanderbilt Institutional Animal Care and Use Committee (IACUC) has determined that avian embryos developmental day 17 and younger are not considered vertebrate animals and therefore do not require specific

protocol approval. Vanderbilt IACUC has reviewed and approved the following experimental and euthanasia procedures.

Spontaneous metastasis (Xenografting)

Fertilized chicken eggs (Tyson Foods, Inc., Springdale, Arkansas) were placed in a 37°C incubator at 55% relative humidity on day 1 post-fertilization. The chorioallantoic membranes (CAM) of day 10 embryos were dropped away from the eggshell by displacing the air cell. Cells were dissociated, counted, and resuspended in sterile 0.9% saline at 20 x 10^6 cells/mL. The dropped CAM was damaged slightly with sterile cotton tipped swabs. 25 µL of cell suspension (500,000 cells) were placed on the dropped CAM and eggs were returned to the incubator. After 5 days of growth, embryos were euthanized by decapitation, and xenografts were harvested, weighed, and fixed in 10% zinc formalin. Fixed tumors were paraffin embedded, sectioned, and stained with hemotoxylin and eosin to visualize local invasion. To quantify metastasis to the distal CAM, the eggshell was cut in half along the long axis, chicks were dissected from the shell, and sections of the distal CAM were dissected using a cork borer. Dissected CAM tissue was incubated with D-luciferin (600 µg/mL) for 45 minutes, and luciferase activity was quantified using a digital gel documentation system (G:Box; Syngene, Frederick, Maryland) as a measure of cell number.

Experimental metastasis (Intravenous injection)

Fertilized chicken eggs were placed in a 37°C incubator at 55% relative humidity on day 1 post-fertilization. Day 11 embryos were candled to locate the allantoic vein and the direction of blood flow. Cells were dissociated, counted and resuspended at 0.25 x 10^6 cells/mL in sterile 0.9% saline. A window was cut into the eggshell at the injection site using a Dremel™ tool (Racine, Wisconsin). 100 µL of cell suspension (25,000 cells) were injected intravenously using an insulin syringe. Eggs were returned to the incubator for 5 days. Upon harvest, embryos are euthanized by decapitation and metastasis was quantified by luciferase activity as described above.

Ex Vivo imaging of tumor colonies

To analyze colony morphology, we performed the experimental metastasis assay as described above. However, upon harvest at 6 days post-injection, eggs were cut in half along the long axis, chicks were dissected from the shell, euthanized by decapitation, and three sections of CAM were dissected using a cork borer. Colonies were imaged using an upright fluorescent microscope (BX-61 WI, Olympus, Pittsburgh, Pennsylvania) and Volocity Imaging Software (Perkin Elmer, Waltham, Massachusetts). Colony size was determined using a custom KNIME (169) workflow (Zurich, Switzerland). In brief, images were thresholded and segmented, after which object size, reflective of colony size and morphology, was determined for each colony. All images were processed with the same workflow. Objects were assigned to one of four bins by size including single cells (150-1,000 pixels), small colonies (1,001-20,000 pixels), medium colonies (20,001-100,000 pixels), and large colonies (>100,000 pixels). Data are presented as percent of total area for each bin category.

Detecting ALCAM shedding

Cells were plated in 6-well plates at 80% confluency and allowed to adhere overnight. Complete medium was removed and cells were incubated with indicated protease inhibitors or vehicle in serum-free medium for 24 h (Table 2). Conditioned medium was collected, centrifuged at 500 g for 5 min to remove cell debris and half of the sample was concentrated 25X by acetone precipitation. Cells were lysed using 1% Triton X-100 lysis buffer for 30 min on ice. Lysates were clarified by centrifugation at 14,000 g for 15 min at 4°C. Following deglycosylation with PNGase-F (New England Biolabs, Ipswitch, MA), ALCAM protein expression (whole cell lysate) and shedding (conditioned medium) were detected by immunoblot with anti-ALCAM (intracellular domain; 1G3A (113) and anti-ALCAM (extracellular domain; MOG/07, Leica Biosystems, Buffalo Grove, Illinois), respectively. ALCAM protein expression and shedding were quantified using human ALCAM DuoSet ELISA (R&D Systems) from un-concentrated whole cell lysate and conditioned medium, respectively.

Adhesion to immobilized ALCAM-Fc

A 96-well high-binding plate was coated with protein G (2 µg/mL in 100 mM bicarbonate/carbonate buffer, pH 9.2) overnight at 4°C. The plate was washed with phosphate buffered saline (PBS) and coated overnight at 4°C with recombinant Fc-tagged ALCAM extracellular domain (ALCAM-Fc, 1 µg/mL) in appropriate wells, negative control wells were not coated with ALCAM-Fc. The plate was washed with PBS and positive control wells (equated to 100% binding) were then coated with Collagen Type 1 (100 µg/mL) overnight at 4°C. The plate was washed with PBS and 2.5 x 10^4 cells/well were added and incubated at 37°C and 5% CO_2 for 4 h. Non-adherent cells were washed away by gentle pipetting and aspiration. Cells were fixed with 4% paraformaldehyde (4% w/vol) and stained with crystal violet (0.5% vol/vol in 20% methanol). Stain was extracted with acetic acid (20% vol/vol). Absorbance was read on automated plate reader (BioTek, Winooski, VT). Cell adhesion was quantified as percent of adhesion compared to wells coated with collagen type I coated (considered 100% adhesion).

In vitro cell aggregation

Cells were detached using non-enzymatic cell dissociation buffer and plated in 24-well low-attachment plates at 2.5 x 10^4 cells/well. For conditioned medium experiments, EGTA was added to a final concentration of 1 mM to inhibit calcium-dependent cell adhesion. Cells were incubated with indicated treatments for 12 hours and cell clusters were imaged using a light microscope (TMS-F, Nikon, Tokyo, Japan) fitted with a D90 SLR camera (Nikon). Ten images were captured for each experimental group and analyzed in FIJI (ImageJ, (170)) by segmenting with Weka Trainable Segmentation (171) and calculating cluster size with the Particle Analysis plug-in. Clusters were assigned to one of four bin categories by size including single cells (200-400 pixels), small colonies (401-2,000 pixels), medium colonies (2,001-4,000 pixels), large colonies (4,001-10,000 pixels), and extra-large (>10,000 pixels). Data are presented as percent of total area for each bin category.

Isoform expression in human tissue

GTEx Transcript reads per kilobase per million mapped reads (RPKMs) were downloaded from the GTEx Portal (172) (Analysis version 6, normal bladder tissue), and transcripts ENST00000306107.5 (ALCAM-Iso1) and ENST00000306107.5 (ALCAM-Iso2) were analyzed. For TCGA (urothelial bladder carcinoma, (173)), per quantile normalized RPKMs for bladder cancer were downloaded from the GDC portal (https://portal.gdc.cancer.gov), and transcripts ENST00000306107.5 (ALCAM-Iso1) and ENST00000306107.5 (ALCAM-Iso2) were analyzed. RPKM values were transformed using $Log_2(x+1)$ for ALCAM-Iso1 and -Iso2 and reported for normal bladder (GTEx Portal) and bladder cancer (TCGA) datasets. In addition, the relative abundance of ALCAM-Iso2 was calculated for each patient and used to compare isoform expression in normal bladder compared to bladder cancer.

Statistical analysis

All statistical analyses were performed using Prism 5 for Mac OS X (GraphPad Software, Inc, La Jolla, California). For statistical analysis of xenograft weight, metastasis to distal CAM, ELISA quantifications, and colony size, experimental groups were compared to control groups using Kruskal-Wallis test with Dunn's post-test. Chi-square test for trend was used to determine statistically significant differences in size distribution between two groups for colony sizes and aggregation assays. All pair-wise Chi-square test for trends are reported in Tables 3, 4, 5, and 6. ALCAM-Iso1 expression was compared to ALCAM-Iso2 expression in both normal bladder and bladder cancer using paired t-test on $Log_2(x+1)$ transformed data, while Mann-Whitney U was used to compare differences in relative abundance of ALCAM-Iso2 between normal bladder and bladder cancer.

Data availability

The datasets analyzed in this manuscript are publicly available using the GTEx Portal (https://www.gtexportal.org/home/) and The Cancer Genome Atlas (TCGA) urothelial bladder carcinoma cohort (https://cancergenome.nih.gov/cancersselected/UrothelialBladderCarcinoma). ALCAM

isoform expression was extracted for transcript accession codes ENST00000306107.5 (ALCAM-Iso1) and ENST00000306107.5 (ALCAM-Iso2).

Results

Alternative splicing of *ALCAM* (ALCAM-Iso2) promotes metastatic dissemination

ADAM17 is known to cleave its substrates in the “stalk region”, which is the extracellular region between the transmembrane motif and the first globular region of the protein (174-176). In ALCAM-Iso1, the stalk region corresponds to amino acids 502-527 (Uniprot (177)) encoded by exons 12-14. Alternative splicing of exon 13 in ALCAM-Iso2 removes the majority of the stalk region (13 amino acids), which could impact the proteolytic processing of ALCAM-Iso2 (Figs. 4a, 5a) and therefore alter its adhesion function (122,165). Since ALCAM ectodomain shedding is elevated in patients with advanced disease (114,149,165) and both isoforms are present in many tissues (Fig. 4b), we hypothesized that alternative splicing could impact metastatic dissemination. To test this hypothesis, we generated a panel of HT1080 cell lines in which expression of the ALCAM isoforms was experimentally controlled (Fig. 6). Overexpression (OE) of ALCAM-Iso1 or ALCAM-Iso2 (Iso1- and Iso2-OE, Fig. 5b, Fig. 6a) generated a modest increase in surface ALCAM compared to levels observed in the parental HT1080 cells (Fig. 6b). Using the avian embryo spontaneous metastasis assay (Fig. 5c, (167,168,178)) no differences in xenograft size were observed (Fig. 5d, e). However, overexpression of ALCAM-Iso2 showed increased incidence of intravascular invasion, as scored by a pathologist (Fig. 7), with a concomitant, four-fold increase in spontaneous metastasis compared to overexpression of ALCAM-Iso1, as quantified by bioluminescent detection of tumor cells (Fig. 5d, f).

To distinguish defects in distant site colonization from defects in primary tumor dissemination, ALCAM-mediated changes in colonization were evaluated in the avian embryo experimental metastasis model, where colony formation within the CAM is evaluated following intravenous injection (Fig. 8a). Quantification of colonization by bioluminescent activity revealed no significant difference in the number of colonies formed by parental, Iso1-OE or Iso2-OE cells (Fig. 8b, c). These observations suggest

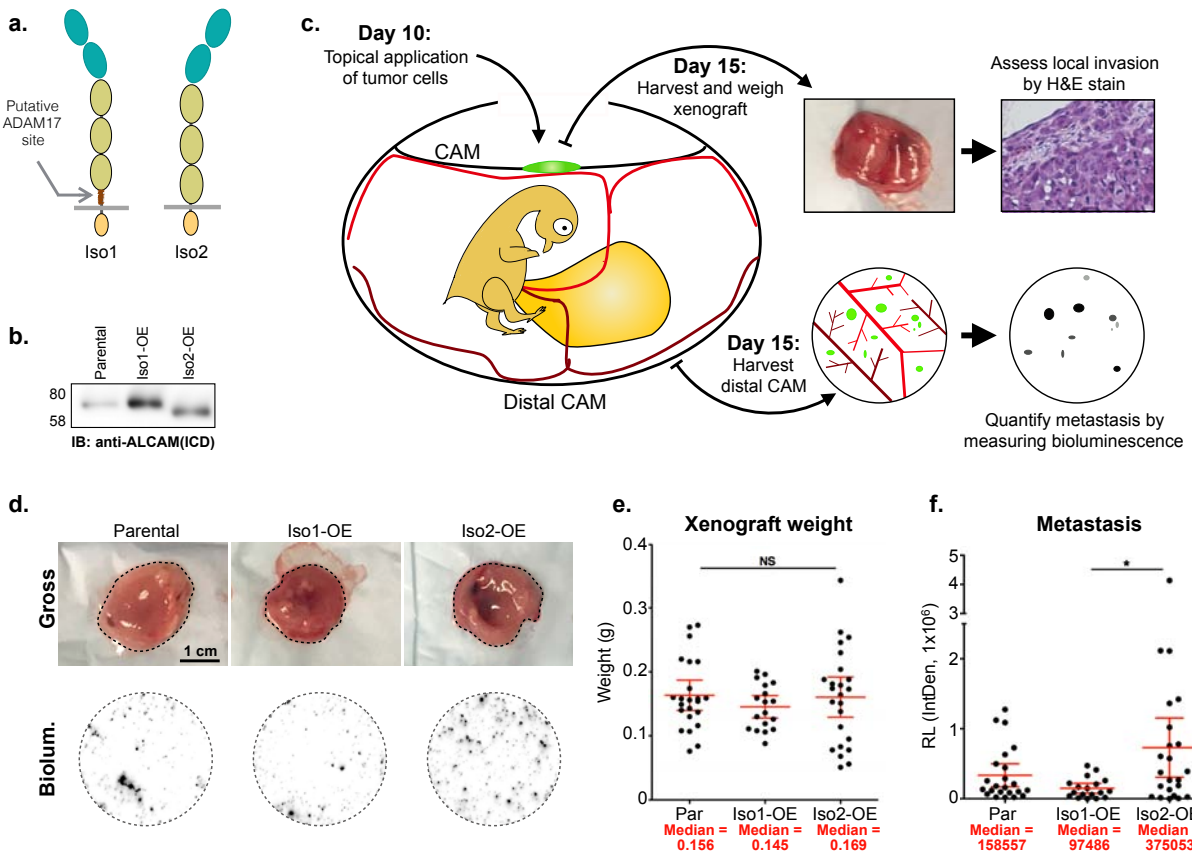

Figure 5. Alternative splicing of *ALCAM* (ALCAM-Iso2) promotes metastatic dissemination. (**a**) Schematic describing ALCAM splice isoforms 1 and 2. (**b**) Immunoblot of parental HT1080 cells (Par) and HT1080 cells stably overexpressing ALCAM-Iso1 (Iso1-OE) or ALCAM-Iso2 (Iso2-OE); ICD: intracellular domain. (**c**) Schematic describing avian embryo spontaneous metastasis assay. (**d**) Representative images of gross (tumor is outlined in dashed line) HT1080 xenografts and metastasis to the distal chorioallantoic membrane (CAM), indicated by bioluminescence (Biolum.). (**e**) Wet weight of HT1080 xenografts removed from CAM of chicken embryos. Three independent experiments were combined for the analysis (N= 23,18, 25, respectively). (**f**) Quantification of metastasis. Metastasis was measured by luciferase activity in a 1.5 cm core of distal CAM. Two cores per embryo from at least 10 embryos were measured. Relative bioluminescence (RL) represents mean value of two CAM sections per chick and was calculated using the integrated density tool (IntDen, $1x10^6$) in ImageJ. (**e, f**) P-values were calculated using Kruskal-Wallis test with Dunn's post-test, ns: not significant, *P<0.05. Graphs display mean with 95% confidence interval. Medians are reported.

a.

	Parental HT1080			ALCAM-knockout HT1080		
Name	**Parental**	**Iso1-OE**	**Iso2-OE**	**KO**	**KO+Iso1**	**KO+Iso2**
ALCAM variant	-	Iso1	Iso2	-	Iso1	Iso2
CRISPR KO	No	No	No	Yes	Yes	Yes
pRBow label	RFP	Cerulean	RFP	RFP	RFP	RFP

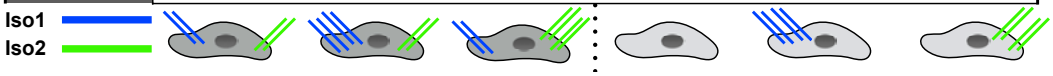

b.

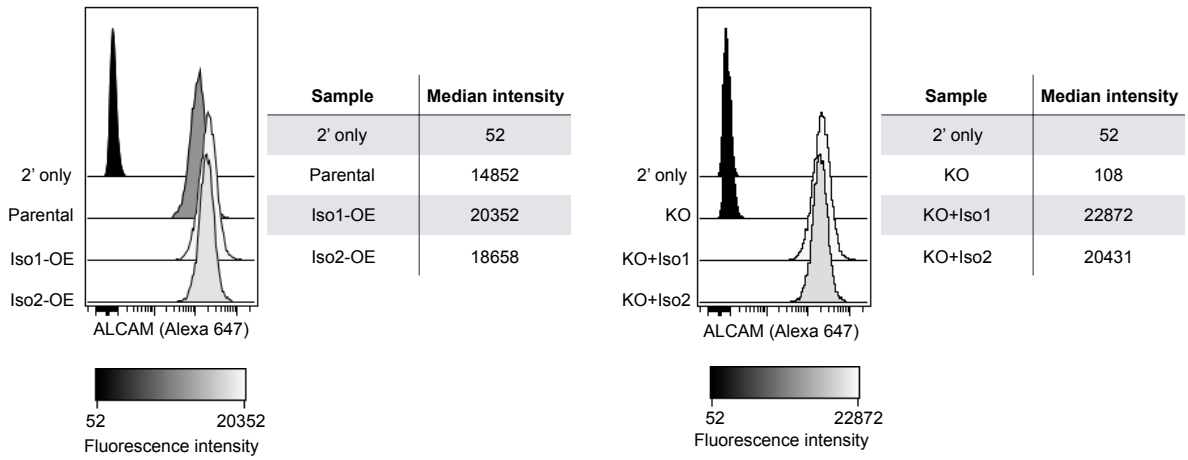

Sample	Median intensity
2' only	52
Parental	14852
Iso1-OE	20352
Iso2-OE	18658

Sample	Median intensity
2' only	52
KO	108
KO+Iso1	22872
KO+Iso2	20431

Figure 6. Stable cell line description. (**a**) Table describing each of the main stable cell lines used. (**b**) Surface ALCAM expression of cells described in (a), as determined by flow cytometry.

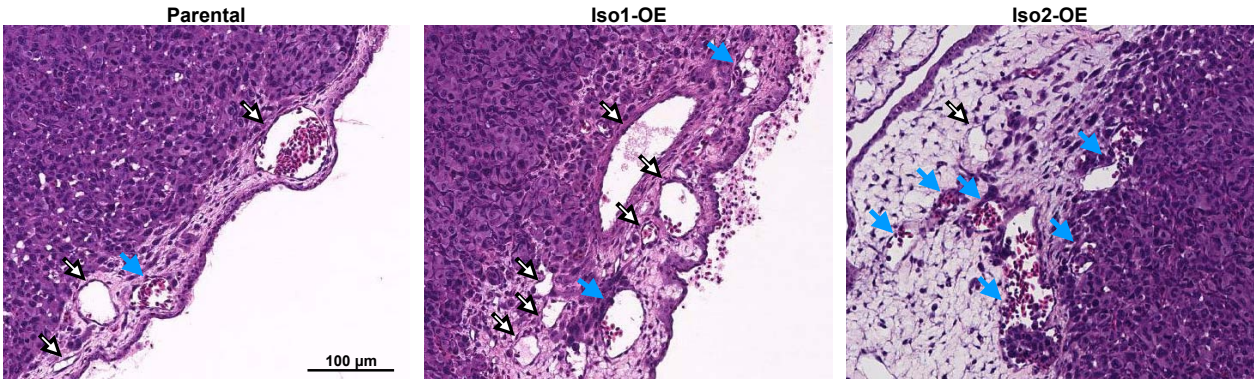

Figure 7: ALCAM-Iso2 cells show higher incidence of intravascular invasion at the primary site. Hematoxylin and Eosin (H&E) stained tumor sections from xenografts of parental HT1080 cells overexpressing ALCAM-Iso1 (Iso1-OE) or ALCAM-Iso2 (Iso2-OE). Tumor adjacent blood vessels were scored positive (➔) or negative (➪) for intravascular invasion by a blinded pathologist.

that alternative splicing of *ALCAM* alters metastatic success by contributing to dissemination from the primary tumor.

Full length ALCAM (ALCAM-Iso1) mediates tumor cell cohesion

While growth of metastatic colonies was not diminished, close examination of colony morphology revealed dense cell-cell cohesion among cells overexpressing ALCAM-Iso1 (Iso1-OE, Fig. 8d-g). High magnification *ex vivo* imaging of metastatic colonies formed in the CAM after intravenous injection revealed dense, multicellular colonies formed by HT1080 cells overexpressing ALCAM-Iso1 (Iso1-OE) while the colonies of the parental line were comprised of dispersed, single cells (Fig. 8d). Conversely, HT1080 cells overexpressing ALCAM-Iso2 (Iso2-OE) formed colonies composed of both diffuse single cells as well as densely-packed, cohesive cell colonies (Fig. 8d). Unbiased quantification of colony size confirmed a five-fold increase in cohesive colonies formed by Iso1-OE cells compared to parental cells (Fig. 8e). Each colony was subsequently classified as “Single Cell”, “Small Colony”, “Medium Colony”, and “Large Colony” based on its pixel area. This classification was pseudo-colored in the original image for visualization (Fig. 8f) and significant differences were assessed by Chi-squared test for trend (Fig. 8g). This analysis revealed that Iso1-OE cells primarily formed large colonies (50%) while the parental cells formed mostly single cells and small colonies (91%). In contrast to Iso1-OE, Iso2-OE cells formed few large colonies (14%) and persisted primarily as small colonies and dispersed single cells (61%) similar to the parental cells (Fig. 8g). These data suggest that ALCAM-Iso1 promotes cell-cell adhesion while ALCAM-Iso2 enables single cell dispersion.

Alternative splicing of *ALCAM* leads to enhanced proteolytic susceptibility

Because ALCAM-Iso2 is generated through the loss of 13 amino acids in the stalk region of the protein, we hypothesized that the functional difference between these two isoforms may be driven by changes in ADAM17-mediated shedding of the ectodomain. To assess this, shedding of ALCAM-Iso1 and ALCAM-Iso2 was quantified by ELISA, with detection of intact ALCAM in the whole cell lysate (WCL) and shed ALCAM in the conditioned medium (CM). Unexpectedly, ectodomain shedding from

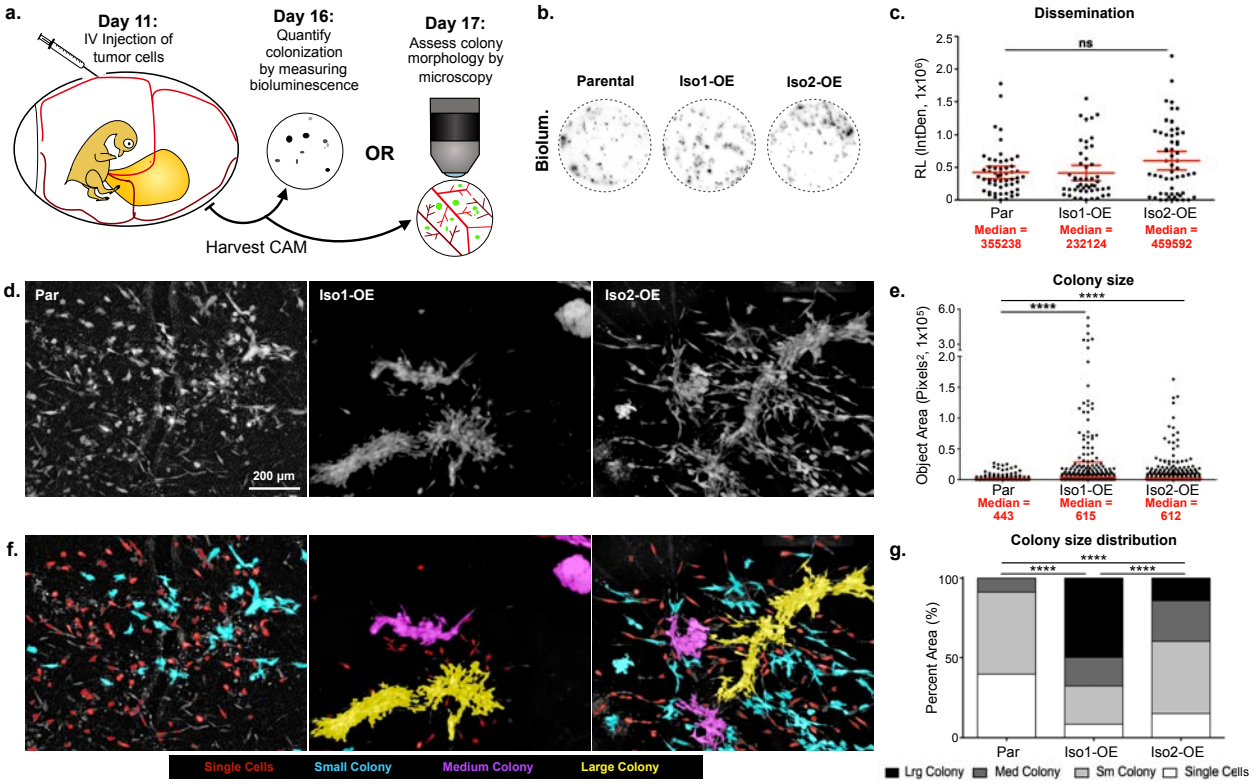

Figure 8. Full length ALCAM (ALCAM-Iso1) mediates tumor cell cohesion. (**a**) Schematic describing avian embryo experimental metastasis assay. (**b**) Representative images of CAM colonization, measured by bioluminescence, following intravenous (IV) injection of indicated HT1080 cells. (**c**) CAM colonization was quantified using luciferase activity in a 1.5 cm core of CAM. Two cores per embryo from at least 10 embryos were measured. Relative bioluminescence (RL) represents mean value of two CAM sections per chick and was calculated using the integrated density tool (IntDen, $1x10^6$) in ImageJ. P-values were calculated using Kruskal-Wallis test with Dunn's post-test, ns: not significant. (**d**) Representative images of metastatic colonies imaged 6 days post intravenous injection into CAM of chicken embryo. (**e**) Colony size was quantified using custom KNIME workflow. P-values were calculated using Kruskal-Wallis test with Dunn's post-test, ****P<0.0001. Graphs display mean with 95% confidence interval. Medians are reported. (**f**) Colonies were binned into single cell, small, medium, and large colonies using KNIME. Colonies are pseudo colored by size bin: Single Cells (Red), Small colonies (Cyan), Medium Colonies (Magenta), and Large colonies (Yellow). (**g**) Distribution of colonies across size bins was represented as percent of total area of all colonies. P-values were calculated using Chi-square test for trend, ****P<0.0001. Graphs display mean with 95% confidence interval. Medians are reported.

Iso1-OE cells was ten-fold lower than that from Iso2-OE cells, despite nearly equal expression of ALCAM-Iso1 and ALCAM-Iso2 (Fig. 9a). To verify that the proteolytic susceptibility was a function intrinsic to the isoforms, rather than dominant-negative or dominant-active interactions between the isoforms, CRISPR/Cas9-mediated ALCAM-KO cells (KO) were generated along with re-expression of either ALCAM-Iso1 or ALCAM-Iso2 (KO+Iso1 and KO+Iso2, respectively, Fig. 6). The difference in ALCAM shedding was recapitulated in KO+Iso1 and KO+Iso2 cells, demonstrating that the increased susceptibility to proteolysis is intrinsic to the alternative splicing of *ALCAM* (Fig. 9a).

Analysis by immunoblotting with antibodies specific to the intracellular domain (ICD) and extracellular domain (ECD) of ALCAM was subsequently used to assess intact ALCAM in the WCL and shed ALCAM in the CM, respectively (Fig. 9b). This not only confirmed that the loss of exon 13 in ALCAM-Iso2 led to an increase in the proteolytic sensitivity, but also showed a change in the proteolytic profile, as evidenced by the production of two distinct soluble fragments (Fig. 9b, right panel). CM from KO+Iso1 cells contains a single ECD of relative molecular weight (rMW) 58 kDa (ECD-58), which corresponds to the expected ALCAM-ECD shed by ADAM17 (Fig. 9b, right panel). However, CM from Iso2-OE and KO+Iso2 cells contain the predicted ECD of rMW 55 kDa (ECD-55), as well as a second, more abundant ECD fragment of rMW 40 kDa (ECD-40) (Fig. 9b, right panel). While the residual ICD generated by ECD shedding from ALCAM Iso1 is undetectable, the appearance of a new intracellular fragment of rMW 20 kDa (ICD-20) in the WCL from ALCAM Iso2 indicates that the alternative splicing has exposed a novel proteolytic site (Fig. 9b, left panel). Based on relative molecular weights, this cleavage is predicted to occur at a site distal to the membrane in the fourth IgG-like domain (Fig. 9c).

Alternative splicing of *ALCAM* introduces sensitivity to MMP14 dependent shedding

Because ADAM17 has been identified as the sheddase of ALCAM-Iso1, we performed a directed protease inhibitor screen to determine if this protease was also responsible for the shedding of ECD-40 from ALCAM-Iso2. Following treatment with indicated protease inhibitors, immunoblotting for ALCAM was performed in WCL and

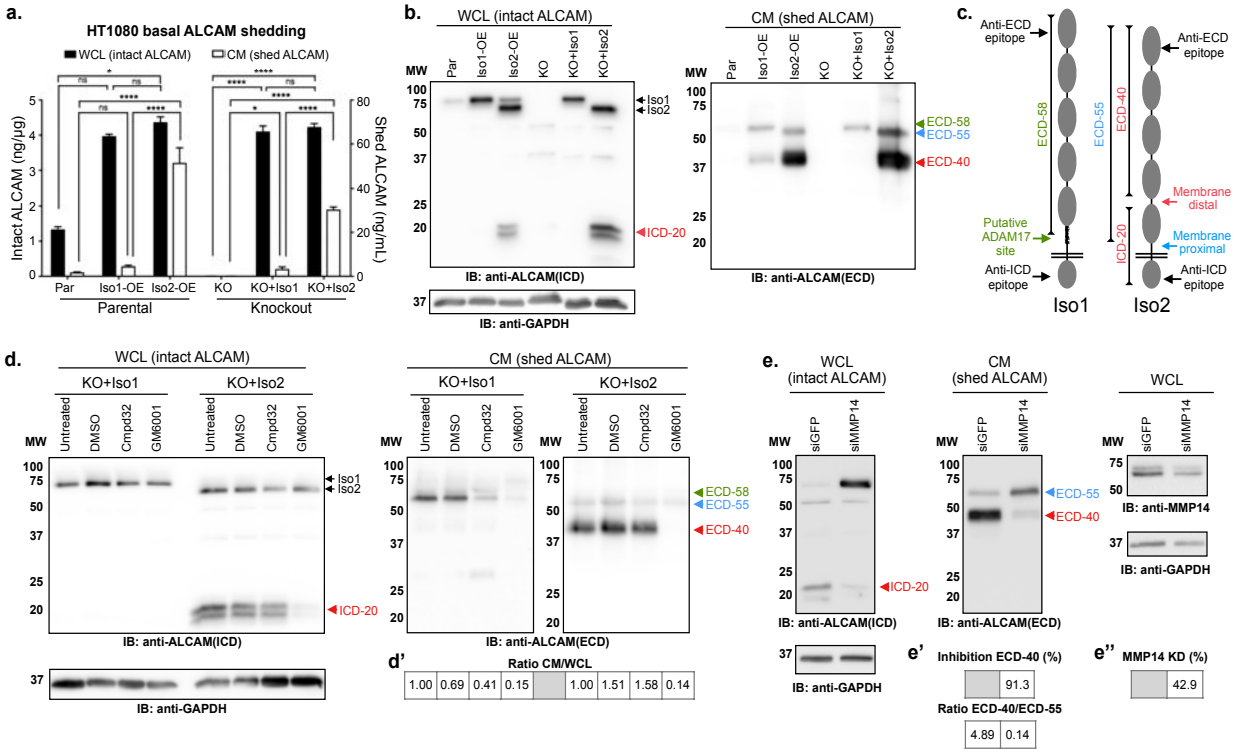

Figure 9. Alternative splicing of *ALCAM* introduces sensitivity to a metalloprotease other than ADAM17. (**a**) ALCAM ELISA for quantification of basal extracellular domain shedding in parental HT1080 cells (Par) overexpressing ALCAM-Iso1 (Iso1-OE) or ALCAM-Iso2 (Iso2-OE), as well as in ALCAM-KO HT1080 cells (KO) rescued with either ALCAM-Iso1 (KO+Iso1) or ALCAM-Iso2 (KO+Iso2). ALCAM expression was measured in whole cell lysate (WCL) and shedding was measured in conditioned medium (CM). P-values were calculated using Kruskal-Wallis test with Dunn's post-test; ns: not significant, *P<0.05, ****P<0.0001. (**b**) Immunoblot analysis of ALCAM expression and basal extracellular domain shedding in indicated cell lines. ICD: intracellular domain, ECD: extracellular domain. ALCAM fragments generated by shedding are marked as follows: 20 kDa intracellular domain fragment (ICD-20, ◀), 58 kDa extracellular domain fragment (ECD-58, ◀), 55 kDa extracellular domain fragment (ECD-55, ◀), and 40 kDa extracellular domain fragment (ECD-40, ◀). (**c**) Schematic of antibody epitopes and cleavage sites in ALCAM-Iso1 and ALCAM-Iso2. (**d**) Immunoblot analysis of extracellular domain shedding of indicated cell lines treated with an ADAM17-specific inhibitor, Compound 32 (Cmpd32, 10µM), or a global metalloprotease inhibitor, GM6001 (10µM). (**d'**) Changes in shedding were quantified as a ratio between intact ALCAM (WCL), and shed ALCAM (CM), with the untreated control normalized to 1. Samples were derived from the same experiment. Gels and blots were processed in parallel. (**e**) Immunoblot analysis of extracellular domain shedding of ALCAM-KO HT1080 cells expressing ALCAM-Iso2 (KO+Iso2) transfected with anti-MMP14 siRNA. Results are representative of two independent experiments. (**e'**) Changes in shedding were quantified as percent decrease in ECD-40 band density compared to control (siGRP), or ratio of ECD-40 density to ECD-55 density. Samples were derived from the same experiment. Gels and blots were processed in parallel. (**e''**) Knockdown (KD) of MMP14 was quantified as percent decrease in band density compared to control (siGRP). Samples were derived from the same experiment. Gels and blots were processed in parallel. (**b, d, e**) 5 min exposures are shown. Individual blots are outlined in black. WCL blots were redeveloped with HRP-tagged anti-GAPDH for loading control.

CM with antibodies directed to the ICD and ECD, as described above. Changes in shedding were quantified as a ratio between intact ALCAM, detected in the WCL, and shed ALCAM, detected in the CM, with the untreated control normalized to one (1). Treatment of KO+Iso1 with the ADAM17-specific inhibitor (Cmpd32) or a broad-spectrum metalloprotease inhibitor (GM6001) inhibited ALCAM-Iso1 ectodomain shedding (ECD-58) by 60% and 90%, respectively (Fig. 9d, d', right panel). This level of inhibition is consistent with previous publications(147,165). Conversely, the novel proteolytic cleavage of Iso2 that generated ECD-40 was inhibited by GM6001 but not by Cmpd32. (Fig. 9d, d', right panel). The loss of ICD-20 from the WCL upon treatment with GM6001, but not with Cmpd32 (Fig. 9d, left panel), suggests that ICD-20 and ECD-40 are indeed the products of the same novel cleavage event. The activity of other classes of proteases against ALCAM-Iso2 was analyzed with a panel of broad spectrum protease inhibitors targeting metallo-, serine, cysteine, aspartyl, and trypsin-like proteases (Table 2). ALCAM-Iso2 shedding was only inhibited by the broad-spectrum metalloprotease inhibitor GM6001 (Fig. 10).

Because the novel cleavage site was more distal to the typical juxtamembrane ADAM sites, we focused on matrix metalloproteases (MMP) as the most likely candidate metalloprotease family. MMP14, also known as membrane-type 1-MMP-1 (MT1-MMP), was the top candidate because ALCAM expression is associated with the upregulation of MMP14 expression and subsequent MMP2 activation (111). Specific siRNA-mediated knockdown of MMP14 in KO+Iso2 cells significantly decreased the generation of ECD-40 in the conditioned medium (91%), indicating that MMP14 is a novel participant in ALCAM-Iso2 ectodomain shedding (Fig. 9e, e', right panel). Taken together, these data confirm that ALCAM-Iso1 is shed by ADAM17 through membrane-proximal cleavage in the stalk region, while ALCAM-Iso2 is predominantly shed in a MMP14-dependent manner at a novel, membrane-distal proteolytic site.

Alternative splicing of *ALCAM* diminishes ALCAM-ALCAM adhesion

To further assess the functional consequences of this alternatively-spliced *ALCAM* isoform, we examined ALCAM-dependent adhesion *in vitro*. HT1080 ALCAM-knockout (KO) cells expressing ALCAM-Iso1 (KO+Iso1) or ALCAM-Iso2 (KO+Iso2)

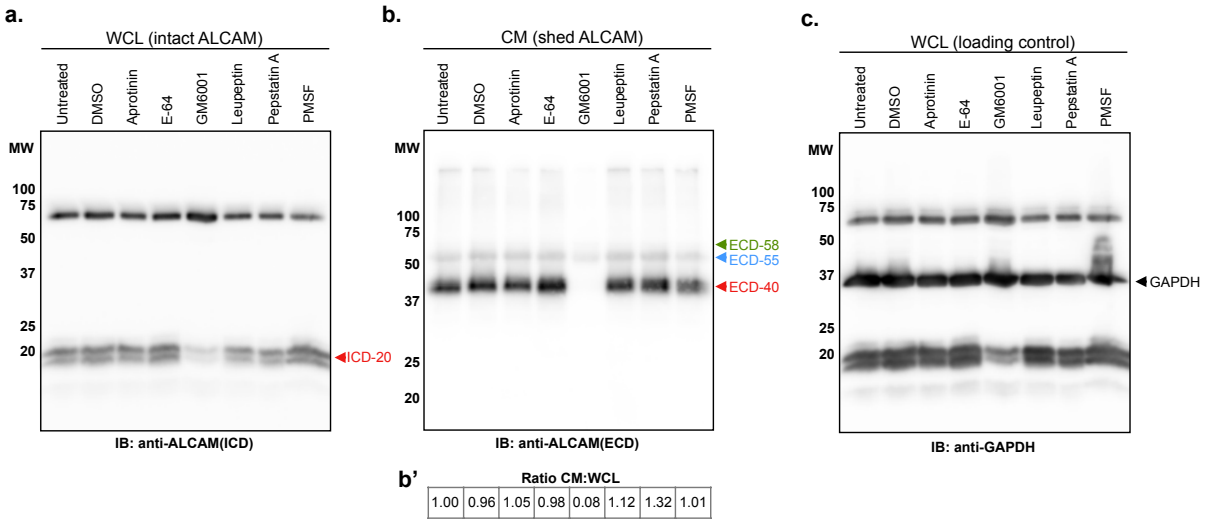

Figure 10. ALCAM-Iso2 shedding is dependent on metalloprotease activity. Immunoblot analysis of extracellular domain shedding of ALCAM-KO HT1080 cells expressing ALCAM-Iso2 (KO+Iso2) treated with various protease inhibitors (listed in Table 2). Results are representative of three independent experiments. (**a**) whole cell lysate (WCL), (**b**) conditioned medium (CM), (**b'**) Changes in shedding were quantified as a ratio between intact ALCAM (WCL), and shed ALCAM (CM), with the untreated control normalized to 1. Samples were derived from the same experiment. Gels and blots were processed in parallel, (**c**) WCL GAPDH loading control, (**a, b, c**) 5 min exposures are shown. Individual blots are outlined in black. WCL blots were redeveloped with HRP-tagged anti-GAPDH for loading control. ICD: intracellular domain, ECD: extracellular domain. ALCAM fragments generated by shedding are marked as follows: 20 kDa intracellular domain fragment (ICD-20, ◀), 58 kDa extracellular domain fragment (ECD-58, ◀), 55 kDa extracellular domain fragment (ECD-55, ◀), and 40 kDa extracellular domain fragment (ECD-40, ◀).

Inhibitor	Targets	Concentration
Aprotinin	Serine proteases	0.3 μM
Compound 32	ADAM17	10 μM
E64	Cysteine proteases	10 μM
GM6001	Metalloproteases	10 μM
Leupeptin	Trypsin-like proteases Serine proteases	100 μM
Pepstatin A	Aspartic proteases	1 μM
PMSF	Serine proteases Papain	1 mM

Table 2. Compounds used in protease inhibitor panel (Fig. 10).

were seeded onto ALCAM-Fc directionally adhered to protein G-coated surfaces (Fig. 11a). KO+Iso1 cells adhered to ALCAM-Fc two-fold more than KO+Iso2 cells (Fig. 11b), suggesting that the differences in cell-cell adhesion in Iso1-OE cells and Iso2-OE cells are caused by differences in homophilic ALCAM interactions.

Isoform-specific differences in cell-cell adhesion are controlled by ectodomain shedding

The enhanced colony cohesion *in vivo* (Fig. 8) and enhanced ALCAM-ALCAM adhesion of ALCAM-Iso1 *in vitro* (Fig. 11) suggests that the differential shedding between ALCAM-Iso1 and ALCAM-Iso2 (Fig. 9) controls the cell-cell adhesion function of ALCAM. To test this hypothesis, we evaluated *ALCAM* splicing and proteolysis-dependent changes in cell-cell adhesion using a cell aggregation assay (Fig. 12). Representative phase contrast images taken at 100x magnification are shown (Fig. 12a). Unbiased automated image analysis was used to quantify the cell cluster size. Similar to our *in vivo* colony size analysis, we analyzed cell cluster size distribution within each group (Fig. 12b) and used Chi-square analysis to define the significance of the changes across groups (Table 3).

Untreated parental HT1080 cells and ALCAM-KO cells maintained for 12 h in suspension persisted primarily as a mixture of single cells (34% and 37%, respectively) and small clusters (51% and 50%, respectively) with a few medium size clusters (14% and 12%, respectively) but no large or extra-large clusters (Fig. 12a, b). Expression of ALCAM-Iso1 greatly enhanced cohesion and caused untreated KO+Iso1 cells to form mostly large and extra-large clusters (78%) with few small clusters and single cells (21%) (Fig. 12a, b). Conversely, the expression of ALCAM-Iso2 caused a significantly smaller portion of the untreated KO+Iso2 cells to form large and extra-large clusters (18%), with the majority of cells persisting as small clusters and single cells (57%, Fig. 12a, b, $p<0.0001$, *Untreated*, Table 3).

Disruption of ALCAM-ALCAM interactions by incubation with soluble recombinant ALCAM-Fc diminished aggregation by significantly inhibiting the formation of medium, large and extra-large clusters in all cell lines (Fig. 12a, b, *A-Fc,* $P=0.0022$ - <0.0001, Table 3), except in ALCAM-KO cells, where aggregation was already at a minimum (Fig. 12a, b, *A-Fc*). Preventing ALCAM shedding with a metalloprotease inhibitor (MPi;

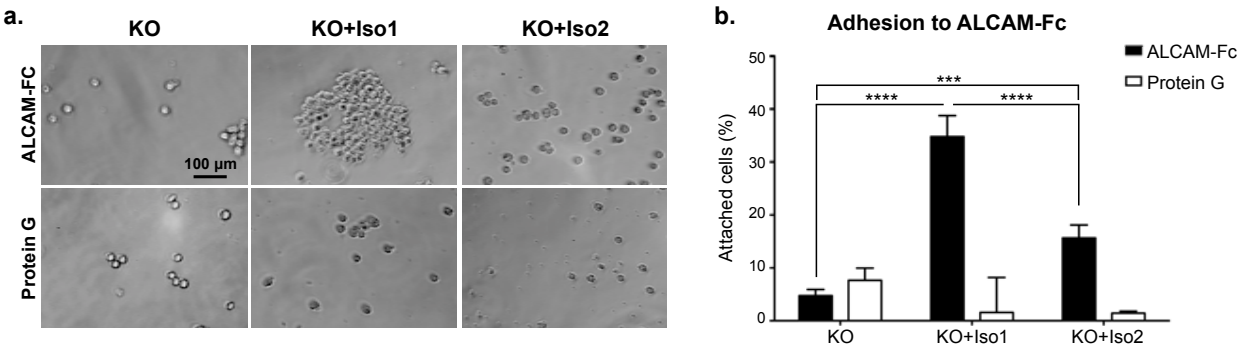

Figure 11. Alternative splicing of *ALCAM* diminishes ALCAM-ALCAM adhesion. (**a**) Representative images of ALCAM-KO HT1080 cells (KO) expressing ALCAM-Iso1 (KO+Iso1) or ALCAM-Iso2 (KO+Iso2) adhered to immobilized ALCAM-Fc. (**b**) Cells attached to ALCAM-Fc were stained with crystal violet dye. Percent of cells attached at 4 hours was quantified compared to cells attached to collagen type I coated wells. P-values were calculated using Kruskal-Wallis test with Dunn's post-test, ***P<0.001, ****P<0.0001.

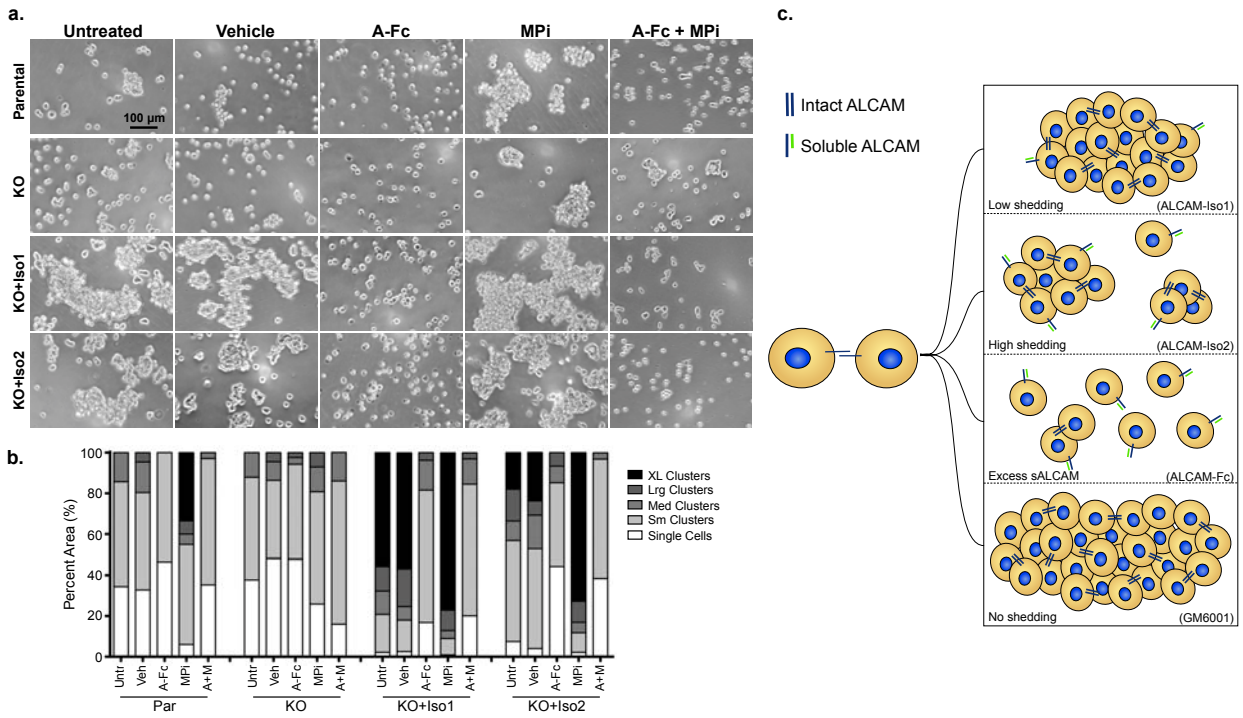

Figure 12. Isoform-specific differences in cell-cell adhesion are controlled by ectodomain shedding. (**a**) Representative images of *in vitro* cell aggregation analysis of parental HT1080 (Par) and ALCAM-KO HT1080 cells (KO) expressing ALCAM-Iso1 (KO+Iso1) or ALCAM-Iso2 (KO+Iso2). Veh: vehicle (0.4% DMSO), A-Fc: soluble ALCAM-Fc (10 µg/mL), MPi: metalloprotease inhibitor (GM6001, 10 µM). (**b**) Quantification of *in vitro* cell aggregation assay. Clusters were binned into single cell, small (Sm), medium (Med), large (Lrg) or extra-large (XL) clusters based on pixel area. Distribution of clusters across size bins was represented as percent of total area of all clusters. P-values were calculated using Chi-square test for trend and are listed in Table 3. Results are representative of three independent experiments. (**c**) Diagram representing aggregation phenotypes observed in indicated conditions. sALCAM: soluble ALCAM.

		Par					KO					KO+Iso1					KO+Iso2				
		Untr	Veh	A-Fc	MPi	A-Fc+MPi	Untr	Veh	A-Fc	MPi	A-Fc+MPi	Untr	Veh	A-Fc	MPi	A-Fc+MPi	Untr	Veh	A-Fc	MPi	A-Fc+MPi
Par	Untr		ns	**0.0022**	**<0.0001**	**ns**	ns					**<0.0001**					**<0.0001**				
	Veh			0.0001	<0.0001	0.0119		ns					<0.0001					<0.0001			
	A-Fc				**<0.0001**	**ns**			ns					<0.0001					0.0281		
	MPi					**<0.0001**				<0.0001					<0.0001					<0.0001	
	A-Fc+MPi										<0.0001					0.0003					ns
KO	Untr							ns	**ns**	**0.0141**	**0.0077**	**<0.0001**					**<0.0001**				
	Veh								ns	0.0058	0.0031		<0.0001					<0.0001			
	A-Fc									**0.0001**	**<0.0001**			<0.0001					ns		
	MPi										**ns**				<0.0001					<0.0001	
	A-Fc+MPi															ns					<0.0001
KO+Iso1	Untr												ns	**<0.0001**	**0.0004**	**<0.0001**	**<0.0001**				
	Veh													<0.0001	0.0037	<0.0001		<0.0001			
	A-Fc														**<0.0001**	**ns**			0.0096		
	MPi															**<0.0001**				ns	
	A-Fc+MPi																				0.0002
KO+Iso2	Untr																	ns	**<0.0001**	**<0.0001**	**<0.0001**
	Veh																		<0.0001	<0.0001	<0.0001
	A-Fc																			**<0.0001**	**ns**
	MPi																				**<0.0001**
	A-Fc+MPi																				

Table 3. P-values for Chi-square test for trend of data in Figure 12b. Comparisons discussed in text are bolded.

GM6001) promoted cell-cell adhesion leading to the formation of large and extra-large clusters in parental cells (from 0% to 35%), while ALCAM-KO cells had an increase in large clusters (from 0% to 7%), but no extra-large clusters with MPi treatment (Fig. 12a, b, *MPi,* P<0.0001 and P=0.0141, respectively, Table 3). Conversely, aggregation in KO+Iso1 cells was enhanced modestly (1.4-fold for extra-large clusters) when shedding was inhibited by GM6001 (Fig. 12a, b, P=0.0004, Table 3). Unlike KO+Iso1 cells, aggregation in KO+Iso2 cells was strongly increased by treatment with GM6001 (four-fold for extra-large clusters, Fig. 12a, b, p<0.0001,Table 3). All of these findings were recapitulated in parental HT1080 cells overexpressing ALCAM-Iso1 or -Iso2 (ISO1-OE and Iso2-OE, respectively, Fig. 13, Table 4). Finally, upon co-treatment with ALCAM-Fc, the clustering in response to MPi treatment was significantly diminished, resulting in dispersed single cells and small clusters for all cell lines, except ALCAM-KO cells which are incapable of ALCAM-ALCAM mediated clustering (Fig. 12a, b, *A-Fc+MPi,* P<0.0001). Together, these data support our hypothesis that alternative splicing of *ALCAM* increases the sensitivity of ALCAM-Iso2 to proteolysis, leading to increased shedding and isoform-specific differences in cell-cell cohesion (Fig. 12c).

Shed ALCAM-Iso2 can disrupt ALCAM-Iso1-mediated cell-cell adhesion in paracrine-like manner

In order to determine if elevated ectodomain shedding from ALCAM-Iso2 could antagonize ALCAM-mediated cell-cell adhesion, we analyzed cell aggregation, as described above, in the presence of fresh complete medium (Untreated), conditioned medium from ALCAM-KO cells (KO CM), or conditioned medium from KO+Iso2 cells (Iso2 CM). EGTA was added to inhibit non-specific effects from calcium-dependent adhesion molecules. In the presence of EGTA, KO+Iso1 cells formed significantly larger clusters than KO+Iso2 cells (P=0.0031, Table 5), confirming that this phenotype is ALCAM specific and Ca^{2+} independent (Fig. 14, *Untreated*). Treatment of KO+Iso1 or KO+Iso2 cells with KO CM did not substantially alter their ability to aggregate nor did the treatment with Iso2 CM affect aggregation of parental or ALCAM-KO cells (Fig. 14, *KO CM and Iso2 CM*). Conversely, the treatment of KO+Iso1 and KO+Iso2 cells with Iso2 CM greatly reduced the formation of extra-large and large clusters, respectively

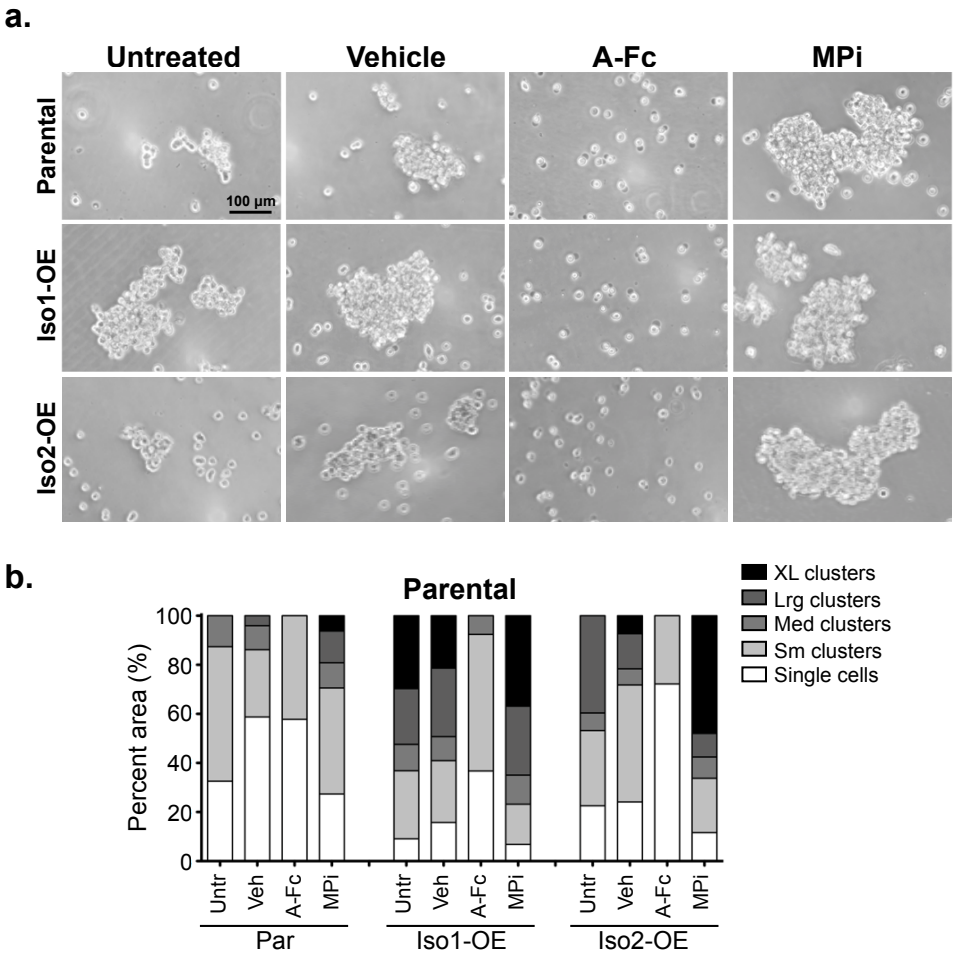

Figure 13. ALCAM-Iso1 promotes cell-cell adhesion through intercellular homotypic ALCAM interactions. (**a**) Representative images of *in vitro* cell aggregation analysis of parental HT1080 cells overexpressing ALCAM-Iso1 (Iso1-OE) or ALCAM-Iso2 (Iso2-OE). Veh: vehicle (DMSO), 0.4%; A-Fc: ALCAM-Fc, 10 µg/mL; MPi: metalloprotease inhibitor (GM6001), 10 µM. (**b**) Quantification of *in vitro* cell aggregation assay. Clusters were binned into single cell, small, medium, large, or extra-large clusters based on pixel area. Distribution of clusters across size bins was represented as percent of total area of all clusters. P-values were calculated using Chi-squared test for trend and are listed in Table 4. Results are representative of three independent experiments.

		Par				Iso1-OE				Iso2-OE			
		Untr	Veh	ALCAM-Fc	GM6001	Untr	Veh	ALCAM-Fc	GM6001	Untr	Veh	ALCAM-Fc	GM6001
Par	Untr		ns	**0.0041**	**0.0002**	**<0.0001**				**<0.0001**			
	Veh			<0.0001	0.0089		<0.0001				0.0362		
	ALCAM-Fc				**<0.0001**			ns				<0.0001	
	GM6001								<0.0001				<0.0001
Iso1-OE	Untr						ns	**<0.0001**	**0.0492**	**0.002**			
	Veh							<0.0001	0.0026		<0.0001		
	ALCAM-Fc								**<0.0001**			**<0.0001**	
	GM6001												**ns**
Iso2-OE	Untr										ns	**<0.0001**	**<0.0001**
	Veh											<0.0001	<0.0001
	ALCAM-Fc												**<0.0001**
	GM6001												

Table 4. P-values for Chi-square test for trend of data in Figure 13. Comparisons discussed in text are bolded.

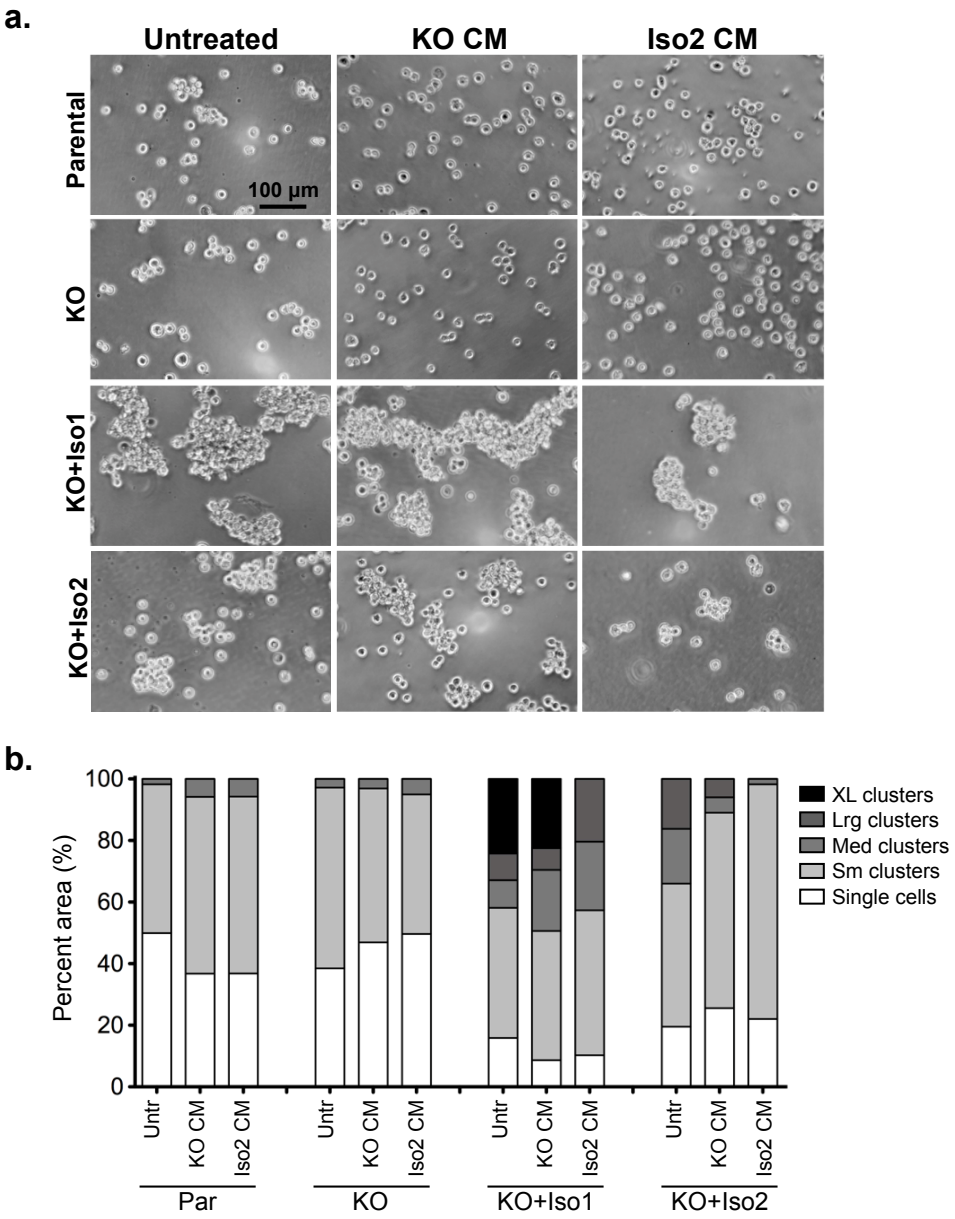

Figure 14. The shedding of alternatively spliced *ALCAM* (ALCAM-Iso2) can disrupt cell-cell adhesion mediated by full-length ALCAM (ALCAM-Iso1) in paracrine-like manner. (**a**) Representative images of *in vitro* cell aggregation analysis of parental HT1080 (Par) and ALCAM-KO HT1080 cells (KO) expressing ALCAM-Iso1 (KO+Iso1) or ALCAM-Iso2 (KO+Iso2) treated with 24 hr conditioned medium (CM) collected from either HT1080 ALCAM-KO cells (KO CM) or HT1080 KO+Iso2 cells (Iso2 CM). (**b**) Quantification of *in vitro* cell aggregation assay. Clusters were binned into single cell, small (Sm), medium (Med), large (Lrg) or extra-large (XL) clusters based on pixel area. Distribution of clusters across size bins was represented as percent of total area of all clusters. P-values were calculated using Chi-square test for trend and are listed in Table 5. Results are representative of three independent experiments.

		Par			KO			KO+Iso1			KO+Iso2		
		Untr	KO CM	Iso2 CM	Untr	KO CM	Iso2 CM	Untr	KO CM	Iso2 CM	Untr	KO CM	Iso2 CM
Par	Untr		0.0298	0.0309	**ns**			**<0.0001**			**<0.0001**		
	KO CM			**ns**		ns			<0.0001			0.0179	
	Iso2 CM						ns			<0.0001			ns
KO	Untr					ns	ns	**<0.0001**			**<0.0001**		
	KO CM						**ns**		<0.0001			0.0002	
	Iso2 CM									<0.0001			0.0013
KO+Iso1	Untr								ns	0.0079	**0.0031**		
	KO CM									**0.0144**		<0.0001	
	Iso2 CM												<0.0001
KO+Iso2	Untr											ns	<0.0001
	KO CM												**0.0015**
	Iso2 CM												

Table 5. P-values for Chi-square test for trend of data in Figure 14b. Comparisons discussed in text are bolded.

(Fig. 14, *KO CM vs. Iso2 CM*, P<0.0001 and P=0.0015, Table 5). In fact, KO+Iso1 cells treated with Iso2 CM formed clusters nearly identical in size to untreated KO+Iso2 cells (P=0.1013, Table 5). Taken together, these data indicate that alternative splicing of *ALCAM* not only diminishes intrinsic adhesion, but that shed ALCAM-Iso2 (ECD-55 and ECD-40) can also disrupt cell-cell adhesion by antagonizing homophilic ALCAM interactions in a paracrine-like manner.

Isoform-specific differences in cell-cell adhesion are controlled by ectodomain shedding in a bladder cancer cell line

Previously, we have shown that shed ALCAM is detected in the serum and urine of bladder cancer patients at a median level of 74.880 and 2.177 ng/mL, respectively (114). Our current data suggest that shed ALCAM-Iso2 can antagonize homophilic ALCAM interactions at a concentration of 30 ng/mL (Fig. 9a, Fig. 14). Because shed ALCAM-Iso2 can disrupt cell-cell adhesion at a physiologically relevant concentration and high ALCAM shedding is prognostic of poor patient outcome in bladder cancer (114), we explored the phenotype of ALCAM-Iso1 and ALCAM-Iso2 in the bladder cancer cell line, UMUC-3. Similar to HT1080 cells, UMUC-3 ALCAM-KO cells (KO) transfected with ALCAM-Iso2 (KO+Iso2) shed ALCAM 2.3-fold more than cells transfected with ALCAM-Iso1 (KO+Iso1, Fig. 15a). Additionally, by immunoblot, ALCAM-Iso2 is shed equally at two distinct sites in the ECD, while ALCAM-Iso1 is shed primarily at the site corresponding to ADAM17 proteolysis (Fig. 15b). These data suggest that the differential processing of ALCAM-Iso1 and ALCAM-Iso2 is evident in multiple cancer cell types.

We then used parental UMUC-3 transiently transfected with control vector (U_Par) and ALCAM-KO UMUC-3 cells transiently transfected with control vector (U_KO), ALCAM-Iso1 (U_KO+Iso1), or ALCAM-Iso2 (U_KO+Iso2) to verify that alternative splicing of *ALCAM* confers differential susceptibility to proteolysis and controls cell-cell adhesion. U_Par cells formed cell clusters of varying sizes with 17% extra-large clusters, 34% large clusters, 21% medium clusters, 23% small clusters, and 5% single cells, while U_KO cells formed significantly smaller clusters with single cells and small clusters accounting for 69% of the cells and medium and large clusters

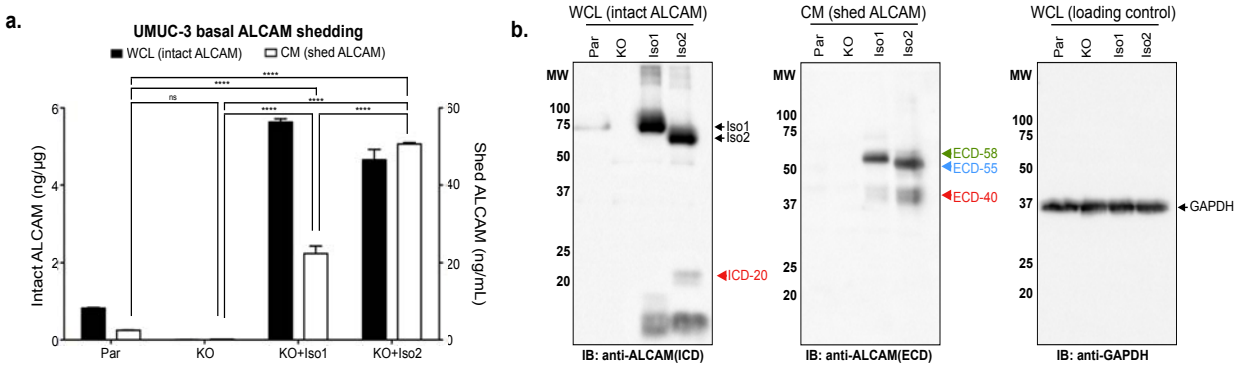

Figure 15. Alternative splicing of ALCAM leads to enhanced proteolytic susceptibility in the bladder cancer cell line UMUC-3. (**a**) ALCAM ELISA for quantification of basal extracellular domain shedding in parental UMUC-3 cells (U_Par) and UMUC-3 ALCAM knockout cells (U_KO) transiently expressing ALCAM-Iso1 (U_KO+Iso1) or ALCAM-Iso2 (U_KO+Iso2). WCL: whole cell lysate, CM: conditioned medium. P-values were calculated using Kruskal-Wallis test with Dunn's post-test, ns=not significant, ****P<0.0001. (**b**) Immunoblot analysis of basal extracellular domain shedding of ALCAM-Iso1 and ALCAM-Iso2 in parental UMUC-3 cells (U_Par) and UMUC-3 ALCAM knockout cells (U_KO) transiently expressing ALCAM-Iso1 (U_KO+Iso1) or ALCAM-Iso2 (U_KO+Iso2). ICD: intracellular domain, ECD: extracellular domain. ALCAM fragments generated by shedding are marked as follows: 20 kDa intracellular domain fragment (ICD-20, ◀), 58 kDa extracellular domain fragment (ECD-58, ◀), 55 kDa extracellular domain fragment (ECD-55, ◀), and 40 kDa extracellular domain fragment (ECD-40, ◀). 5 min exposures are shown. Individual blots are outlined in black. WCL blots were redeveloped with HRP-tagged anti-GAPDH for loading control. Full-length blots are shown.

accounting for 31% of cells (Fig. 16a, b, *Untreated*, p<0.0001, Table 6). Rescue with ALCAM-Iso1 (U_KO+Iso1) promoted cell clusters larger than that of parental cells with extra-large clusters accounting for 41% of cells and large clusters accounting for 25% of cells (Fig. 16a, b, P=0.0113, Table 6). Meanwhile, cells with ALCAM-Iso2 rescue (U_KO+Iso2) formed clusters significantly smaller than both U_Par and U_KO+Iso1 cells (P=0.0094, P<0.0001, respectively, Table 6) with 41% small clusters and single cells and only 35% large and extra-large clusters (Fig. 16a, b, *Untreated)*.

Consistent with our previous findings (Fig. 12), soluble ALCAM-Fc disrupted ALCAM-ALCAM interactions in all groups except KO cells, leading to significantly smaller cell clusters (Fig. 16a, b, *A-Fc*; p<0.0001, Table 6). In U_Par cells, small clusters and single cells accounted for 83% of the cell distribution after ALCAM-Fc treatment, while ALCAM-Fc treatment in U_KO+Iso1 and U_KO+Iso2 resulted in 70% and 69% small clusters and single cells, respectively (Fig. 16a, b). Finally, treatment with GM6001 significantly increased the size of cell clusters in U_KO+Iso2 cells, increasing large and extra-large clusters to 54% (Fig. 16a, b, *MPi*; P=0.0003, Table 6). Again, these data suggest that the effects of alternative splicing of ALCAM on cell-cell cohesion persist across multiple cancer cell types.

Changes in *ALCAM* isoform expression correlate with disease progression in bladder cancer

Together, these data indicate that differences in *ALCAM* isoform expression can be important for bladder cancer progression. To investigate this further, we evaluated *ALCAM* expression in both normal bladder and bladder cancer tissue. Using the publicly available Genotype-Tissue Expression (GTEx Portal, (172)) dataset, we quantified ALCAM-Iso1 and ALCAM-Iso2 expression in normal bladder and showed that ALCAM-Iso1 and ALCAM-Iso2 are expressed in relatively equal levels (Fig. 16c, left panel). Additionally, using The Cancer Genome Atlas (TCGA) urothelial bladder carcinoma cohort (173), we quantified *ALCAM* isoform expression in human bladder tumors and showed that ALCAM-Iso2 is expressed two-fold higher than ALCAM-Iso1 (P<0.0001, Fig. 16c, right panel). These data indicate that there is a switch to ALCAM-Iso2 dominated expression in bladder cancer, compared to normal tissue. This was validated

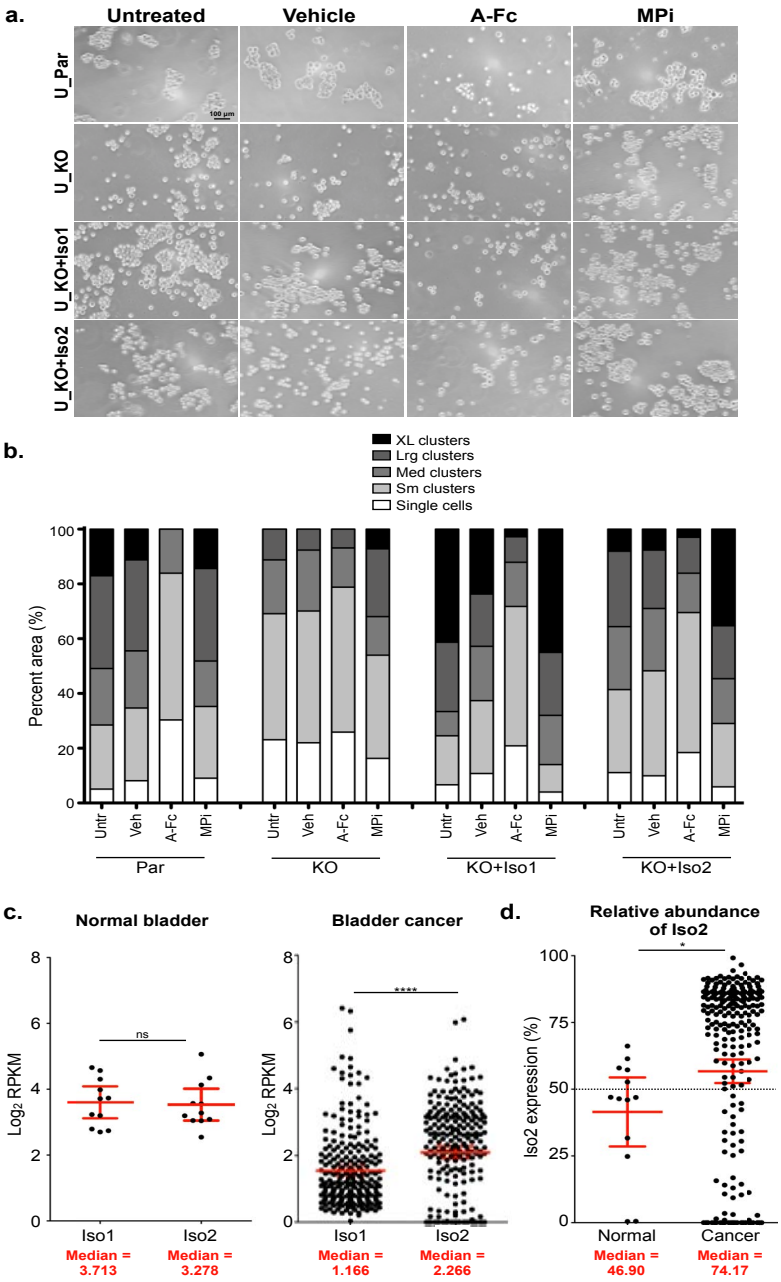

Figure 16. ALCAM-Iso2 expression correlates with disease progression. (**a**) Representative images of *in vitro* cell aggregation analysis of parental UMUC-3 cells (U_Par) and UMUC-3 ALCAM knockout cells (U_KO) transiently expressing ALCAM-Iso1 (U_KO+Iso1) or ALCAM-Iso2 (U_KO+Iso2). Veh, vehicle (0.4% DMSO), A-Fc, soluble ALCAM-Fc (10 µg/mL), MPi, metalloprotease inhibitor (GM6001, 10 µM). (**b**) Quantification of *in vitro* cell aggregation assay. Clusters were binned into single cell, small (Sm), medium (Med), large (Lrg) or extra-large (XL) clusters based on pixel area. Distribution of clusters across size bins was represented as percent of total area of all clusters. P-values were calculated using Chi-square test for trend and are listed in Table 6. Results are representative of three independent experiments. (**c**) Expression of ALCAM-Iso1 and ALCAM-Iso2 in normal bladder and bladder cancer. Data for normal bladder tissue were extracted from the GTEx Portal. Data for bladder cancer tissue were extracted from the TCGA bladder cancer cohort. p-values were calculated using paired t-test, ****p<0.0001. Graphs display mean with 95% confidence interval. Medians are reported. (**d**) Relative abundance of ALCAM-Iso2 in normal and bladder cancer tissue. P-value calculated with Mann-Whitney U test. Graphs display mean with 95% confidence interval. Medians are reported.

		Par				KO				KO+Iso1				KO+Iso2			
		Untr	Veh	ALCAM-Fc	GM6001	Untr	Veh	ALCAM-Fc	GM6001	Untr	Veh	ALCAM-Fc	GM6001	Untr	Veh	ALCAM-Fc	GM6001
Par	Untr		ns	**<0.0001**	**ns**	**<0.0001**				**0.0113**				**0.0094**			
	Veh			<0.0001	ns		<0.0001				ns				0.0339		
	ALCAM-Fc				**<0.0001**			ns				0.0035				0.0005	
	GM6001								0.0058				<0.0001				0.0307
KO	Untr						ns	**ns**	**0.0014**	**<0.0001**				**<0.0001**			
	Veh							ns	0.0004		<0.0001				<0.0001		
	ALCAM-Fc								**0.0002**			ns				0.0342	
	GM6001												<0.0001				<0.0001
KO+Iso1	Untr										ns	**<0.0001**	**ns**	**<0.0001**			
	Veh											<0.0001	<0.0001		0.0209		
	ALCAM-Fc												**<0.0001**			**ns**	
	GM6001																**0.0350**
KO+Iso2	Untr														ns	**<0.0001**	**0.0003**
	Veh															0.0012	<0.0001
	ALCAM-Fc																**<0.0001**
	GM6001																

Table 6. P-values for Chi-square test for trend of data in Figure 16b. Comparisons discussed in text are bolded.

by directly comparing the relative abundance of ALCAM-Iso2 between the GTEx (normal bladder) and TCGA (bladder cancer) cohorts (P=0.0224, Fig. 16d). This clinical data supports our mechanistic data and suggests that ALCAM-Iso1 expression promotes high cell-cell cohesion, while a switch to ALCAM-Iso2 dominated expression promotes lower cell-cell adhesion, a permissive environment for single cell dispersion and, as a result, enhanced migration and metastasis. Thus, we suggest that differential splice isoform expression provides an explanation for increased ALCAM shedding in patients with cancer and provides a mechanism by which ALCAM detected in biofluids is prognostic of poor outcome.

Discussion

The overarching goal of this study was to determine how ALCAM shedding regulates tumor cell biology. In this manuscript we describe how alternative splicing of *ALCAM* controls the functional contribution of ALCAM to tumor biology.

Dynamic alteration of cell adhesion is an integral step to cancer progression (21,179). While many adhesion molecules can control cancer progression, the mechanisms underlying dynamic control of these molecules remain unclear. Unlike many of the classic oncogenes and tumor suppressors, the cell adhesion molecules that control malignant progression are rarely genetically mutated, amplified or deleted. Rather than genomic alterations, the contributions of these adhesion factors appear to be controlled primarily at the transcriptional and post-transcriptional level. The function of many Ig-CAMs, including ALCAM, is regulated through proteolytic shedding of the ectodomain from the cell surface (104). ALCAM's participation in malignant progression has been recognized in numerous studies (22,111,112,134,160-163), and we recently linked elevated ALCAM shedding directly to poor patient outcome (113,114). However, the mechanism controlling proteolytic shedding of ALCAM was unknown.

In this study, we demonstrate that alternative splicing is responsible for controlling the susceptibility of ALCAM to proteolytic shedding. Loss of exon 13 in ALCAM-Iso2 allows for MMP14-dependent proteolytic cleavage at a membrane-distal site which leads to a 10-fold increase in ALCAM-Iso2 shedding compared to the

canonical isoform, ALCAM-Iso1 (Fig. 9). Since many proteases are promiscuous and target several substrates (180,181), changing proteolytic susceptibility through alternative splicing allows for specific and dynamic control of ALCAM proteolysis. Therefore, differential expression of ALCAM-Iso1 and ALCAM-Iso2, as opposed to altering protease activity, allows for intrinsic control of ALCAM shedding and adhesion function without affecting other targets of ADAM17 or other metalloproteases.

We originally hypothesized that exon 13 might contain the ADAM17 cleavage site and the splicing would therefore remove proteolytic susceptibility to ADAM17 in a manner similar to what has been reported for Cell Adhesion Molecule 1 (CADM1) and the epithelial growth factor receptor family member (ErbB4) (182,183). However, we discovered that the loss of exon 13 by splicing is unique in the fact that it makes ALCAM more susceptible to proteolytic cleavage in a separate, membrane-distal site, outside of exon 13. Moreover, this proteolytic event is MMP14-dependent and distinct from ADAM17 activity. Thus, the ALCAM ectodomain appears to contain a second proteolytic site that is exposed or unmasked upon alternative splicing of exon 13. To our knowledge, this is the first observation of a masked proteolytic site revealed distal to an alternatively spliced exon.

The specific regulation of ALCAM function through differential expression of *ALCAM* isoforms has implications in various biological processes. ALCAM has known roles in non-pathologic processes requiring static and stable cell adhesion such as T-cell activation and maintenance of the blood-brain barrier (108,124,158), as well as roles in dynamic processes such as transendothelial migration and neuronal guidance (109,159). To this point, the vast majority of ALCAM function has been investigated using the canonical isoform, ALCAM-Iso1. We hypothesize that dynamic regulation of cell adhesion through differential expression of *ALCAM* isoforms would be vital to all ALCAM-mediated functions, both pathological and non-pathological. Our results clearly indicate that the role of ALCAM in many physiological processes may be more complicated and more dynamic than first indicated.

While broadly applicable in the field of cell adhesion, our findings highlight the importance of regulating ALCAM shedding in cancer progression. In our direct comparison of ALCAM-Iso1 and -Iso2, we show that expression of ALCAM-Iso2

increases ectodomain shedding up to ten-fold (Fig. 9a, 15a) which diminishes cell-cell adhesion (Fig. 12, 13, 14, 16) while promoting metastasis and tumor cell dissemination (Fig. 5f & 8d-g). We also show a switch from nearly equal isoform expression in normal bladder tissue to ALCAM-Iso2-dominated expression in bladder cancer (Fig. 16c, d). While the regulation of alternative splicing has not been studied for *ALCAM* specifically, aberrations in alternative splicing in cancer can be attributed to several factors such as genetic abnormalities in spliceosome machinery or, more commonly, to dysregulation of expression and localization of *trans*-acting splicing factors (184). Therapeutic targeting of alternative splicing in cancer is an active field of research; therefore, identifying the regulatory mechanisms guiding alternative splicing in *ALCAM* could potentially lead to novel cancer therapies. Additionally, given our previous work that indicates that high ALCAM shedding is predictive of poor patient outcome (113,114), we hypothesize that elevated ALCAM-Iso2 expression may be the cause of increased ALCAM shedding in patients with aggressive disease. This combination of experimental and clinical observations warrants future investigations into the value of ALCAM-Iso2 tissue expression as a predictive and prognostic biomarker.

Although this is the first study that attributes differential proteolysis of ALCAM to alternative splicing, smaller soluble forms of ALCAM generated by proteolysis of the ECD have been observed in other studies. Fabbi and colleagues observed the generation of two soluble ALCAM fragments (95 kDa and 65 kDa (glycosylated)) and attributed the generation of both fragments to ADAM17 activity in neuroblastoma cell lines (185). Bongarzone and colleagues also observed the generation of soluble ALCAM fragments at 96 kDa and 60 kDa (glycosylated) or 55 kDa and 35 kDa (deglycosylated) in thyroid cancer cell lines (147). These soluble forms align well with the soluble forms we observed from the proteolysis of ALCAM-Iso2 and may indicate that the cell lines used in these reports may express ALCAM-Iso2. The findings we report here enable further interpretation of the existing literature on ALCAM and its function.

Our work also provides an opportunity to direct further research into the biology of ALCAM and the cell-adhesion it controls. Understanding how the alternative splicing is regulated and identifying the mechanism by which MMP14 selectively cleaves

ALCAM-Iso2 will provide further insight into the intrinsic regulatory mechanisms that control the physiology and pathology of multi-cellular adhesions. Further structure-function studies of this masked proteolytic site can reveal dynamic regulatory systems intrinsic to normal physiology that are co-opted by cancer to provide this disease a dynamic and tunable mechanism to control migration, dissemination, and metastasis. In cancer, detecting ALCAM shedding, as well as the switch from ALCAM-Iso1 to ALCAM-Iso2, may function as an indicator of disease progression. Additionally, it may be possible to target this regulatory process with a therapeutic intervention that can benefit cancer patients as well as other individuals with cell adhesion-related pathologies.

In conclusion, we have shown that alternative splicing of *ALCAM* can specifically and dynamically regulate ALCAM-mediated cell-cell adhesion by introducing a proteolytic susceptibility adjacent to the spliced exon (Fig. 17). The increased shedding of ALCAM-Iso2 leads to reduced cell-cell adhesion and increased metastasis in experimental models, while differential expression of *ALCAM* isoforms is evident in the tumor tissue from bladder cancer patients. Given our previous work that indicates that high ALCAM shedding is predictive of poor patient outcome (113,114), we hypothesize that elevated ALCAM-Iso2 expression may be the cause of increased ALCAM shedding in patients with aggressive disease. This is the first evaluation of biochemical and functional differences between ALCAM-Iso1 and ALCAM-Iso2, and our results warrant further investigation into the role of alternative splicing of *ALCAM* in both normal and pathological processes.

Acknowledgements

We want to thank Dr. Barbara Fingleton (Vanderbilt University) and Henar Suarez (Centro de Biologia Molecular Severo Ochoa) for insightful discussion of MMP biology. AZ was supported by R01CA143081. KEH was supported by the Microenvironmental Influences in Cancer Training Program (NIH/NCI T32CA009592) and F31CA189764. SAE was supported by the Department of Veterans Affairs IK2BX002498. Flow Cytometry experiments were performed in the VMC Flow Cytometry Shared Resource. The Translational Pathology Shared Resource and the

VUMC Flow Cytometry Shared Resource is supported by the Vanderbilt Ingram Cancer Center (P30 CA68485) as well as the Vanderbilt Digestive Disease Research Center (DK058404). The Genotype-Tissue Expression (GTEx) Project was supported by the Common Fund of the Office of the Director of the National Institutes of Health, and by NCI, NHGRI, NHLBI, NIDA, NIMH, and NINDS. The data used for the analyses described in this manuscript were obtained from: the GTEx Portal on 08/01/2017. The results shown here are in part based upon data generated by the TCGA Research Network: http://cancergenome.nih.gov/.

Author Contributions

Study was conceived and designed by KEH and AZ. Experiments were performed by KEH with help from EYL on avian embryo metastasis assays, AKvL on knockdown of MMP14, CT on immunoblots, AE on evaluation of primary tumor invasion, JH on generation of ALCAM-KO cell lines, and DKF on FACS and flow cytometry. TPS extracted, aligned, and normalized RNAseq data from the GTEx portal and TCGA. Data analysis was performed by KEH with help from SAE and AZ. Manuscript was written by KEH, SAE, and AZ and edited by EYL.

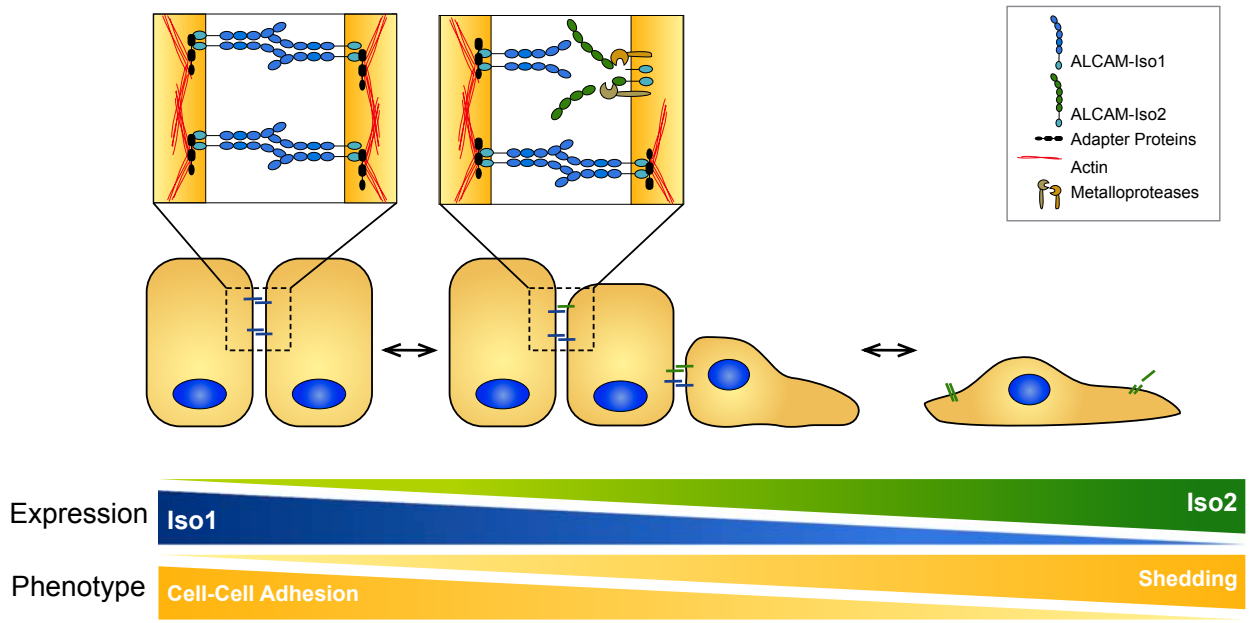

Figure 17. Expression of alternative *ALCAM* splice isoforms modulates cell-cell adhesion through differential susceptibility to proteolysis. Our data demonstrate that alternative splicing of *ALCAM* can alter cell-cell adhesion through differential susceptibility to proteolysis of the extracellular domain. Cells expressing ALCAM-Iso2 are more likely to undergo single cell dispersion and, therefore, metastasize more frequently from the primary tumor.

CHAPTER III:

INTEGRIN-FREE CD151 CONTROLS TUMOR CELL ADHESION, MIGRATION, AND METASTASIS VIA A TRIMERIC COMPLEX WITH ALCAM AND SYNTENIN-1

Contributing Authors: Katie E. Hebron, Trenis D. Palmer, Ariana K. Von Lersner, Elizabeth Y. Li, Antonio Mazzocca, Amanda G. Hansen, Hiroaki Ishida, Matthew E. Hyndman, Hans J. Vogel, and Andries Zijlstra

Summary

Members of tetraspanin superfamily (TSPAN) are important membrane scaffolding proteins responsible for controlling the availability, organization and activity of non-TSPAN membrane partners. The TSPAN CD151 is a key regulator of cellular adhesion and motility. Much of the TSPAN's ability to regulate migration was initially linked to its association with laminin-binding integrins. However, integrin-free CD151 ($CD151^{free}$) was revealed to be a potent regulator of adhesion whose clustering on the cell surface led to increased cellular cohesion and reduced tumor cell migration and metastasis. Utilizing an antibody specific for $CD151^{free}$, we investigated partners that associate with this specific CD151 population in order to elucidate the mechanism by which $CD151^{free}$ controls adhesion, motility and metastasis. Proteomic analysis of $CD151^{free}$-associated proteins identified Activated Leukocyte Cell Adhesion Molecule (ALCAM) as a novel CD151 partner that is required for $CD151^{free}$ to control adhesion. NMR of interacting peptides and subsequent co-immunoprecipitation revealed that $CD151^{free}$ interacts with ALCAM through the scaffolding protein syntenin-1. Furthermore, we show that the intracellular domain of ALCAM (ALCAM-ICD) is susceptible to ɣ-secretase cleavage which releases a PDZ-binding peptide capable of disrupting the CD151/syntenin-1/ALCAM trimeric complex. Disruption of this complex by expression of free ALCAM-ICD or genetic ablation of ALCAM impedes $CD151^{free}$-mediated regulation of tumor cell adhesion and metastasis. Together, these

observations demonstrate that CD151^{free} controls tumor cell migration through a trimeric complex of CD151/syntenin-1/ALCAM.

Introduction

While clinical progression to metastasis is a lethal aspect of cancer, the process of tumor cell dissemination is highly inefficient. The speed at which this sequential, multistep process progresses is dependent on the contribution of many individual molecular processes (9). Because tumor cells must actively modulate adhesive interactions as they disseminate from their point of origin, the dynamic regulation of cell adhesion becomes a major contributor to metastatic success (21). TSPANs, such as CD9 and CD151, are membrane scaffolding proteins that have been shown to be important regulators of adhesion and cancer progression (186-189). They organize macromolecular complexes known as TSPAN-Enriched Microdomains (TERM) by facilitating interactions between themselves and their non-TSPAN partners, such as integrins, immunoglobulin-like cell adhesion molecules, proteases, and signaling receptors (reviewed in (190,191)). The interactions between TSPAN and their binding partners have been shown to modulate adhesive processes that are critical to tumor cell dissemination such as matrix remodeling, migration, and extravasation (reviewed in (191,192)).

The TSPAN CD151 is a potent regulator of cell adhesion, migration, and metastasis. In mice and humans, the genetic loss of CD151 disrupts epithelial integrity leading to physiological malfunction in kidney, lung, and the endothelium (193-195). In this context, CD151 is a central component of the laminin-binding integrin complex α3β1 and is required for maintaining adhesion to the basement membrane (196,197). Conversely, genetic ablation of this TSPAN in cancer models diminishes metastasis, suggesting that CD151 contributes to dissemination(198-200). Several CD151-specific antibodies have demonstrated the ability to inhibit cell migration (178). We have demonstrated that these migration-inhibiting antibodies engage integrin-free CD151 (CD151^{free}) through its integrin-binding domain and clusters the TSPAN in a manner that emulates its aggregation at areas of cell-cell contact. This clustering promotes adhesion and subsequently prevents metastatic dissemination by inhibiting migration

(178,189). These observations demonstrate that CD151 can control migration through a α3β1-independent mechanism, which is particularly relevant in tumors that exhibit reduced α3β1 after oncogenesis (189).

To determine the mechanism by which CD151^{free} could achieve α3β1-independent regulation of motility, we set out to identify CD151^{free}-associated proteins and dissect the underlying mechanism. We identified Activated Leukocyte Cell Adhesion Molecule (ALCAM), a member of the immunoglobulin-like superfamily of cell adhesion molecules, as a CD151^{free}-associated protein and performed structure-function analyses to determine how this complex could control adhesion and metastasis. We discovered that this interaction, enabled by the scaffolding protein syntenin-1, is required for CD151^{free}-mediated control of cell adhesion, motility, and metastasis. This work reveals a novel integrin-independent mechanism by which CD151 regulates adhesion and migration and suggests that CD151 may modulate adhesion and motility by switching binding partners.

Methods

Cell culture, plasmids, transfections, inhibitors, and antibodies

HT1080 (fibrosarcoma) cells were obtained from the ATCC (CCL-121) and maintained in RPMI supplemented with penicillin/streptomycin, sodium pyruvate, nonessential amino acids, and 10% fetal bovine serum and cultured at 37°C with 5% CO_2. Knockout cell lines were generated using a CRISPR/Cas9 gRNA targeting the signal peptide of ALCAM (AGACGGTGGCGGAGATCAAG, Horizon Discovery). The level of protein expression was verified by flow cytometry for cell surface ALCAM and by immunoblot for total ALCAM expression in whole cell lysates. HT1080 cells expressing the intracellular domain of ALCAM (ALCAM-ICD) were stably transduced with lentiviral particles containing vectors for the ALCAM-ICD fragment as well as a labeling vector containing firefly luciferase with mTagRFP2 fluorescent protein. Viral plasmids were constructed using MultiSite Gateway (ThermoFisher Scientific) on the pLenti6.2/V5-DEST backbone. Viral particles were produced in LentiX 293T cells (Clontech). Transductions were performed with 5 μg/mL polybrene. Transient transfections were

performed using X-tremeGENE HP (Sigma Aldrich) with 2 µg plasmid DNA. CD151-GFP was kindly provided by Dr. Kiyo Sekiguchi (Osaka University, Japan). Syntenin-1-GFP and syntenin-1-PDZ1 plasmids were kindly provided by Dr. Pascale Zimmermann (The Cancer Research Center of Marseille, France). ALCAM and GFP siRNA were purchased from Invitrogen (Grand Island, NY). Anti-CD151 (mAB 1A5) was generated as previously described (201). ALCAM was detected with commercially available antibodies (ThermoFisher Scientific, clone L50; Abcam, Cambridge, Massachusetts, EPR2759 (2); or R&D Systems, MAB6561). Syntenin-1 was detected with commercially available antibody (Abcam, Cambridge, Massachusetts, EPR8102). The control antibody, 29-7, was generated in the same fashion as mAB 1A5 (201). ɣ-secretase activity was inhibited with L-685,458 (InSolution ɣ-secretase Inhibitor X, Millipore Sigma, Burlington, Massachusetts).

Immunoblot and immunoprecipitation analysis

Metabolic labeling

HEp3 cells were labeled overnight in methionine/cysteine free DMEM containing 35S-label. Cells were washed thoroughly with PBS and lysed in 1% Brij 99 lysis buffer. The lysates were incubated with control antibody or mAB 1A5 and immunoprecipitated as described below. The gels were dried and then exposed to film at -80°C .

Cell surface biotinylation

For cell surface labeling, confluent HEp3 cells were treated with mAB 1A5 or control antibody for 1 h on ice and then washed with cold PBS. Cultures were subsequently biotinylated with sulfoccinimidyl-6-[biotin-amido] hexanoate using the EZ-Link Sulfo-NHS-Biotinylation Kit (ThermoFisher Scientific) according to manufacturer's instructions. Cells were lysed in 1% (vol/vol) Brij 99 followed by extraction of the insoluble material in 1% (vol/vol) Triton X-100. Immunoprecipitation was performed as described below. Biotinylated proteins were detected with peroxidase conjugated streptavidin.

Immunoprecipitation

500µg total cell lysate was incubated with 2 µg of the immunoprecipitation antibody and the antibody/lysate solution was incubated overnight at 4°C with end-to-end rotation. Protein/antibody complexes were captured with protein G sepharose beads (GE Healthcare) for 4 h at 4°C with end-to-end rotation. The lysates were cleared by centrifugation at 4000 rpm for 4 min and the unbound material saved for further analysis. The beads were washed 3 times with lysis buffer and the immune complexes were eluted by incubation in 100 µL Laemmli sample buffer (Bio-Rad Laboratories, Hercules, California) for 10 min at 95°C. The samples were then prepared for SDS-Page analysis, as described below.

Immunoblotting

For immunoblot analysis, HT1080 cells were lysed in 1% (vol/vol) Brij-98 lysis buffer and incubated on ice for 30 minutes. The lysates were cleared by centrifugation at 14,000 rpm for 15 min and the cleared lysates were then transferred to fresh tubes. Protein concentrations were determined by BCA assay (ThermoFisher Scientific). Equal amounts of protein were loaded in to SDS-PAGE gels and subsequently transferred to polyvinylidene fluoride membranes (PVDF, Millipore Sigma, Burlington, Massachusetts). The membranes were blocked for 1 h in 5% (wt/vol) non-fat dry milk in phosphate buffered saline with 0.05% Tween-20 (PBSt). The membranes were incubated overnight at 4°C with specific antibodies prepared in blocking buffer; after which the membranes were washed 3 times with PBSt and incubated with the appropriate species-specific horse radish peroxidase-conjugated secondary antibodies for 1 h at room temperature. After washing, antibody binding was visualized by chemiluminescence using a digital gel documentation system (G:Box; Syngene).

<u>Mass spectrometry</u>

HEp3 and HT1080 cells were lysed in 1% (vol/vol) Brij99 lysis buffer as described above. Lysates were incubated with control antibody 29-7 or anti-CD151 antibody (mAB 1A5) overnight at 4°C and immunoprecipitated with protein-G sepharose

beads. The immunoprecipitated complexes were then resolved by SDS-PAGE. Each lane was excised and prepared for mass spectrometry analysis by the Vanderbilt University Mass Spectrometry Core. Mass spectrometry analyses were performed with a LCQ-Deca or LTQ-Orbitrap mass spectrometer (ThermoFisher Scientific). Tandem mass spectra were extracted from raw files and used to search the database. Only proteins identified from two independent matrix preparations were considered candidate components of the matrix.

Nuclear magnetic resonance (NMR)

The ^{15}N- or ^{13}C-labeled syntenin-1 tandem PDZ1/2 fragment (amino acid residues 113-273) was expressed and purified as a GST-fusion protein with a linker containing a TEV-protease cleavage site. A synthetic gene designed with optimized codon usage for expression of PDZ1/2 in *Escherichia coli* was obtained from GeneArt. The *E. coli* BL21(DE3) strain was used for protein expression and the protein was purified on a glutathione-Sepharose column. The GST-tag was removed by on-column cleavage with the TEV-protease (202). NMR samples contained 0.2-0.3 mM isotope-labeled syntenin-1 PDZ1/2, 150 mM KCl, 20 mM Bis-Tris (pH 6.9), 10 mM ^{2}H-labelled dithiothreitol, and 0.5 mM 2,2-dimethyl-2-silapentane-5-sulfonate (DSS) in 10% D_2O/90%H_2O. Chemical shift assignments for syntenin-1 PDZ1/2 were obtained on a Bruker Avance 700 MHz NMR spectrometer by acquiring three-dimensional HNCACB, CBCA(CO)NH, HN(CA)CO, HNCO, HNCA, and HN(CO)CA experiments using the ^{13}C,^{15}N-labeled protein. Peptides corresponding to the PDZ binding motifs from CD9 (Ac- AIRRNREMV-OH), CD63 (Ac-VKSIRSGYEVM-OH), CD151 (Ac-LYRSLKLEHY-OH), and ALCAM (Ac-KKLEENNHKTEA-OH) in the same buffer were titrated into the NMR sample containing ^{15}N-labeled protein up to a 1:6 protein-peptide ratio. All peptides were purchased from Genscript (San Diego, CA) and were synthesized with >98% purity. The peptide titrations were monitored by serial ^{1}H,^{15}N-HSQC experiments performed on a Bruker Avance 500 MHz NMR spectrometer at 30°C. DSS was used as a reference to obtain the ^{1}H, ^{13}C, and ^{15}N chemical shifts. The spectra were processed with NMRPipe (203) and analyzed using NMRView (204).

In vitro cell aggregation

Cells were detached using non-enzymatic cell dissociation buffer and plated in 24-well low-attachment plates at 2.5 x 10^4 cells/well. Cells were incubated with indicated treatments for 8 h and cell clusters were imaged using a light microscope (TMS-F, Nikon) fitted with a D90 SLR camera (Nikon). Ten images were captured for each experimental group and analyzed in FIJI (ImageJ, (170)) by segmenting with Weka Trainable Segmentation (171) and calculating cluster size with the Particle Analysis plug-in. Clusters were assigned to one of four bin categories by size including single cells (300-600 pixels), small colonies (601-3,000 pixels), medium colonies (3,001-6,000 pixels), large colonies (6,001-12,000 pixels), and extra-large (>12,000 pixels). Data are presented as percent of total area for each bin category.

Avian embryo metastasis models

Spontaneous and experimental metastasis experiments were performed as described previously (167,168). In accordance with the Public Health Services policy on Humane Care and Use of Laboratory Animals, Vanderbilt Institutional Animal Care and Use Committee (IACUC) has determined that avian embryos developmental day 17 and younger are not considered vertebrate animals and therefore do not require specific protocol approval. Vanderbilt IACUC has reviewed and approved the following experimental and euthanasia procedures.

Spontaneous Metastasis (Xenografting)

Fertilized chicken eggs (Tyson Foods, Inc) were placed in 37°C incubator at 55% relative humidity on day 1 post-fertilization. The chorioallantoic membranes (CAM) of day 10 embryos were dropped away from the eggshell by displacing the air cell. Cells were dissociated, counted, and resuspended in sterile 0.9% saline at 20 x 10^6 cells/mL. The dropped CAM was damaged slightly with sterile cotton tipped swabs. 25 µL of cell suspension (500,000 cells) were placed on the dropped CAM and eggs were returned to the incubator. After 5 days of growth, embryos were euthanized by decapitation, and xenografts were harvested and weighed. To quantify metastasis to the distal CAM, the

eggshell was cut in half along the long axis, chicks were dissected from the shell, and sections of the distal CAM were dissected using a cork borer. Dissected CAM tissue was incubated with D-luciferin (600 µg/mL) for 45 minutes and luciferase activity was quantified using a digital gel documentation system (G:Box; Syngene) as a measure of cell number.

Experimental Metastasis (Intravenous Injection)

Fertilized chicken eggs were placed in a 37°C incubator at 55% relative humidity on day 1 post-fertilization. Day 11 embryos were candled to locate the allantoic vein and the direction of blood flow. Cells were dissociated, counted, and resuspended at 0.25 x 10^6 cells/mL in sterile 0.9% saline. A window was cut into the eggshell at the injection site using a Dremel™ tool. 100 µL of cell suspension (25,000 cells) was injected intravenously using an insulin syringe. Eggs were returned to the incubator for 5 days. Upon harvest, embryos are euthanized by decapitation, and metastasis was quantified by luciferase activity as described above.

Ex Vivo Imaging of Tumor Colonies

To analyze colony morphology, we performed the experimental metastasis assay as described above. However, upon harvest at 6 days post-injection, eggs were cut in half along the long axis, chicks were dissected from the shell, euthanized by decapitation, and three sections of CAM were dissected using a cork borer. Colonies were imaged using an upright fluorescent microscope (BX-61 WI, Olympus) and Volocity Imaging Software (Perkin Elmer). Colony size was determined using a custom KNIME (169) workflow. In brief, images were thresholded and segmented, after which object size, reflective of colony size and morphology, was determined for each colony. All images were processed with the same workflow. Objects were assigned to one of four bins by size including single cells (150-1,000 pixels), small colonies (1,001-20,000 pixels), medium colonies (20,001-100,000 pixels), and large colonies (>100,000 pixels). Data are presented as percent of total area for each bin category.

Migration assays

In vitro transwell migration

Tumor cells in a single cell suspension were plated into the top chamber of 8 μm Transwell inserts (Corning, Tewksbury, Massachusetts) in the presence of serum free/insulin free media. Cell culture media containing 10% fetal bovine serum was placed in the bottom chamber to serve as a chemoattractant. Migration assays were carried out for 12 h in a 37°C cell culture incubator containing 5% CO. The top surface of the inserts was cleaned with a cotton swab soaked with PBS to remove the non-migrated cells. The Transwell inserts were subsequently fixed in methanol and stained with 0.2% crystal violet. Migrated cells were counted in 3 independent fields under 20x magnification with a light microscope (TMS-F, Nikon) fitted with a D90 SLR camera (Nikon).

Two-dimensional migration

Tumor cell migration on immobilized ALCAM-Fc was performed by adhering it to glass coverslips with protein-G. Briefly, glass coverslips were coated with protein-G (2 μg/ml) followed by rat tail collagen type 1 (100 μg/ml). Unbound surface was blocked with BSA (0.5% in PBS), the surface was washed then incubated with ALCAM-Fc in 0.5% BSA. Control migration was performed on identical surfaces with the exception of ALCAM-Fc. Tumor cells were seeded at low density and tracked by live cell imaging every 10 min over a 6 h period with a fully-automated microscope (BX61, Olympus) equipped with a digital camera (Orca ER, Hammatsu). Data acquisition and analysis was performed using Volocity image acquisition software (Perkin Elmer).

Statistical analysis

All statistical analyses were performed using Prism 5 for Mac OS X (GraphPad). For statistical analysis of xenograft weight, metastasis to distal CAM, ELISA quantifications, and colony size, experimental groups were compared to control groups using Mann-Whitney-U test. Chi-square test for trend was used to determine statistically

significant differences in size distribution between two groups for colony sizes and aggregation assays.

Results

Identification of CD151^{free} associated proteins

The ability of TSPAN to organize higher-order structures in the membrane, known as TSPAN-enriched microdomains (TERM), leads to complex interactions of variable affinity with a variety of transmembrane and membrane proximal proteins (Fig. 18, (205)). Immunoprecipitation (IP) of CD151^{free} with the motility-inhibiting antibodies mAB 1A5 and 14A2 from lysates extracted with mild detergents (Brij) or stringent detergent (TX-100) co-precipitates several proteins visible after metabolic labeling (S35), and cell-surface biotinylation (Biotin) (Fig. 19a). In order to identify the components of the CD151-TERM complex responsible for regulating tumor cell motility and metastasis, we used tandem Mass Spectrometry (LC-MS-MS) to identify CD151^{free} partners that co-IP with mAB 1A5 (Fig. 19b). IPs were performed with the CD151^{free}-binding antibody mAB 1A5. Control samples included IPs with an isotype-matched control IgG and protein G alone. The precipitated complexes were separated by SDS-PAGE, excised, and analyzed by LC-MS-MS. CD151-specific candidates were identified by eliminating non-specific targets precipitated with an isotype control or protein G. Candidates identified by two or more peptides in two or more independent analyses were selected as viable targets. A total of 228 proteins were identified, of which 51 candidates distributed across five phenotypic subgroups were detected repeatedly (Fig. 19b, pie chart).

To prioritize candidates with the potential to participate in CD151^{free} regulation of migration, we emphasized candidates with the potential to influence cell-cell adhesion Based on validated interactions from published studies and the observed cell-cell accumulation, a short list of known binding partners (Fig. 19c, established partners) and possible novel partners (Fig. 19c, putative partners) was established. Nearest neighbor analysis was performed on each putative candidate using the Broad Institute Cancer

Cell Line Encyclopedia (http://www.broadinstitute.org/ccle/home, (206)). Activated leukocyte cell adhesion molecule (ALCAM) was identified as the nearest neighbor of

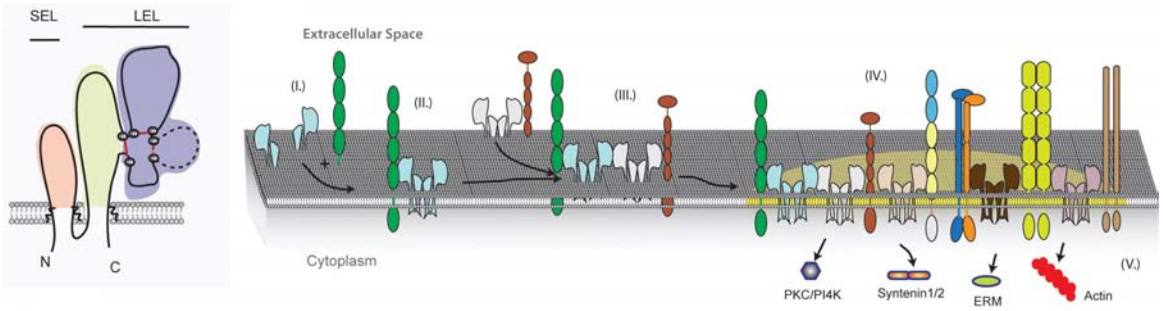

Figure 18. Tetraspanin enriched microdomains. (Left panel) Schematic depeicting general tetraspanin structure with the small extracellular loop (SEL) and the large extracellular loop (LEL) highlighted. (Right panel) Schematic representation of the steps necessary for tetraspanin-enriched microdomain (TERM) assembly including (I. & II.) tetraspanin-partner interaction, (III.) tetraspainin-tetraspanin clustering, (IV.) assembly into lipid raft-independent microdomain, and (V.) interaction with intracellular signaling molecules.

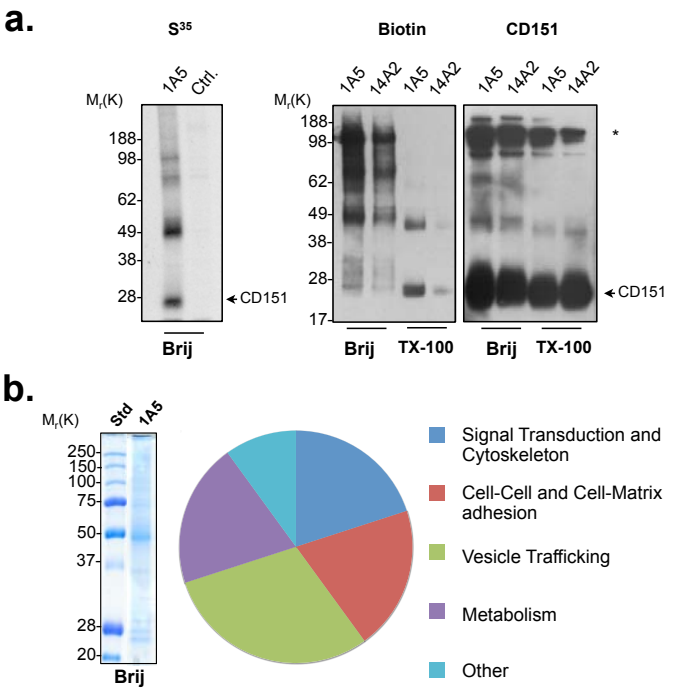

c.

Targets Identified by Mass Spectrometry.

Established Partners	Gene # | Uniprot ID.
CD151 (TSPAN24)	977 | P48509
Integrin subunit α3 (ITGA3)	3672 | P26006
Integrin subunit β1 (ITGB1)	3688 | P05556
MMP14 (MT1-MMP)	4323 | P50281
PI 4-kinase type 2-alpha (PIK42A)	55361 | Q9BTU6
Syntenin-1 (SDCBP)	6386 | O00560
Putative Partners	
ALCAM (CD166)	214 | Q13740
CUB domain-containing protein-1 (CDCP-1)	64866 | Q9H5V8
Claudin domain-containing protein-1 (CLDND1)	56650 | Q9NY35
EGF-like repeat and discoidin I-like domain	10085 | O43854
CD44 antigen precursor	960 | P16070

Figure 19. ALCAM is a novel binding partner of CD151. (**a**) Detection of CD151 and associated proteins by metabolic labeling (S35), cell-surface biotin labeling (biotin), or CD151-specific immunoblot after immunoprecipitation of HEp3 whole cell lysate. (**b**) SDS-PAGE stained with coomassie blue of proteins co-immunoprecipitated with CD151 from HEp3 cell lysates. Proteins were identified by mass spectrometry, filtered to eliminate proteins co-immunoprecipitated by control antibody (29-7), and categorized according to their particular cellular functions, if known. (**c**) Table of known CD151-associated proteins and putative partners that control migration identified by mass spectrometry.

integrin α3, one of the primary partners of CD151. Moreover, ALCAM has been shown to associate with the TSPAN CD9 which can promote *cis* ALCAM clustering at the cell surface and thereby enhance both homophilic and heterophilic ALCAM interactions by (125). Consequently, we prioritized ALCAM as the putative partner of $CD151^{free}$ capable of mediating its ability to control adhesion, migration, and metastasis.

The immunoglobulin-like superfamily member, ALCAM, is coupled to $CD151^{free}$ through syntenin-1

ALCAM is broadly expressed in epithelial tissues, their corresponding tumors, (Fig. 20a), and continuous cell lines derived from these tumors (Fig. 20b,c). Its primary function is to mediate cell-cell adhesions through both heterophilic *trans* interactions with CD6 and homophilic ALCAM-ALCAM *trans* interactions, which enables it to function as a contributing factor in both normal and pathological processes of cell adhesion (105,115,124). ALCAM is a known regulator of cancer cell adhesion, migration and metastasis (111,136,146,165). We have recently demonstrated that the function of this clinically relevant adhesion molecule is largely regulated by proteolytic shedding of the extracellular domain ((114,165), Hebron et al., under review)

ALCAM is anchored to the actin cytoskeleton through the scaffolding protein syntenin-1, enhancing both homophilic and heterophilic interactions (123,124). Since both CD151 and ALCAM contain PDZ-binding motifs, we hypothesized that synthenin-1 might link these two membrane proteins. Indeed, syntenin-1 was among the $CD151^{free}$-associated proteins identified in our LC-MS-MS screen (Fig. 19c). To test this hypothesis, we analyzed the binding of CD151 and ALCAM carboxy-terminal (c-terminal) fragments to the PDZ domains of syntenin-1 by nuclear magnetic resonance (NMR). Incubation with C^{15}-labeled c-terminal fragment of CD151 causes significant chemical shifts in the N^{13}-labeled PDZ-1 domain, indicating protein interactions. Conversely, incubation with the c-terminal fragment of C^{15}-labeled ALCAM causes significant shifts in the N^{13}-labeled PDZ-2 domain of syntenin-1, indicating protein interactions (Fig. 21a). Considering that CD151 and ALCAM interact with distinct, adjacent PDZ domains in the same molecule, these observations indicate that syntenin-

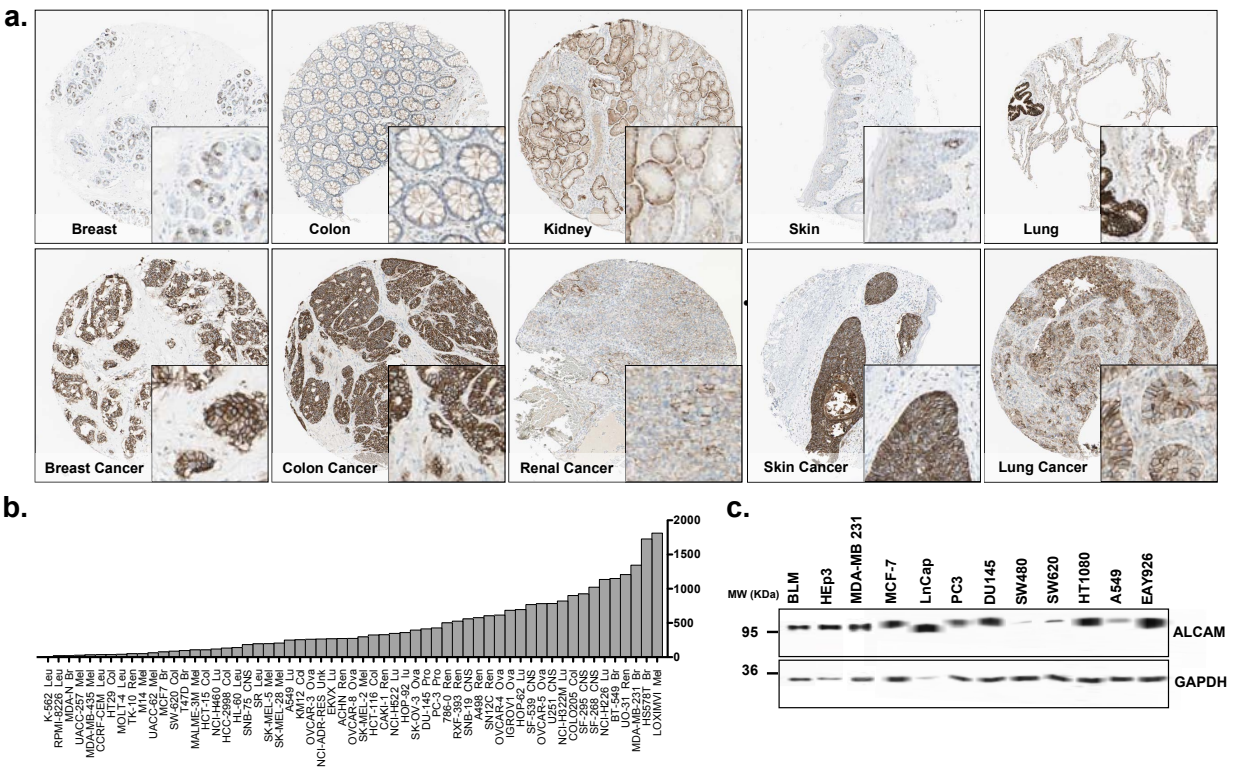

Figure 20. ALCAM is expressed in several tissue types and their corresponding cancers. (**a**) Expression of ALCAM in several tissue types and corresponding cancer tissues. Images obtained from Human Protein Atlas. (**b**) mRNA expression analysis of the NCI-60 dataset demonstrates that the expression of ALCAM varies; however, epithelial derived cancer cell lines have the highest expression. (**c**) Western blot analysis of ALCAM expression in commonly used cancer cell lines. GAPDH is shown for loading control.

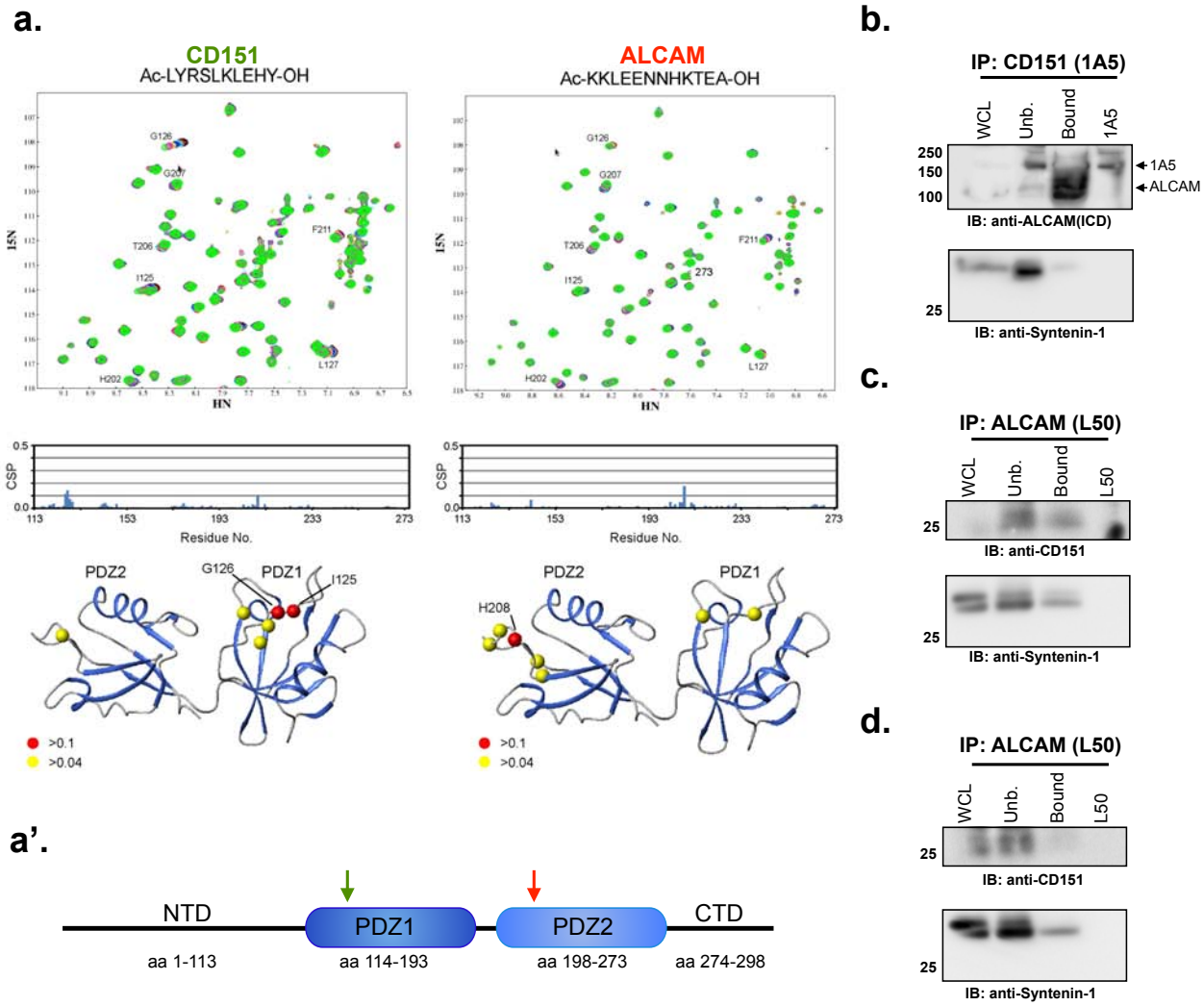

Figure 21. CD151 associates with novel binding partner, ALCAM, through scaffolding protein, syntenin-1. (**a**) Chemical shift perturbations (CSPs) measured in $^{1}H,^{15}N$-HSQC NMR spectra of syntenin-1 PDZ1/2 upon addition of the CD9, and CD63 peptides. HSQC spectra with 0 (black), 1 (red), 2 (cyan), 3 (blue), 4 (yellow), 5 (magenta), and 6 (green) molar equivalents of the peptides are overlaid (top panel). CSPs are plotted as a function of the residue number (middle panel). The residues that experienced CSPs of more than 0.05 (yellow) and 0.1 ppm (red) are highlighted on the crystal structure of syntenin-1 PDZ1/2 (PDB code: 1N99). (**a'**) Schematic depicting putative binding sites of CD151 and ALCAM to syntenin-1. (**b**) Co-immunoprecipitation of ALCAM and syntenin-1 with CD151 (mAB 1A5) from HT1080 cells (**c**) Reciprocal co-immunoprecipitation of CD151 and syntenin-1 with ALCAM from HT1080 cells. WCL: whole cell lysate (10 µg), Unb.: unbound fraction (10 µL), Bound: protein G bound fraction (20 µL), 1A5: anti-CD151 immunoprecipitation anybody (0.1 µg), L50: anti-ALCAM immunoprecipitation antibody, IP: immunoprecipitation, IB: immunoblot. (**d**) Co-immunoprecipitation of CD151 and syntenin-1 with ALCAM (L50) from HT1080 cells overexpressing PDZ1 domain of syntenin-1.

1 may indeed bind to both CD151 and ALCAM to form a previously unknown trimeric complex (Fig. 21a').

The scaffolding protein, syntenin-1 is required for CD151/ALCAM interaction

To validate the existence of a trimeric CD151/syntenin-1/ALCAM complex, we immunoprecipitated CD151-associated proteins from HT1080 cells lysed with 1% Brij-98 lysis buffer using anti-CD151^{free} antibody (mAB 1A5). Both ALCAM and syntenin-1 co-immunoprecipitated with CD151 (Fig. 21b). Additionally, reciprocal immunoprecipitation of ALCAM (L50) resulted in the co-immunoprecipitation of both CD151 and syntenin-1 (Fig. 21c). Overexpression of a single PDZ domain of syntenin-1 can disrupt syntenin-1-coupled complexes (207); therefore, we transiently transfected syntenin-1-PDZ1 into HT1080 cells to determine if ALCAM's interaction with CD151 was syntenin-1 dependent. Immunoprecipitation of ALCAM in cells transfected with PDZ1 reduced co-immunoprecipitation of CD151 by 70%, Conversely, expression of PDZ1 only reduced syntenin-1 co-immunoprecipitation slightly (38%) supporting our NMR data indicating that ALCAM interacts with syntenin-1 through the PDZ2 domain (Fig. 21d).

The intracellular domain of ALCAM is released by ɣ-secretase, disrupting the CD151/syntenin-1/ALCAM complex

Metalloprotease-mediated shedding of the extracellular domain (ECD) disrupts ALCAM-mediated cell-cell adhesion (146), Hebron et al, under review). ECD shedding is a common regulatory mechanism for cell adhesion molecules and is often followed by ɣ-secretase-mediated release of the intracellular domain (ICD) from the plasma membrane (104). However, release of the intracellular domain by ɣ-secretase has not been previously observed in ALCAM. To determine the activity of ɣ-secretase against ALCAM, we treated cells expressing GFP-tagged ALCAM with a ɣ-secretase inhibitor (L-685,458) and monitored the generation of soluble ALCAM-ICD. Immunoblot analysis of cells treated with ɣ-secretase inhibitor (GSI) shows a dose-dependent accumulation of a 38 kDa intracellular ALCAM fragment that corresponds to the membrane-anchored intracellular product that remains after ADAM17-mediated shedding of the ectodomain (ΔECD-GFP, Fig. 22a). Furthermore, treatment with 10 μM GSI inhibits the generation

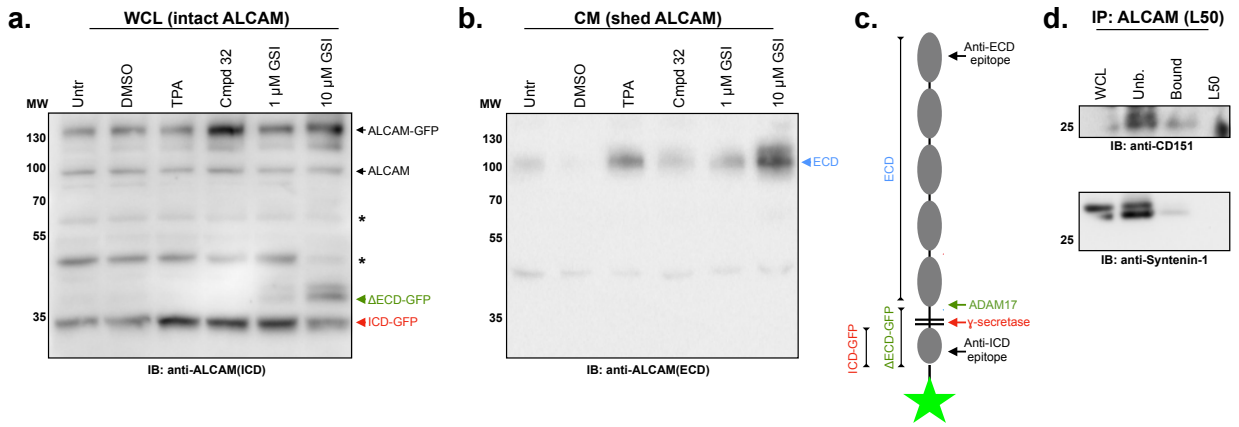

Figure 22. The intracellular domain of ALCAM is released by ɣ-secretase, disrupting the CD151/syntenin-1/ALCAM complex. (**a**) Immunoblot analysis of proteolytic processing of ALCAM. WCL: whole cell lysate; ΔECD-GFP: membrane-anchored ALCAM intracellular domain, (◀) ICD-GFP: soluble ALCAM intracellular domain, (◀); TPA: tetradecanoylphenol-13-acetate; Cmpd32: 10 μM compound 32; GSI: ɣ-secretase inhibitor, L-685,458 (**b**) Immunoblot analysis of proteolytic processing of ALCAM. CM: conditioned medium; ECD: cleaved ALCAM extracellular domain (◀). (**c**) Schematic of ALCAM proteolytic processing by ADAM17 and ɣ-secretase. (**d**) Co-immunoprecipitation of CD151 and syntenin-1 with ALCAM from HT1080 cells overexpressing the intracellular domain of ALCAM (ALCAM-ICD).

of a 34 kDa fragment corresponding to soluble ALCAM-ICD by approximately 50% (ICD-GFP, Fig 22a). These observations indicate that ɣ-secretase indeed cleaves ALCAM and provides an endogenous mechanism by which the interaction of CD151 and ALCAM may be regulated.

The ability of the soluble ALCAM-ICD fragment to disrupt the CD151/syntenin-1/ALCAM complex was investigated by expressing ALCAM-ICD in HT1080 cells and immunoprecipitating the trimeric complex with anti-ALCAM. Similar to overexpression of PDZ1, overexpression of ALCAM-ICD inhibited the co-immunoprecipitation of CD151 and syntenin-1 by 50% and 80%, respectively (Fig. 22c). Taken together, these data indicate that syntenin-1 is necessary for intracellular coupling of CD151 and ALCAM.

CD151^{free} regulation of *in vitro* cell adhesion and migration is ALCAM dependent

To determine if the regulation of cell adhesion and migration through CD151^{free} is ALCAM dependent, the ability of mAB1A5 to promote adhesion and inhibit migration was tested, following disruption of the interaction between CD151 and ALCAM. Two distinct methods of disrupting the CD151/syntenin-1/ALCAM complex were analyzed: 1) Complex formation was disrupted through overexpression of ALCAM-ICD, which mimics the ICD released by ɣ-secretase and antagonizes the ALCAM-syntenin-1 interaction, or 2) The complex was disrupted by CRISPR/Cas9 (Hebron, et al., under review) or RNAi mediated ablation of ALCAM expression (Fig. 24b).

Using cell aggregation assays, we tested the ability of CD151^{free} to mediate cell adhesion after ablation of ALCAM or disruption of the trimeric complex with ALCAM-ICD. Unbiased, automated image analysis was used to determine cell cluster size and each cluster was assigned to indicated size category. Representative bright field images taken at 100X are presented (Fig. 23a). Engaging CD151^{free} with mAB 1A5 promoted cell-cell adhesion and aggregation significantly more than in cells treated with mouse IgG, increasing the number of extra-large cell clusters from 0% to 30% with a concomitant decrease in the number of small clusters and single cells from 69% to 36% (Fig. 23b, *Parental*, $P<0.0001$). Subsequent disruption of the CD151/ALCAM complex by overexpressing ALCAM-ICD or CRISPR-mediated knockout of ALCAM (ALCAM-KO) inhibited the effect of CD151^{free}-mediated clustering. mAB 1A5 treatment of ALCAM-ICD

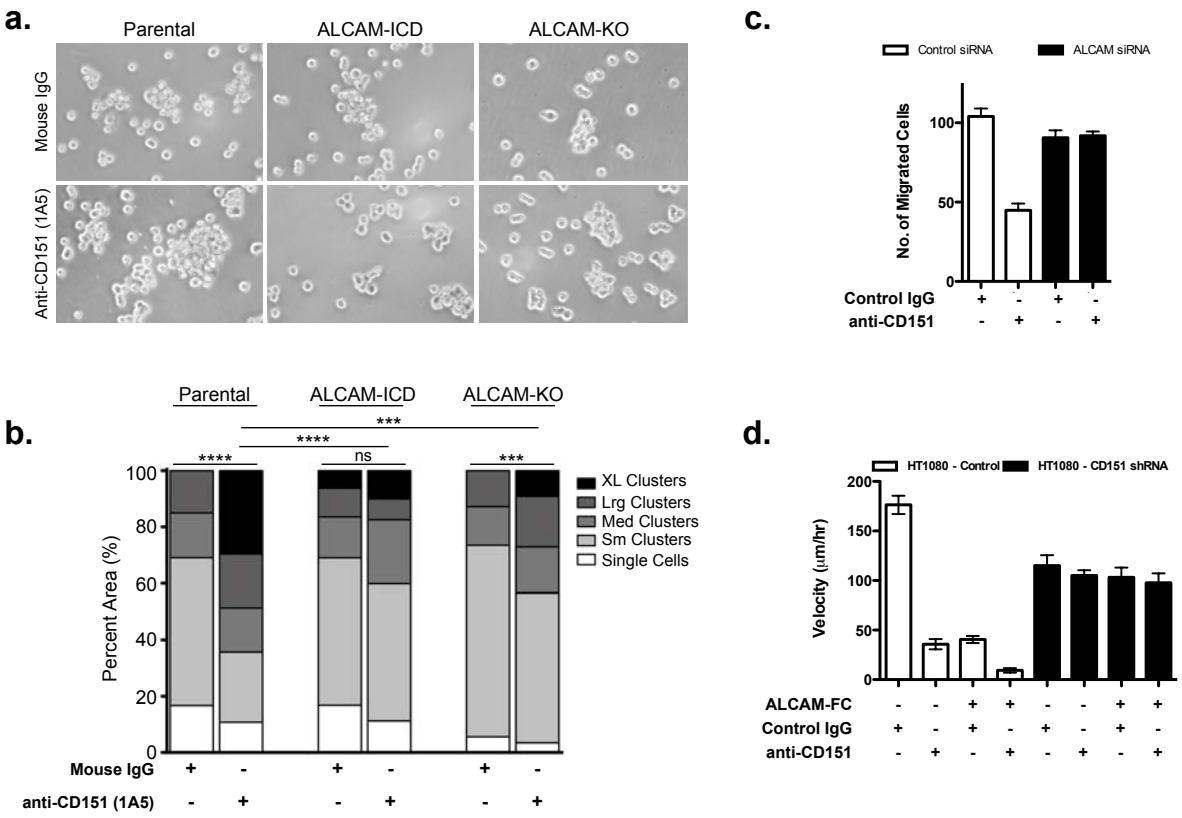

Figure 23. CD151^{free} regulation of *in vitro* cell adhesion and migration is ALCAM dependent.
(**a**) Representative images of *in vitro* cell aggregation analysis of parental HT1080 (Parental) expressing ALCAM-ICD (ALCAM-ICD) and ALCAM-KO HT1080 cells (ALCAM-KO). (**b**) Quantification of *in vitro* cell aggregation assay. Clusters were binned into single cell, small (Sm), medium (Med), large (Lrg) or extra-large (XL) clusters based on pixel area. Distribution of clusters across size bins was represented as percent of total area of all clusters. P-values were calculated using Chi-square test for trend, ****P<0.0001, ns: not significant. Results are representative of three independent experiments. (**c**) Transwell migration of parental HT1080 cells (white bars) or ALCAM-knockdown cells (black bars) in the absence or presence of mAB 1A5. (**d**) 2D migration of parental HT1080 cells (white bars) or CD151-knockdown cells (black bars) in the absence or presence of mAB 1A5. Migration velocities are reported.

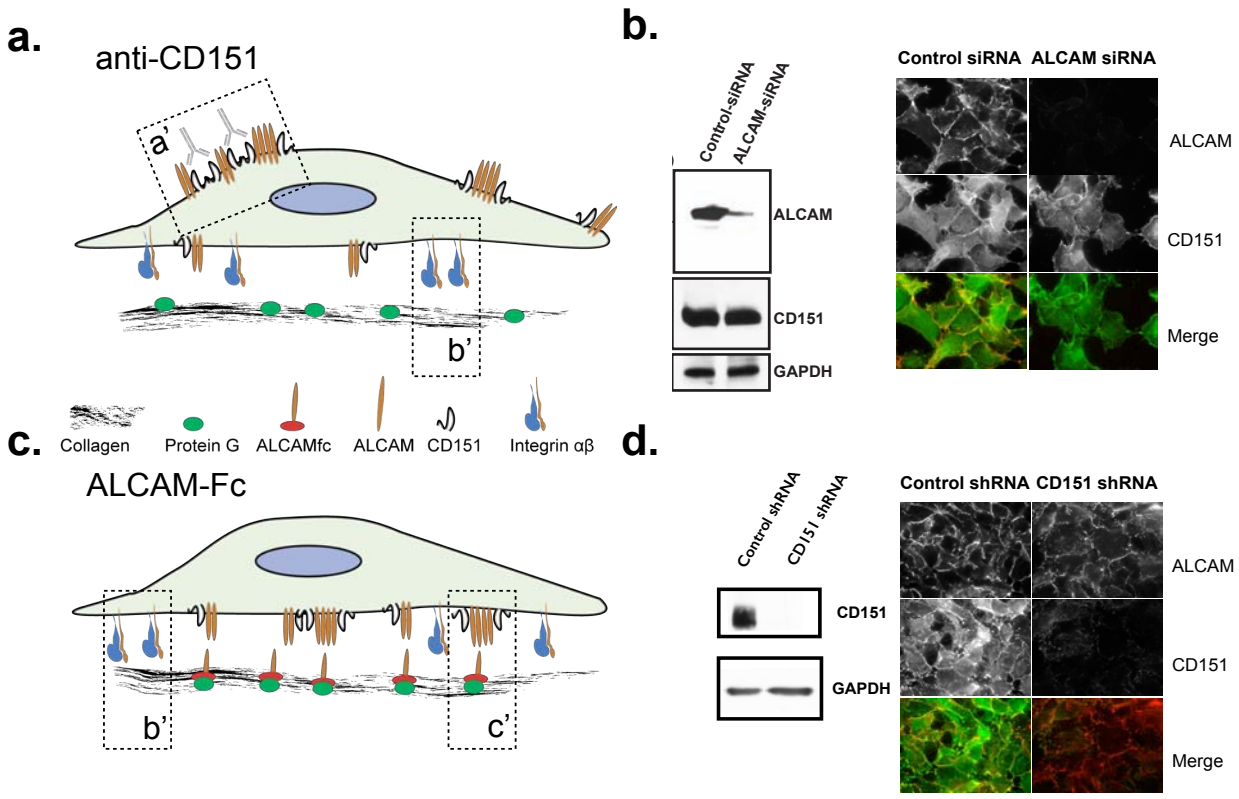

Figure 24. Analysis of CD151 and ALCAM cooperation in the regulation of tumor cell migration. (**a**) Schematic for the analysis of 2D migration in the presence of the anti-CD151 antibody. Tissue culture plates are coated with Rat tail collagen type I, (a') represents the CD151TERM complex being engaged with the anti-CD151 antibody mAB 1A5 (b') depicts the presence of the Integrin α3β1 which is expressed on the surface of HEp3 cells and associates closely with CD151 (mAB 1A5). (**b**) Immunoblot and immunofluorescence analysis of ALCAM and CD151 expression in HT1080 cells transfected with ALCAM-specific siRNA, demonstrating ~90% loss of protein expression compared to the control siRNA transfected cells. (**c**) Schematic for the analysis of 2D migration on immobilized ALCAM-Fc. Tissue culture plates are coated with Rat tail collagen type I and protein G, (b') represents the adhesion mediated by integrin α3β1 binding (c') represents the binding of ALCAM on the tumor cell surface to ALCAM-FC. (**d**) Immunoblot and immunofluorescence analysis of CD151 expression in HT1080 cells transfected with CD151-specific siRNA, demonstrating ~100% loss of protein expression compared to the control siRNA transfected cells.

cells failed to induce cell clustering when compared to mouse IgG-treated ALCAM-ICD cells and, when compared to mAB 1A5-treated parental cells, this prevention of clustering by ICD-expression was highly significant (Fig 23b, *Parental-1A5 vs. ICD-1A5*, P<0.0001). Similarly, the ablation of ALCAM (HT1080-KO) greatly diminished mAB 1A5 induced clustering (*Parental-1A5 vs. KO-1A5*, P=0.0021, 9% vs 30%).

Similarly, ALCAM is required for CD151-regulation of *in vitro* migration. Promoting $CD151^{free}$-mediated cell-cell adhesion with mAB 1A5 inhibits HT1080 tumor cell *in vitro* transwell migration on a collagen matrix (Fig. 24a). After RNAi-mediated depletion of ALCAM (Fig. 24b), tumor cells are no longer sensitive to the immobilization by clustering of CD151 (Fig. 23c). To test if this $CD151^{free}$-mediated regulation of migration extended to collective cell migration, we modeled ALCAM-ALCAM interactions by seeding cells on ALCAM-Fc coated surfaces (Fig. 24c and (125)). Similar to mAB 1A5 treatment, engaging ALCAM-ALCAM interactions inhibited tumor cell motility (Fig. 23d). The inhibition of cell motility upon ALCAM-ALCAM ligation is enhanced by mAB 1A5-induced clustering of CD151 (Fig. 23d). Conversely, shRNA-mediated knockdown of CD151 in HT1080 cells (Fig. 24d) not only eliminates sensitivity to the anti-CD51 antibody mAB 1A5, but also prevents the inhibition of motility by ALCAM-ALCAM ligation (Fig. 23d, black bars).

Taken together, these data demonstrate that the association of ALCAM with $CD151^{free}$ is necessary in order for this adhesion complex to promote adhesion and control migration.

$\underline{CD151^{free}}$ <u>regulation of *in vivo* motility and metastasis is ALCAM dependent</u>

Targeting $CD151^{free}$ with mAB 1A5 *in vivo* inhibits tumor cell migration and metastasis (178,189). To determine if this $CD151^{free}$ functionality is ALCAM dependent, we assayed for mAB 1A5-induced alterations in both tumor cell dissemination and spontaneous metastasis with disruption of the CD151/syntenin-1/ALCAM complex. Tumor cell migration was analyzed using the avian embryo model of experimental metastasis (Fig. 25). In this model, local dispersion of tumor cells within a metastatic colony is indicative of tumor cell motility (178).

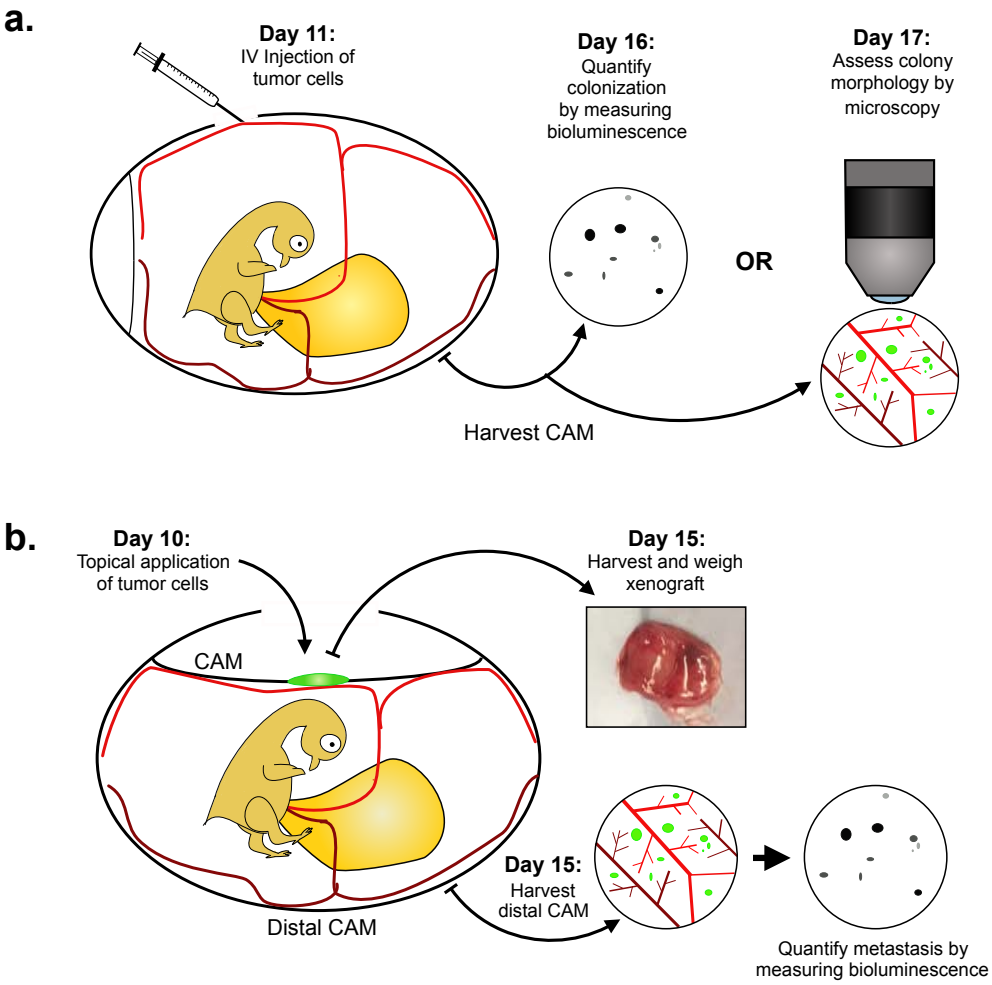

Figure 25. Avian embryo models of metastasis. (**a**) Schematic describing avian embryo experimental metastasis assay. (**b**) Schematic describing avian embryo spontaneous metastasis assay.

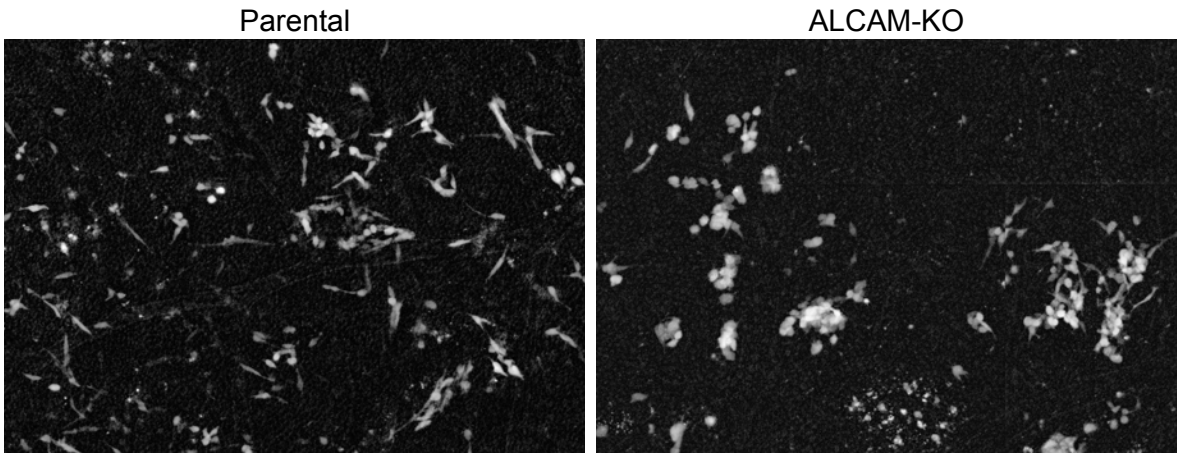

Figure 26. ALCAM-KO promotes amoeboid migration. Representative images of metastatic colonies imaged 6 days post intravenous injection of parental HT1080 or ALCAM-KO cells into CAM of chicken embryo.

Because colonies formed by ALCAM-KO HT1080 cells display a morphology indicative of ameboid migration with poorly dispersed colonies (Fig. 26), the effect of disrupting the CD151/ALCAM complex on mAB 1A5-mediated inhibition of motility was investigated through antagonistic disruption of the CD151/syntenin-1/ALCAM complex using cells overexpressing ALCAM-ICD. As expected, colonies formed by parental HT1080 cells exhibit a highly motile phenotype while treatment with mAB 1A5 strongly inhibits migration and gives rise to compact colonies (Fig. 27a), which reflected quantitatively by the increase in large clusters (Fig. 27b) and is indicative of inhibited tumor cell migration. Conversely, HT1080 cells overexpressing ALCAM-ICD were largely unaffected by treatment with mAB 1A5, with no significant increase in cluster size over ALCAM-ICD treated with mouse IgG (Fig. 27a,b, ns) and colony size remaining significantly smaller than mAB 1A5-treated parental cells (Fig. 27a,b, $P>0.0001$).

Concomitant with the inhibition of mobility, mAB 1A5 inhibits spontaneous dissemination from the primary tumor (178). Using the avian embryo model of spontaneous metastasis (Fig. 25b), we determined that mAB 1A5 suppressed metastasis of parental HT1080 cells 3-fold without affecting xenograft growth (Fig. 27c,d). Conversely, knockout of ALCAM in HT1080 cells completely abrogated the effect of 1A5 on metastasis (Fig. 27d). Interestingly, overexpression of ALCAM-ICD alone significantly decreased spontaneous metastasis over 7-fold (Fig. 28). This suggests that dynamic regulation of the interaction between ALCAM and CD151 may be critical to efficient metastasis because both overt disruption (by ALCAM-ICD) and long-term stabilization (by mAB 1A5) are capable of suppressing spontaneous metastasis. However, ALCAM-ICD-mediated suppression of metastasis was lost in the experimental metastasis model (Fig. 25a, 29), indicating that the interaction between ALCAM and CD151 may be most critical in the initial steps of metastasis.

Cumulatively, these data demonstrate that the association of ALCAM with $CD151^{free}$ is necessary in order for this adhesion complex to inhibit motility and metastasis *in vivo*.

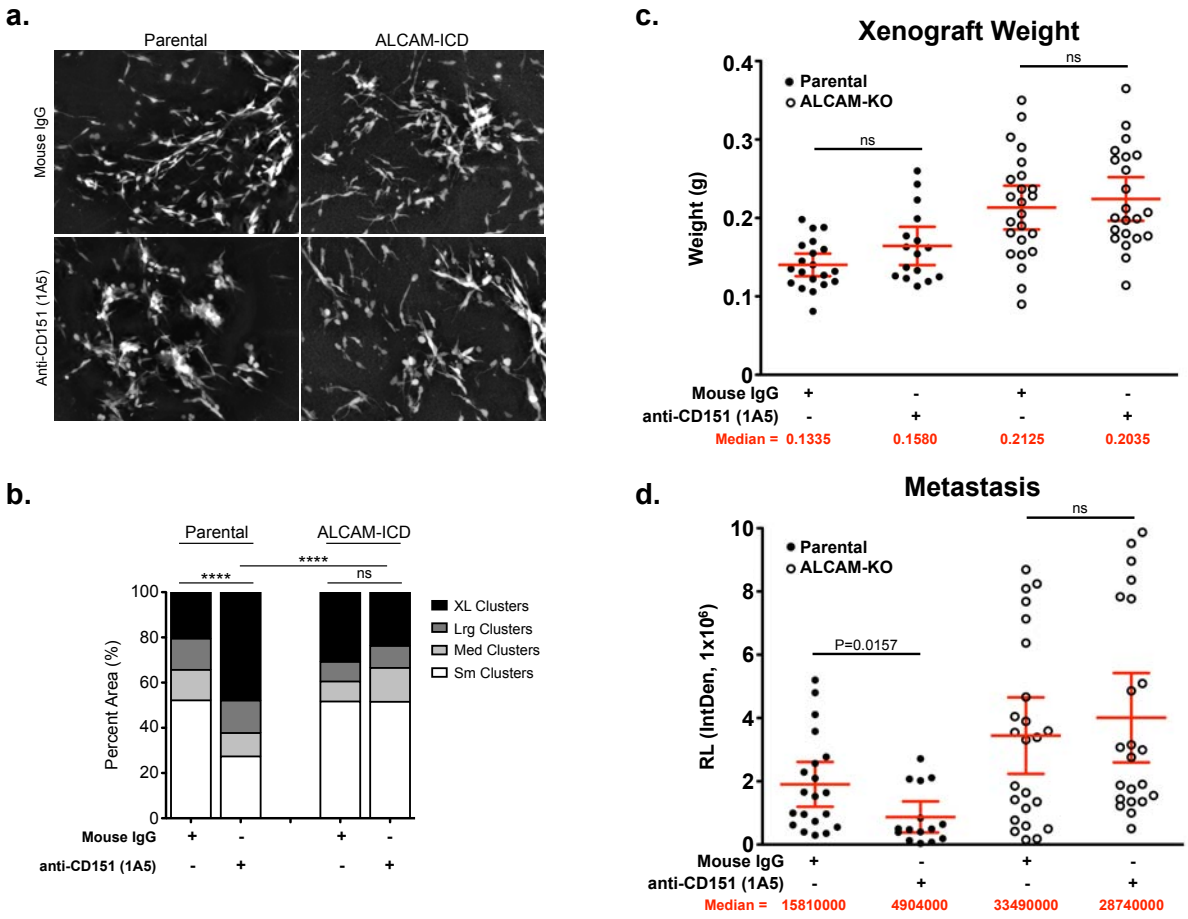

Figure 27. CD151^{free} regulation of *in vivo* motility and metastasis is ALCAM dependent.
(**a**) Representative images of metastatic colonies of parental HT1080 cells (Parental) and HT1080 cells expressing ALCAM-ICD (ALCAM-ICD) imaged 6 days post-intravenous injection into CAM of chicken embryo in the absence and presence of mAB 1A5. (**b**) Colony size was quantified using custom KNIME workflow. P-values were calculated using Mann-Whitney-U test, ****P<0.0001. Graphs display mean with 95% confidence interval. Medians are reported. Parental: closed circles; ALCAM-ICD: open circles. (**c**) Wet weight of HT1080 xenografts removed from CAM of chicken embryos. Three independent experiments were combined for the analysis (N= 20, 15, 24, 22 respectively). P-values were calculated using Mann-Whitney-U test, ns: not significant. Graphs display mean with 95% confidence interval. Medians are reported. Parental: closed circles; ALCAM-KO: open circles. (**d**) Quantification of metastasis. Metastasis was measured by luciferase activity in a 1.5 cm core of distal CAM. Two cores per embryo were measured. Relative bioluminescence (RL) represents mean value of two CAM sections per chick and was calculated using the integrated density tool (IntDen, 1x10^6) in ImageJ. Three independent experiments were combined for the analysis (N= 20, 15, 24, 22 respectively). P-values were calculated using Mann-Whitney-U test, ns: not significant. Graphs display mean with 95% confidence interval. Medians are reported. Parental: closed circles; ALCAM-KO: open circles.

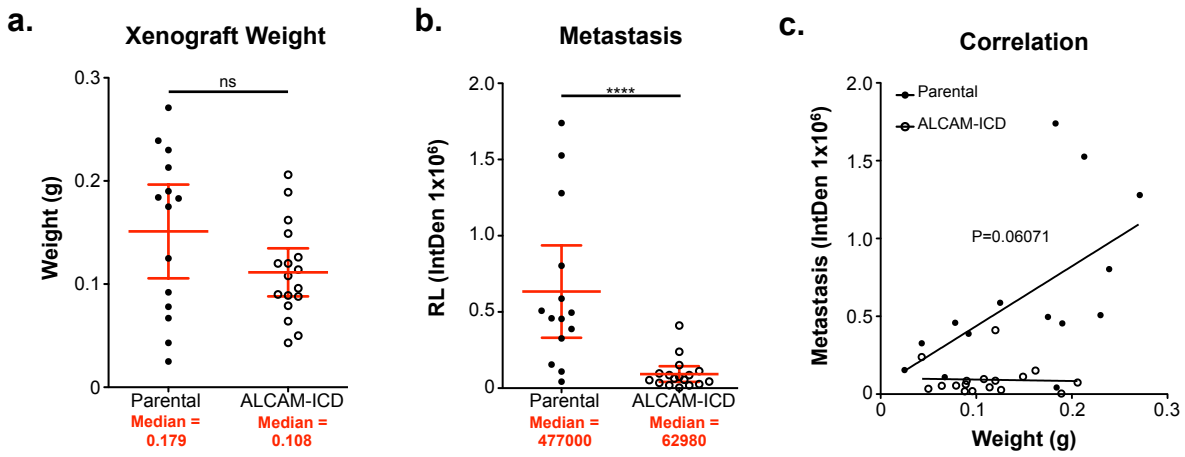

Figure 28. Intracellular disruption of the CD151/syntenin-1/ALCAM inhibits metastasis. (**a**) Wet weight of HT1080 xenografts removed from CAM of chicken embryos. Three independent experiments were combined for the analysis (N= 14 and 17, respectively). (**b**) Quantification of metastasis. Metastasis was measured by luciferase activity in a 1.5 cm core of distal CAM. Two cores per embryo from at least 10 embryos were measured. Relative bioluminescence (RL) represents mean value of two CAM sections per chick and was calculated using the integrated density tool (IntDen, $1x10^6$) in ImageJ. (**c**) Correlation of tumor size to respective metastatic burden. P-value corresponds to difference in slopes of linear regression.

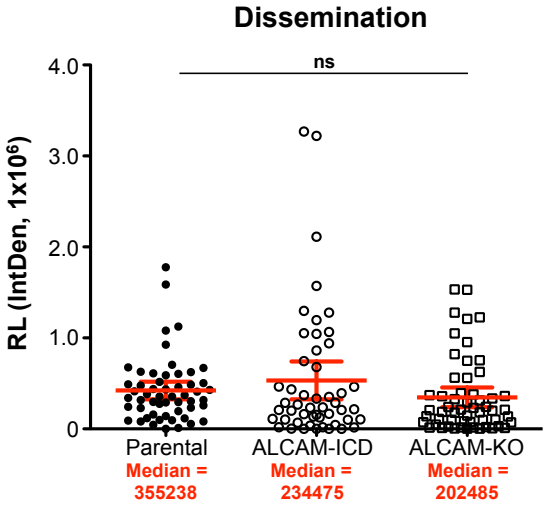

Figure 29. Overexpression of ALCAM-ICD suppresses spontaneous metastasis, but not experimental metastasis. CAM colonization was quantified using luciferase activity in a 1.5 cm core of CAM. Two cores per embryo were measured. Relative bioluminescence (RL) represents mean value of two CAM sections per chick and was calculated using the integrated density tool (IntDen, $1x10^6$) in ImageJ. P-values were calculated using Kruskal-Wallis test with Dunn's post-test, ns: not significant. (n= 27, 25, 28)

Discussion

The regulation of migration is a complex process that relies on the integration of many different molecular processes. TSPAN-driven molecular scaffolding is one mechanism by which signal integration is accomplished. Like many biological functions, cell adhesion is “tunable”, meaning that it is neither “on” nor “off” but rather in a perpetually dynamic state in which activity can range from promoting to inhibiting adhesions (5,208). Consequently, many factors that control adhesion can both promote and inhibit migration. There have been several investigations into the molecular mechanism(s) by which CD151 regulates cell motility (reviewed in (5,209,210)). The characterization of direct interaction with laminin-binding integrins evolved to define the ability of CD151 to promote adhesion and migration through direct interaction with these integrins. Consistent with this hypothesis is the reduction of migration on a laminin substrate (211) and the reduction in metastasis seen with CD151 knockout mice (199). However, recent work has revealed that direct interactions with laminin-binding integrins may not be responsible for some of the cancer-associated activities of CD151 (189). In fact, the loss of α3β1 in prostate cancer cells promotes, rather than inhibits, metastasis (95), suggesting that CD151 may regulate cell motility through α3β1-independent mechanisms. Indeed, α3β1 expression is frequently reduced during carcinogenesis while $CD151^{free}$ becomes detectable in the tumor tissue and is prognostic of cancer progression and patient survival (189).

In the present study we identify ALCAM as a novel CD151 partner that associates with integrin-free CD151 via the intracellular scaffolding protein syntenin-1. ALCAM is a cell adhesion molecule belonging to the immunoglobulin superfamily (IgSF). ALCAM is expressed broadly in human tissues and cells, with predominant expression in neuronal cells, immune cells, epithelial cells, and stem cells of hematopoietic and mesenchymal origin. It is functionally associated with many cell adhesion events including T-cell activation, endothelial adherence junction formation, neuronal guidance, and epithelial integrity (Fig. 2, (212,213)). ALCAM expression and function has been associated with many solid cancers and their progression. While the

molecular mechanism of action has not been defined, its expression has been broadly recognized to be altered during cancer progression (Fig. 20, (116)).

The data presented in this study strongly suggest that the interaction between CD151 and its novel binding partner, ALCAM, is very dynamic and enables tunable regulation of cell-cell adhesion, migration, and metastasis. Our data suggest that the CD151/ALCAM interaction closely represents the classical dogma that adhesion and metastasis interact on a bell shaped curve, whereby very weak adhesion is just as inhibitory to efficient metastasis as very strong adhesion. Disruption of the CD151/syntenin-1/ALCAM complex by antagonistic overexpression of ALCAM-ICD significantly inhibits metastasis (Fig. 28), as does stabilization of this complex by treatment with mAB 1A5 (Fig. 27d, (178)). However, the molecular switch of CD151 from integrin-binding to integrin-free promotes migration and correlated with poor patient survival in prostate cancer (189). Because the dynamic regulation of tumor cell adhesion is essential for efficient metastasis, understanding the regulation of this elastic complex during cancer progression presents an attractive therapeutic target.

One potential mechanism regulating CD151/ALCAM-mediated adhesion and migration is the proteolytic processing of ALCAM. Similar to many Ig-CAMs, the function of ALCAM, is regulated through proteolytic shedding of the ectodomain from the cell surface by the metalloprotease ADAM17 (104,146). Moreover, high levels of ALCAM shedding are associated with poor patient outcome in several cancers (113,114,146). While it is well established that ADAM17 is responsible for shedding the ectodomain of ALCAM (146,165), less is known about how this shedding is regulated. Previous studies have associated the interaction of ALCAM and TSPAN CD9 with a decrease in ALCAM shedding by ADAM17. This interaction with CD9 has been shown to stabilize and strengthen ALCAM-mediated cell adhesion in immune cells. The effect of CD151 binding on ALCAM shedding has yet to be explored, however it is reasonable to hypothesize that the proteolytic processing of ALCAM can be regulated through its TSPAN binding partners, thus regulating ALCAM-mediated adhesion. Beyond shedding, ALCAM-mediated adhesion is also known to be positively regulated by it’s interaction with the actin cytoskeleton (123,124,214). ALCAM’s association with the actin cytoskeleton is dependent on PKCα activation (214) and PKCα is a known binding

partner of CD151 (215,216). Therefore, PKCα may regulate ALCAM adhesion through CD151.

Here, we explore the interaction of CD151 in the context of cancer progression and metastasis. However, this data also has implications for several biological processes. As previously mentioned, both ALCAM and CD151 are critical to processes requiring dynamic regulation of cell adhesion, raising the questions: 1) Does CD151 interact with ALCAM in normal tissue? and 2) If so, does this interaction facilitate any of these processes?

TSPAN interactions with, and organization of, seemingly unrelated and divergent proteins and signaling molecules allow them to function as molecular integrators of cellular behaviors. In the present study, we aimed to determine the mechanism by which the clustering of CD151 is able to promote adhesion and control tumor cell motility. As motility is required for metastasis, TSPANs are considered attractive targets in the design of anti-metastatic treatment (5,103). These data demonstrate that the novel binding partner, ALCAM, is required for clustering of integrin-free CD151, and subsequent inhibition of motility and metastasis. Considering that both CD151 and ALCAM are strongly associated with increased virulence in cancer, this interaction is an attractive target for understanding tumor cell dissemination.

Acknowledgements

We want to thank Dr. Guido Swart for insightful discussion of ALCAM biology. AZ was supported by R01 CA143081, P01 CA040035, and R01 CA120711. KEH was supported by the Microenvironmental Influences in Cancer Training Program (NIH/NCI T32CA009592) and F31CA189764. TDP was supported by F31 CA136228. AGH was supported by P50 CA098131.

Author Contributions

Study was conceived and designed by KEH, TDP and AZ. Experiments were performed by KEH and TDP with help from EYL on avian embryo metastasis assays, AKvL on immunoblots, AGH on evaluation of ALCAM expression, AM on mass spectrometry and surface labeling assays, and HV, HI, and MEH on NMR experiments. Data analysis was performed by KEH with help from AZ. Manuscript was written by KEH, and AZ and edited by EYL.

CHAPTER IV:

DISCUSSION AND FUTURE DIRECTIONS

Summary

In Chapter I, I outlined an unanswered question remaining in the field of metastasis research: How are the normal mechanisms that regulate dynamic cell adhesion appropriated by tumor cells to promote cancer progression and dissemination? The data presented in this dissertation begin to address that question and provide two novel mechanisms by which ALCAM's function is regulated to modulate cell-cell adhesion and allow it to function as a tunable element that can be adjusted to suppress or promote migration and dissemination. ALCAM, a member of the immunoglobulin superfamily of cell adhesion molecules, has been shown to mediate several processes requiring dynamic regulation of cell adhesion, including T-cell activation, transendothelial migration, and axon fasciculation (107,109,110). However, in the absence of a conventional activation mechanism, such as phosphorylation, binding of a metal ion cofactor, or conformational change, the regulation of ALCAM's function was not self-evident. Currently, two processes have been shown to contribute to ALCAM's function: 1) The proteolytic processing of the extracellular domain (ECD) (146,165), Hebron et al. under review) and 2) Anchoring ALCAM to the actin cytoskeleton though the intracellular domain (123,125). However, the regulation of ALCAM's function in these processes remain unclear.

In Chapter II, we present the first study to examine the biochemical and functional consequences of alternative splicing of exon 13 in *ALCAM*. We show that alternative splicing of *ALCAM* alters susceptibility to proteolysis and, in turn, modulates tumor cell adhesion, dissemination, and metastasis. Moreover, we show that ALCAM-Iso2, which is more susceptible to proteolysis than ALCAM-Iso1, is preferentially expressed in bladder cancer, compared to normal bladder tissue. Together, these data present an alternative splicing-dependent mechanism by which tumor cells alter cell adhesion to promote metastasis. Furthermore, this work raises several novel questions

including: 1) ALCAM-Iso2 is expressed in normal tissues, what is its role in normal physiology? 2) How does the loss of 13 amino acids in the juxtamembrane region of ALCAM-Iso2 both increase ectodomain shedding and unmask a novel proteolytic site? 3) To our knowledge, this is the first documented observation in which alternative splicing is responsible for unmasking a cleavage site distal to the spliced exon. Is this a common mechanism by which the function of immunoglobulin superfamily of cell adhesion molecules is regulated?

In Chapter III, we identify ALCAM as a novel binding partner of tetraspanin (TSPAN) CD151. We have previously shown that integrin-free CD151 ($CD151^{free}$, which is not associated with its canonical partner, integrin α3β1) is an important regulator of cancer metastasis that can be targeted by a metastasis-inhibiting monoclonal antibody mAB 1A5 (178,189). We show integrin-free CD151 ($CD151^{free}$) binds to ALCAM through intracellular interaction with the scaffolding protein, syntenin-1. This interaction is necessary for regulation of cell adhesion, migration, and metastasis by $CD151^{free}$ in response to mAB 1A5. Disruption of the interaction between ALCAM and syntenin-1 by release of the intracellular domain or ablation of ALCAM expression prevents $CD151^{free}$ from promoting adhesion and inhibiting metastasis in response to mAB 1A5. Moreover, ablation of CD151 expression prevents ALCAM from suppressing motility. Cumulatively, our observations describe a unique trimeric complex responsible for tunable regulation of cell adhesion. These findings prompt further investigation into several areas: 1) Is this complex found in normal cells? If so, what is its role? Is it cell type-specific? 2) Disruption of the CD151/syntenin-1/ALCAM complex significantly dampened the effect of mAB 1A5, but did not completely ablate it. Does $CD151^{free}$ have other undiscovered binding partners that participate in the regulation of tumor cell behavior? 3) Does ɣ-secretase-mediated cleavage regulate ALCAM's interaction with molecules other than CD151 and syntenin-1? 4) Does the ALCAM-ICD released by ɣ-secretase antagonize other PDZ motifs other than syntenin-1? If so, what are the broader consequences of antagonizing syntenin-1 and other PDZ-containing proteins?

This dissertation identifies two regulatory mechanisms of ALCAM function that are broadly applicable to both normal and pathological processes requiring modulation of adhesion. ALCAM has known roles in non-pathologic processes requiring static and

stable cell adhesion such as T-cell activation and maintenance of the blood-brain barrier (108,124,158), as well as roles in dynamic processes such as transendothelial migration and neuronal guidance (109,159). Additionally, CD151 has known roles in platelet aggregation, maintenance of epithelial integrity, and tubule formation. To this point, the vast majority of ALCAM function has been investigated using the canonical isoform, ALCAM-Iso1, and much of the investigation into CD151 has been in the context of its integrin-binding partners. We hypothesize that dynamic regulation of cell adhesion through either differential expression of *ALCAM* isoforms or through novel binding partners, such as CD151, would vastly improve our understanding of ALCAM- and CD151-mediated functions, both pathological and non-pathological.

Below, I highlight the major metastasis-related questions raised by the two regulatory mechanisms described in this dissertation.

Future Directions

With more than 90% of cancer-related deaths being attributed to metastatic spread of the disease, a deeper understanding of tumor cell dissemination has the potential to significantly improve patient care. The investigation of metastasis has three overarching objectives: (1) Identifying the patients most likely to progress to metastatic disease, (2) preventing the spread of localized disease, and (3) discovering therapies that effectively target both localized and systemic disease. The work presented herein has the potential to impact all three objectives.

Alternative splicing of ALCAM as a prognostic marker of progression

The expression of ALCAM has been examined extensively as a marker of tumor progression with conflicting results (111,112,134,135,162). However, shedding of the ALCAM ectodomain has consistently correlated with aggressive disease and poor patient outcome (113,114,147,149). In Chapter II, I demonstrated that the alternatively spliced ALCAM-Iso2 is significantly more susceptible to ectodomain shedding than the canonical isoform, ALCAM-Iso1. Additionally, I demonstrated that ALCAM-Iso2 is expressed 3-fold higher than ALCAM-Iso1 in bladder cancer tissue. Taken together,

these data present a strong foundation for an investigation into using the expression of ALCAM isoforms as a prognostic marker.

While ALCAM shedding has emerged as a reliable marker of aggressive disease, quantifying this process is not always straightforward. Quantification of ALCAM shedding in biofluids by ELISA is an attractive and clinic-friendly method, but not a viable option for all tumor types. In tumors with adjacent biofluids, such as ovarian (ascites) and bladder (urine), proteolysis of ALCAM is strongly associated with poor survival; however, that association is weakened or lost when it is measured in patient serum (114,149). Therefore, this method is not ideal for tumors without adjacent biofluids available. Direct detection of intratumoral ALCAM shedding by immunofluorescence is possible (113); however, standardizing quantification of immunofluorescence in the clinical environment is difficult. Examining ALCAM isoform expression as a prognostic biomarker may resolve this issue.

ALCAM isoform expression can be measured by two means. Traditional RNAseq analysis of isoform expression from bulk tumor tissue is straightforward and has been used extensively in the establishment of databases such as The Cancer Genome Atlas (TCGA, (173)). Because ALCAM is expressed in both stromal and tumor cells, it may be useful to analyze ALCAM isoform expression by cell type, rather than in the bulk tumor tissue. A commercial mRNA *in situ* hybridization technology called RNAscope® is a promising candidate for quantifying isoform expression *in situ* (217). This technology requires the detection of mRNA at two distinct sites for signal amplification to occur, thereby reducing noise and increasing specificity. With this technology, the quantification of ALCAM isoform expression *in situ* in paraffin embedded tissue may be developed as a reliable prognostic marker in several tumor types.

Combining ALCAM shedding and CD151^{free} as prognostic markers in prostate cancer

In Chapter III, we describe the discovery that ALCAM is a novel binding partner of integrin-free CD151 (CD151^{free}). We demonstrated that modulation of this complex regulates adhesion, migration, and metastasis. Previously, ALCAM was shown to interact with TSPAN CD9. This TSPAN stabilizes ALCAM's interaction with the actin cytoskeleton and prevents ADAM17-mediated ectodomain shedding of ALCAM (125). In

Chapter II, we show that alternative splicing of exon 13 in ALCAM-Iso2 unmasks a MMP14-sensitive proteolytic site distal from the previously identified ADAM17 site. This discovery is especially interesting and exciting because this site is outside of the alternatively spliced exon 13. Therefore, both ALCAM-Iso1 and ALCAM-Iso2 contain the site, yet only ALCAM-Iso2 seems to be cleaved at this membrane distal site. This suggests that either 1) the alternative splicing of exon 13 causes structural changes that reveal a cryptic proteolysis site, or 2) that structural modifications in the juxtamembrane region regulate intramembrane protein interactions (such as with TSPANs) that facilitate proteolytic processing at this membrane distal binding site. I hypothesize that differential TSPAN binding partners could be the mechanism by which ALCAM isoform shedding is regulated.

TSPAN are scaffolding proteins known to regulate the activity of their binding partners by coupling extracellular, transmembrane, and intracellular binding partners to potentiate transmembrane signaling (190,191). In Chapter III, we show that ALCAM and CD151 are linked through the scaffolding protein syntenin-1. NMR data suggests that the carboxy-terminal cytoplasmic tail of CD151 interacts with syntenin-1 PDZ1 domain while the intracellular domain of ALCAM interacts with syntenin-1 PDZ2. We also have data suggesting that TSPANs CD9 and CD63 interact with syntenin-1 PDZ1 (Fig. 30). Furthermore, CD151 is known to associate with and regulate MMP14. Remembering that CD9 has been previously shown to dampen ALCAM shedding (125) and that we have shown that ALCAM-Iso1 is shed up to 10-fold less than ALCAM-Iso2, it is reasonable to hypothesize that ALCAM-Iso1 may associate with CD9 while ALCAM-Iso2 may associate with CD151.

By identifying isoform-specific binding partners, we not only learn more about the regulation of ALCAM's function, but we may also strengthen the prognostic value of

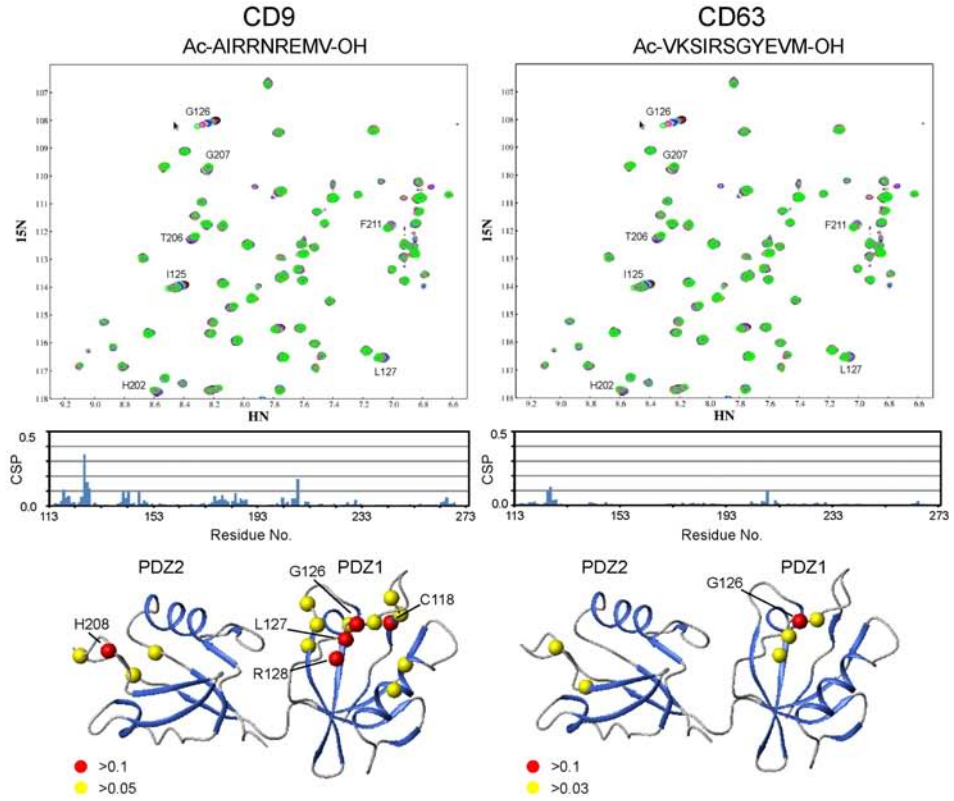

Figure 30. Tetraspanins CD9 and CD63 interact with syntenin-1 through PDZ1. Chemical shift perturbations (CSPs) measured in $^{1}H,^{15}N$-HSQC NMR spectra of syntenin-1 PDZ1/2 upon addition of the CD9, and CD63 peptides. HSQC spectra with 0 (black), 1 (red), 2 (cyan), 3 (blue), 4 (yellow), 5 (magenta), and 6 (green) molar equivalents of the peptides are overlaid (top panel). CSPs are plotted as a function of the residue number (middle panel). The residues that experienced CSPs of more than 0.05 (yellow) and 0.1 ppm (red) are highlighted on the crystal structure of syntenin-1 PDZ1/2 (PDB code: 1N99).

ALCAM by combining it with the expression of CD151^{free}. We have shown that CD151^{free} correlates with poor patient outcome in prostate cancer patients (189). We have also demonstrated that ALCAM is necessary for bone metastasis in mouse models of prostate cancer (165). We are currently investigating ALCAM shedding as a prognostic biomarker in bone metastatic prostate cancer with promising preliminary results (data not shown). Future investigations into isoform-specific TSPAN binding partners may support combining both ALCAM shedding or isoform expression with CD151^{free} to create a robust model for predicting prostate cancer patient outcome.

Modulating ALCAM function to prevent tumor cell motility

This thesis describes two mechanisms by which ALCAM function is regulated. It may be possible to exploit these two mechanisms to prevent the dissemination of tumor cells from the primary tumor. In Chapter II, I show that expression of ALCAM-Iso1 increases cell-cell adhesion, thereby reducing metastasis. In Chapter III, we show that tumor cells maybe immobilized through clustering of CD151^{free} in an ALCAM-dependent manner. Together, these data suggest that manipulation of ALCAM, either by modulation of alternative splicing, or through the TSPAN CD151, may be a mechanism by which tumor cell dissemination can be prevented.

Currently, the mechanisms controlling alternative splicing of ALCAM are unknown. However, controlling alternative splicing is emerging as an attractive therapeutic target in cancer research (184). Collaborations with the laboratory of John Lewis have also identified Serine/Arginine-Rich Splicing Factor Kinase 1 (SRPK1) as a metastasis promoter in a tumor migration screen deployed in the chick CAM, which further supports the notion that alternative splicing mechanisms are altered during cancer progression. Significant effort has been made to understand how aberrant dysregulation of alternative splicing occurs in cancer. Similar to adhesion molecules, spliceosome machinery is rarely mutated or deleted in cancer. The most common mechanism by which alternative splicing is dysregulated in cancer is through changes in expression or mislocalization of spliceosome *trans*-actors. By identifying the mechanism by which *ALCAM* is alternatively spliced, we may be able to promote cell-cell adhesion

and reduce tumor cell dissemination by therapeutically targeting alternative splicing machinery to promote ALCAM-Iso1 expression.

In Chapter III, we show that stabilization of the CD151/syntenin-1/ALCAM complex increases cell-cell adhesion, thereby decreasing cell motility and metastasis. While mAB 1A5 is capable of stabilizing this complex, it is not a viable therapy because of severe on-target side effects, such as blot clotting due to platelet aggregation. Because we now know that ALCAM is necessary for the effect of mAB 1A5, it may be possible to identify other antibodies or biotherapeutics capable of stabilizing the complex through either ALCAM or syntenin-1, in order to avoid these on-target side effects.

ALCAM-Iso1 and ALCAM-Iso2 have diverging effects on proliferation

Although this dissertation focuses on the effect ALCAM in the context of cell adhesion, it has been investigated in several other biological processes including proliferation and prevention of apoptosis (112,165,218). We have preliminary evidence suggesting that alternative splicing of *ALCAM* may affect tumor cell proliferation. Both *in vitro* and *in vivo,* cells expressing ALCAM-Iso2 proliferated significantly faster than cells expressing ALCAM-Iso1 (Fig. 31). *In vitro*, cells expressing ALCAM-Iso1 have a doubling time of 38.7 h, while ALCAM-Iso2 cells have doubling time of just 25.4 h, indicating that expression of ALCAM-Iso1 slows cell proliferation by more than 50% (Fig. 31a). *In vivo,* this translates to a two-fold reduction in tumor size for cells expressing ALCAM-Iso1 (Fig. 31b). Because of this drastic difference in proliferation, cells expressing ALCAM-Iso2 may be more sensitive to chemotherapeutics than cells expressing ALCAM-Iso1. If this hypothesis is indeed true, ALCAM isoform expression may emerge as a useful biomarker capable of predicting response to therapy.

ALCAM-mediated regulation of adhesion is cell- and context-dependent

Data in Chapter III suggests that KO of ALCAM in the fibrosarcoma cell line HT1080 not only increases cell proliferation (as measured by xenograft weight), but also

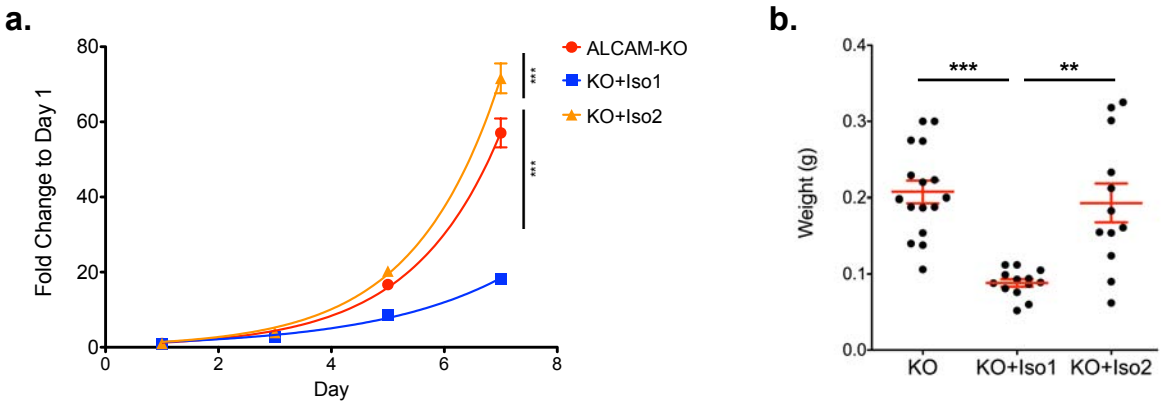

Doubling Time (h)

ALCAM-KO	26.0
KO+Iso1	38.7
KO+Iso2	25.4

Figure 31. Alternative splicing of ALCAM affects tumor cell proliferation. (**a**) *In vitro* proliferation of ALCAM-knockout HT1080 cells (ALCAM-KO) expressing ALCAM-Iso1 (KO+Iso1) or ALCAM-Iso2 (KO+Iso2). Proliferation was measured as fold change in bioluminescence compared to initial reading (day 1). ***P<0.0001. (**b**) Wet weight of HT1080 xenografts removed from CAM of chicken embryos. Three independent experiments were combined for the analysis (N= 16, 13, 12, respectively). P-values were calculated using Mann-Whitney-U test, **P<0.001, ***P<0.0001.

promotes metastasis in the avian embryo model of metastasis. However, we have previously shown that ALCAM knockdown in the epithelial-derived PC3 prostate cancer cell line inhibits the formation of bone metastases in nude mice (165). Because these data differ in both cell type and model, the conflict is difficult to interpret and warrants further investigation into the effect of the loss of ALCAM on metastasis. These data suggest that ALCAM's contribution to metastasis is likely very cell-type and context dependent. This emphasizes the need to investigate the modulation of ALCAM function in multiple models and, most importantly, to validate as many of these findings in human tissue as possible.

Concluding Statements

This dissertation identifies two mechanisms by which the function of ALCAM is regulated. The nuances of the data suggest that processes such as alternative splicing and microdomain localization are largely responsible for regulation of ALCAM's function. As we learn more about how the function of ALCAM is regulated, we will be able to better predict the effect of ALCAM in specific contexts by considering isoform expression as well as known binding partners. Our work presented herein not only furthers our understanding of the ALCAM's contribution to tumor cell adhesion and dissemination, but also lays the groundwork for future studies with the potential to advance cancer patient care through the establishment of a robust biomarker of cancer progression, as well as revealing previously unexplored therapeutic targets.

Furthermore, our work focuses on the role of ALCAM in metastasis. However, the impact of our findings reaches far beyond cancer. ALCAM has established roles in hematopoiesis, immune cell function, and neuronal migration (108-110,219). The function of ALCAM in these processes must be re-examined in the context of our findings, especially the differential function of ALCAM isoforms. By reevaluating the function and expression of individual ALCAM isoforms in each of these processes, we will exponentially increase our understanding of ALCAM as an adhesion molecule.

Finally, this work provides two mechanisms of function regulation that may be broadly applicable to other cell adhesion molecules. Many Ig-CAMs lack the

aforementioned traditional activation motifs. The function of these molecules is often context dependent. This work warrants further investigation into the alternative splicing and differential binding partners of Ig-CAMs whose regulation is not yet elucidated.

Appendix A:

FLUORESCENT BARCODING OFFERS INCREASED DIMENSIONALITY IN TRACKING TUMOR CELLS *IN VITRO* AND *IN VIVO*

Contributing Authors: Katie E. Hebron, Tatiana Ketova, Shanna Arnold Egloff, Patrick Mulcrone, H. Charles Manning, Julie Sterling, Florent Elefteriou, and Andries Zijlstra

Summary

The understanding of metastasis has greatly improved as the field has developed tools allowing researchers to visualize the process. However, investigators are still quite limited in their ability to track the metastasis of multiple cell populations. This is becoming increasingly important because tumor heterogeneity has been shown to significantly affect metastasis. Therefore, it is important to develop novel technologies that will help us investigate tumor heterogeneity and how it affects patient care. Here we present a novel fluorescent protein barcoding system that will aid in the study of tumor heterogeneity and metastasis. Real-time and longitudinal imaging of tumors in animal models is a critical element in monitoring tumor burden, growth, and metastatic dissemination. To improve utility of current imaging technologies, we have developed a library of fluorescent and luminescent tracking vectors designed to permit *in vivo* multiplexing through fluorescent barcoding. Our vectors express firefly luciferase and one of six unique fluorescent proteins. The combination of luciferase and fluorescent labeling allows us to monitor tumor growth by luciferase activity and distinguish individual cell populations by their fluorescent label. Using barcoded cell lines, we have demonstrated that the six FPs are uniquely identifiable by spectral imaging and by flow cytometry. We have improved quantification and evaluation of metastasis in avian embryo metastasis models. We have used these lines to investigate tumor heterogeneity in a mouse model of skeletal metastasis. Additionally, we determined that dissemination of breast cancer cells to the bone is a cooperative event, whereby multiple tumor cells are able to seed and proliferate in a single site.

Introduction

The vast majority of cancer-related deaths are due to dissemination from the primary tumor (2). However, improvement to the care of patients with metastatic disease has been slow. Metastasis research often revolves around three broad questions: 1) Why do tumor cells leave the primary tumor microenvironment? 2) What mechanisms allow tumor cells to leave the primary tumor and survive at a secondary site? 3) Why do metastases often respond to therapy differently from the primary tumor? While the field has made significant advances in understanding the process of metastasis, technical difficulties limiting the visualization and quantification of metastasis continue to hinder metastasis research (36, 220). Furthermore, the inherent heterogeneity of metastasis calls for the examination of several subpopulations in a single experiment (221). The development of tools that allow for the simultaneous tracking and quantification of several cell populations would greatly improve investigators' ability to address the three major questions outlined above.

Several technologies have been developed in the past two decades in an effort to aid metastasis research, however, the visualization and quantification of multiple cell populations in a single model remains difficult without the use of highly specialized equipment that is not commonly accessible. For example, intravital multiphoton microscopy has revolutionized realtime, *in vivo* investigation of cell behavior (36, 220). However, this technology is not readily accessible to all investigators. Furthermore, while this technology is well suited for analysis of individual cell phenotypes, it is not particularly useful for broad quantification of metastatic subpopulations.

Another imaging modality, bioluminescence, has greatly improved investigators' ability to quantify tumor burden in a highly sensitive, non-invasive, longitudinal fashion (222). However, due to lack of diversity in the luciferase genes, multiplexing the analysis of several cell populations within a single *in vivo* model is difficult. Renilla and firefly luciferases (RLuc and FLuc, respectively) are often multiplexed *in vitro* for dual reporter assays, but their usefulness as dual quantitative markers *in vivo* is complicated by substrate bioavailability and enzyme kinetics (223).

Cloning and exogenous expression of green fluorescent protein (GFP) from

Aequorea victoria, allowed for direct visualization of cells and proteins marked with this gene (224, 225). This finding lead to significant advances in the understanding of cell and molecular biology. The discovery and development of additional fluorescent proteins with different spectral profiles has allowed for the effective marking, tracing, and multiplexed analysis of several cell populations at once. To date, the most notable uses of this technology rely on red-green-blue (RGB) marking, which is the random expression of one or more fluorescent proteins in each cell and it's subsequent progeny (226, 227). This method of cell marking provides an effective method of lineage tracing and has lead to significant discoveries in the investigation of the cell of origin in several cancers (228, 229). However, because this technology relies on random recombination, it does not provide investigators complete control over the labeling of diverse cell populations.

DNA barcoding, which is the insertion of short DNA tags into a cell's genome, allows for effective quantification of subpopulations, but lacks modalities for *in vivo* visualization and tracking (230). Additionally, because the DNA barcode is quantified by polymerase chain reaction, concomitant analysis of cell properties, such as protein expression, is difficult.

Ideally, to effectively investigate the heterogeneity of metastasis, and thereby begin to address the three questions posed above, investigators require accessible tools that 1) allow directed and stable labeling of cell subpopulations, 2) provide longitudinal monitoring of tumor burden, 3) enable direct visualization within the model, and 4) permit simultaneous single cell analysis of properties such as protein expression. Herein, we describe a technology, pRainbow, that meets the aforementioned requirements and demonstrate its effectiveness as a tool for metastasis research.

Materials and Methods

Cell culture

HT1080 (fibrosarcoma) and HEK293T cells were obtained from the ATCC (CCL-121 and CRL-1573, respectively). MDA-MB-231 cells were obtained from Dr. Julie Sterling at Vanderbilt University and subsequently genetically fingerprinted to verify identity. To obtain a bone metastatic cell line, MDA-MB-231 cells were injected into a nude mouse via intracardiac injection and subsequently isolated and expanded from tibial metastases to generate bone-specific variants of MDA-MB-231. Cell lines were maintained in RPMI (HT1080) or DMEM (HEK293T and MDA-MB-231) supplemented with penicillin/streptomycin, sodium pyruvate, non-essential amino acids and 10% fetal bovine serum and cultured at 37°C with 5% CO_2.

Vector library construction

The pRainbow vector library was constructed using Gateway Multisite-Pro vector recombination system (ThermoFisher Scientific). Vectors were constructed using a three fragment recombination strategy where fragment “A”, human codon-optimized firefly luciferase gene, was synthesized in pENTR 221 L1-L4, fragment “B”, P2A self cleaving peptide sequence, was synthesized in pENTR 221 L4r-L3r, and fragment “C”, one of the six human codon-optimized fluorescent protein genes (TagBFP (231), Cerulean (232), TagGFP2 (Evrogen), Citrine (233), TagRFP (234), mKate2 (235)), was synthesized in pENTR 221 L3-L2. The three pENTR vectors (50 ng) were mixed with pLenti 6.2/V5-DEST (150 ng) and incubated with LR Clonase II enzyme at room temperature for 1 hour for recombination. Successful recombination was verified by PCR and enzyme digest.

Stable cell line generation

Lentiviral particles were produced in LentiX 293T cells (Clontech). Transductions were performed with 5 μg/mL polybrene. Cells were selected with blasticidin (ThermoFisher Scientific, 25 μg/mL for MDA-MB-231 or 10 μg/mL for HT1080) for 2 weeks. Cells were expanded in the absence of blasticidin for 3-4 weeks and selected for

the top 25% of the fluorescent population by fluorescent activated cell sorting (FACS).

In vitro proliferation assay

MDA-MB-231 cells stably transduced with pRBow vectors and parental MDA-MB-231 cells were plated in 96 well tissue culture treated plates (2,000 cells/well). Plates were incubated at 37°C with 5% CO_2. Beginning 24 h after plating, cells were incubated with 20 µL MTT (5 mg/mL) for 4 h. Medium was gently removed and crystals were dissolved with 150 µL solvent (100% isopropanol, 0.1% w/vol NP-40, 4 mM HCl). Reduction of MTT was quantified by absorbance at 590 nm with reference at 620 nm using an automated plate reader (BioTek).

Avian embryo metastasis assays

Spontaneous and experimental metastasis experiments were performed as described previously (167, 168). In accordance with the Public Health Services policy on Humane Care and Use of Laboratory Animals, Vanderbilt Institutional Animal Care and Use Committee (IACUC) has determined that avian embryos developmental day 17 and younger are not considered vertebrate animals and therefore do not require specific protocol approval. Vanderbilt IACUC has reviewed and approved the following experimental and euthanasia procedures.

Ectopic cell titration

Fertilized chicken eggs were placed in a 37°C incubator at 55% relative humidity on day 1 post-fertilization. On day 15 post-fertilization, eggs were removed from the incubator, the eggshell was cut in half along the long axis, chicks were dissected from the shell, embryos were euthanized by decapitation, and sections of the distal CAM were dissected using a cork borer. HT1080 cells stably expressing pRBow-RFP were dissociated, counted, and resuspended in sterile 0.9% saline at 2.5×10^5 or 2.5×10^4 cells/mL. A suspension of 25,000; 12,500; 6,250; 3,125; 2,500; 1,250; 625; or 312 cells was ectopically placed on dissected CAM sections in duplicate. D-luciferin (150 µg/mL) was added to the cell suspension and luciferase activity was quantified using a digital gel documentation system (G:Box; Syngene).

Ex ovo experimental metastasis (Intravenous injection)

Fertilized chicken eggs were placed in a 37°C incubator at 55% relative humidity on day 1 post-fertilization. On day 4 post-fertilization, embryos were removed from their eggshell, transferred to a sterilized square polystyrene weighing dish, covered with a square petri dish, and returned to the incubator. Day 10 embryos were injected with 100 µL HT1080 pRBow-RFP cell suspension (25,000; 12,500; 6,250; 3,125; or 1,500 cells) and returned to incubator for 72 hours. Day 13 embryos were injected with 50 µL D-luciferin (15 mg/mL) and luciferase activity was quantified using a digital gel documentation system (G:Box; Syngene).

In ovo spontaneous metastasis (Xenografting)

Fertilized chicken eggs (Tyson Foods, Inc., Springdale, Arkansas) were placed in a 37°C incubator at 55% relative humidity on day 1 post-fertilization. The chorioallantoic membranes (CAM) of day 10 embryos were dropped away from the eggshell by displacing the air cell. HT1080 cells stably expressing pRBow-BFP, pRBow-Citrine, or pRBow-RFP were dissociated, counted, and resuspended at a 1:1:1 ratio in sterile 0.9% saline at 20 x 10^6 cells/mL. The dropped CAM was damaged slightly with sterile cotton tipped swabs. 25 µL of cell suspension (500,000 cells) were placed on the dropped CAM and eggs were returned to the incubator. After 5 days of growth, embryos were euthanized by decapitation, xenografts were harvested, the eggshell was cut in half along the long axis, chicks were dissected from the shell, and sections of the distal CAM were dissected using a cork borer. Xenografts and dissected CAM sections were imaged in blue, green and red fluorescent channels using stereo microscope (Lumar.V12, Zeiss, Oberkochen, Germany).

<u>Mouse experimental metastasis assay</u>

Vanderbilt IACUC has reviewed and approved the following experimental and euthanasia procedures.

Intracardiac injection and longitudinal monitoring

Intracardiac (IC) injection was performed as described previously (ref). Briefly, cells were dissociated, counted and resuspended at 1 x 10^6 cells/mL in sterile PBS. All six MDA-MB-231 pRBow cell lines were mixed at equal proportions prior to injection. 100 µL cell suspension (100,000 cells) were injected into the left ventricle of Nude mice. Beginning 72 hours post IC injection, skeletal metastases were monitored weekly by detection of luciferase expressing cells and formation of bone lesion by X-ray. Whole animal luminescent imaging was performed with the IVIS™ system (Caliper Life Sciences, Hopkinton, MA). D-luciferin (150 mg/kg in sterile PBS, Biosynth International, Itasca, IL) was delivered via intraperitoneal injection 10 minutes prior imaging. Radiographic images (Faxitron X-ray Corp, Lincolnshire, IL, USA) were obtained using an energy of 35 kV and an exposure time of 8 seconds.

Sample harvest and preparation

Animals were euthanized upon meeting end point criteria. Lung, liver, brain, long bones, skull, mandible, spine, and pelvis were harvested. Muscle tissue was dissected from bones before *ex vivo* spectral imaging (see below) of all samples. After ex vivo imaging, soft tissue and bone tissues were minced with a clean razor blade and digested for 1.5 h at 37℃ in digestion buffer (2 mg/mL collagenase Type II, 100 U/mL Hyaluronidase in antibiotic free complete medium). As necessary, long bones were flushed with saline using syringe fitted with 18G needle to extract bone marrow prior to digest. Digested samples were strained through 70 µm mesh filters to remove undigested portions. Red blood cells were lysed with RBC lysis buffer (Biolegend, San Diego, California). Cells were stained with Alexa-647 conjugated anti-hCD151 (1A5, (201)) to label human cells, and Zombie NIR Viability Dye (Biolegend).

Spectral imaging

Samples were imaged using Maestro™ multispectral imaging system (CRi, Woburn, Massachusetts). Fluorescence emission was acquired in 10 nm steps from 500 to700 nm. Spectral library was established using pure cell populations and unlabeled mouse tissue, as necessary, with CPS™ (Compute Pure Spectrum) software.

Quantitative spectral unmixing was performed with RCA™ (Real Component Analysis) software.

Flow cytometry

All data was acquired using a Beckton Dickinson LSR Fortessa Special Order Research Product (SORP) (La Jolla, California) with indicated filter configuration (Table 7). During data acquisition 10,000 single tumor cells were collected from each tumor sample, when available. If 10,000 tumor cells were not available, the entire tumor was acquired for analysis. All gated analysis of tumor samples was performed using FlowJo (Tree Star, Inc., Ashland, Oregon). Tumor cells were identified initially by their forward (FSC-A) and side (SSC-A) laser scatter properties. Doublet discrimination-based gating was used to identify single cells. Zombie NIR was plotted against Alexa 647-conjugated anti-hCD151 to further specify viable human tumor cells. Each sample was then analyzed for the presence of: BFP, Cerulean, GFP, Citrine, RFP, or mKate (Fig. 37). The proportion of all cells expressing a fluorescent protein was analyzed and reported per sample in heat map form.

Results

pRainbow labeling vectors offer both longitudinal and endpoint monitoring of up to 6 unique populations

We constructed a panel of labeling vectors, called pRainbow (pRBow) using the MultiSite Gateway vector recombination system (ThermoFisher). The vectors are composed of 3 core sections: A. firefly luciferase gene, B. P2A sequence, C. fluorescent protein (FP) gene on the pLenti6.2/V5-DEST lentiviral backbone (ThermoFisher) with CMV promotor (Fig. 32a). Longitudinal, noninvasive bioluminescent monitoring of tumor burden is made possible with expression of firefly luciferase, while expression of one of six FPs allows for labeling and identification of up to six unique populations. The two genes are separated by self-cleaving P2A peptide sequence to promote equal expression of both genes (236,237). Stable expression of these labeling vectors has no impact on proliferation rate (Fig. 32b).

Laser wavelengh	Fluorophore	Long Pass Mirror (nm)	Bandpass Filter (nm)
405	BFP	N/A	450/50
	Cerulean	470	473/12
488	GFP2	505	515/20
	Citrine	525	530/30
561	RFP	585	585/40
	mKate	635	675/20
640	1a5	N/A	670/14
	Zombie NIR	735	780/60

Table 7. Filter setup for flow cytometry. Instrument configuration for flow cytometry data acquisition.

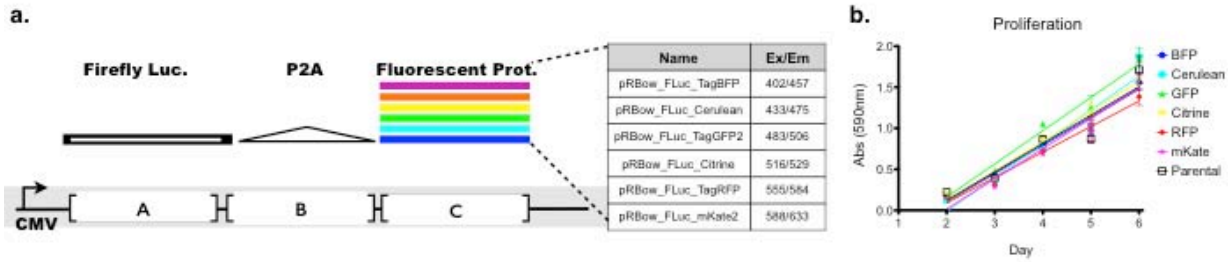

Figure 32. pRainbow design and validation. (**a**) Schematic depicting pRainbow (pRBow) vector design. Luc.: luciferase; FLuc: firefly luciferase. (**b**) *In vitro* proliferation of MDA-MB-231 cells stably expressing one of the six pRBow vectors as indicated, measured by MTT reduction.

Despite overlapping emission spectra of the six FPs (Fig. 33a), advances in spectral imaging and flow cytometry technology allow for unique identification of each FP by different modalities. Using the Maestro™ spectral imaging system, we are able to uniquely identify four populations. Due to physical limits of the instrument, emission spectra below 500 nm are not well tolerated. Therefore, BFP is not detectable and GFP and Cerulean show some overlap (Fig. 33b). In our system, GFP, Citrine, RFP and mKate2 are the best FPs for imaging with the Maestro™ spectral imaging system.

We next tested the unique identification of each FP by flow cytometry. Using the filter configuration described in Table 7, we were able to uniquely identify each of the six FP (Fig. 33c, single color). To confirm that there was no overlap in detection of each FP, we also examined fluorescence minus one (FMO) samples, where each sample is composed of five of the six FPs, systematically removing one FP at a time. Using this approach, we confirmed that each FP was uniquely identifiable by flow cytometry (Fig 33c, FMO).

Prolonged proliferation in the absence of antibiotic selection stabilizes pRBow expression

Stable cells lines were established by lentiviral transduction, antibiotic selection with blasticidin, followed by fluorescent activated cell sorting (FACS) for the top 25% of the fluorescent population. Longitudinal monitoring of pRBow FP expression in stable MDA-MB-231 cells after recovery from cryopreservation showed that the percent of FP expressing cells dropped for 3 weeks and subsequently stabilized (Fig. 34a). Because these cell lines were grown in the absence of blasticidin, we tested if treatment with blasticidin would restore pRBow expression in the negative population. Following one week of blasticidin treatment, the percent of FP cells increased in each stable pRBow cell line (Fig. 34b). There was no significant increase in cell death for blasticidin treated versus untreated cells (data not shown). We hypothesized that the negative population had not lost the pRBow vector, but shut down its expression, and that culture in blasticidin artificially enhanced expression of the pRBow vector. Therefore, we tested the stability of FP expression in the pRBow cell lines after prolonged culture in the absence of blasticidin. The expression of pRBow FP was indeed stable after 5 weeks of

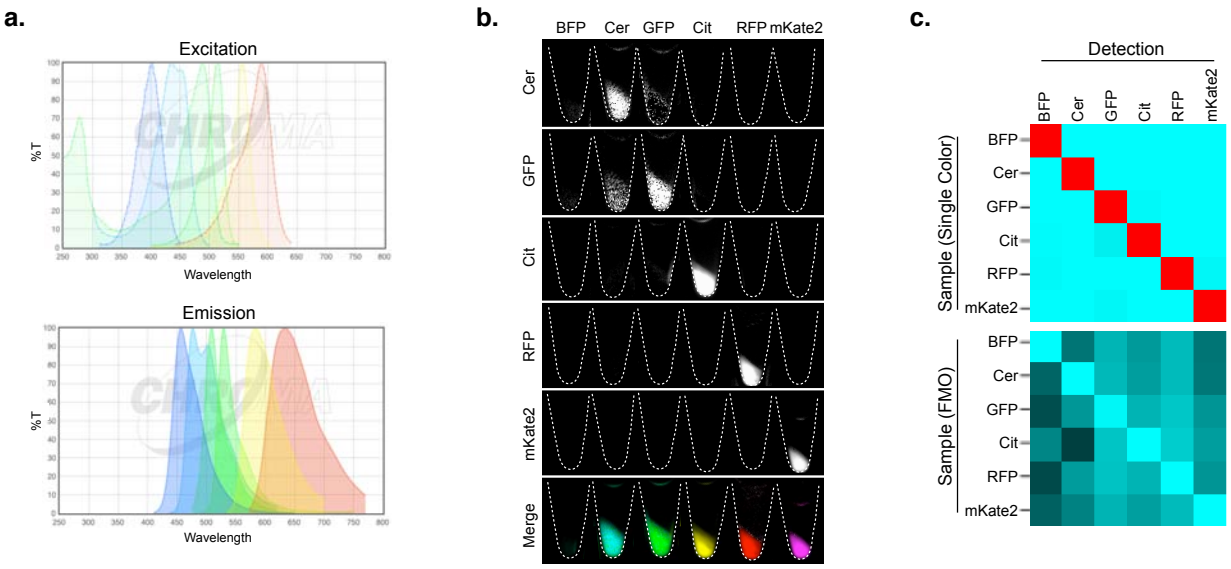

Figure 33. pRainbow vectors are uniquely identifiable by spectral imaging and flow cytometry. (**a**) excitation and emission spectra of each fluorescent protein in pRBow vector library, extracted from **https://www.chroma.com/spectra-viewer**. (**b**) Spectral imaging and subsequent separation of HEK293T cells transiently transfected with indicated pRBow vectors. (**c**) Heat map of fluorescent protein signal from single color controls and fluorescence minus one (FMO) controls as detected by flow cytometry.

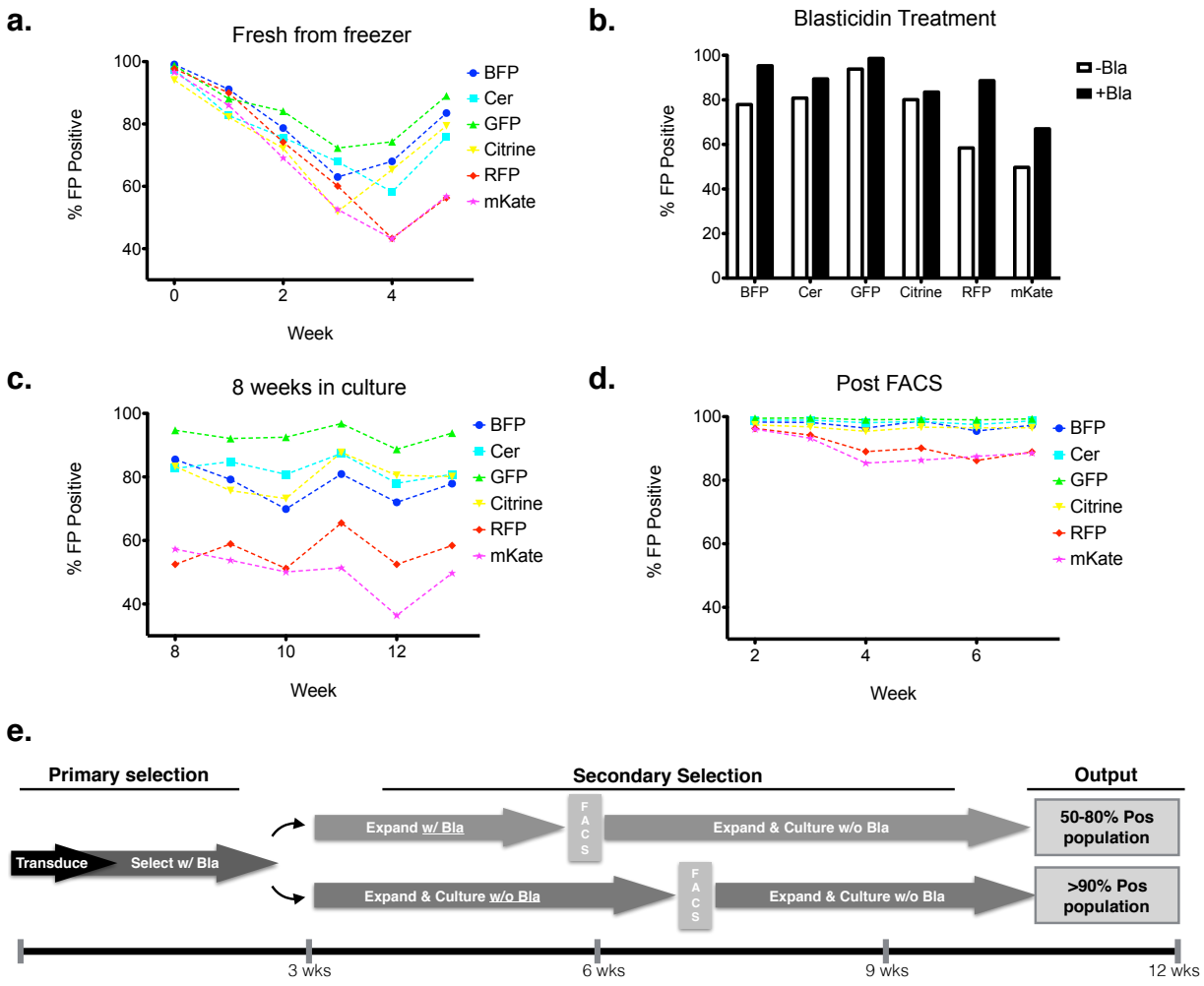

Figure 34. Expression of pRBow vector is stable following three week hiatus from blasticidin selection. (**a**) Longitudinal analysis of MDA-MB-231 cells stably expressing the indicated pRBow vector following recovery from cryopreservation. Percent of fluorescent positive cells determined by flow cytometry. Cells were grown in the absence of blasticidin. (**b**) Percent of fluorescent positive MDA-MB-231 cells stably expressing indicated pRBow vector with and without one week of treatment with blasticidin (25 μg/mL). (**c**) Longitudinal analysis of MDA-MB-231 cells stably expressing indicated pRBow vector. Percent of fluorescent positive cells determined by flow cytometry. Cells were grown in the absence of blasticidin for the indicated time. (**d**) Longitudinal analysis of MDA-MB-231 cells stably expressing indicated pRBow vector after fluorescence-activated cell sorting (FACS) following growth in absence of blasticidin for three weeks. Percent of fluorescent positive cells determined by flow cytometry. Cells were grown in the absence of blasticidin. (**e**) Schematic depicting timeline and outcome of selection with and without blasticidin hiatus.

growth in the absence of blasticidin treatment (Fig. 34c). This phenomenon suggested that the increase in non-fluorescent cells observed after recovery from cryopreservation was not due to expansion of a vector negative population, but is more likely due to silencing of the vector in a subpopulation. FACS following an extended (4 week) blasticidin hiatus resulted in cell lines stably expressing the pRBow vectors in >90% of the cell population even after 6 weeks of growth in the absence of blasticidin (Fig. 34d). Taken together, these data suggest that the most effective method of stable cell line production includes a prolonged blasticidin hiatus prior to FACS (Fig. 34e).

Metastasis in the avian embryo model is efficiently and simply quantifiable using cells expressing pRBow vectors

The avian embryo model is an effective tool for efficient *in vivo* study of angiogenesis and tumor cell motility and metastasis (238). However, quantification of metastasis in the avian embryo model by human alu PCR (167) is both time and resource consuming. We hypothesized that the pRBow labeling vector could improve quantification of metastasis in the avian embryo metastasis models. To test this hypothesis, we analyzed the luciferase activity of HT1080 cells stably expressing pRBow-RFP after ectopic placement on dissected sections of chorioallantoic membrane (CAM). The luciferase activity of these cells linearly correlated with cell number (Fig. 35a, r^2=0.9869), indicating that luciferase activity could be used as a surrogate for cell number in this model.

We next tested the use of luciferase activity as a reporter of metastatic burden in the *ex ovo* experimental metastasis avian embryo model. Shell-less embryos were injected with increasing numbers of HT10080 pRBow-RFP cells into the allantoic vein. After 72 h growth, whole animal luciferase activity was measured. As expected, the number of luciferase positive colonies increased exponentially with the number of cells injected (Fig. 35b, R^2= 0.9391). These data support the use of luciferase activity as a surrogate marker for metastatic burden in the avian embryo model.

Finally, we examined spontaneous metastasis by seeding tri-color (pRBow-BFP, Citrine, or RFP) xenografts (Fig. 35c, i) and detecting metastasis to the distal CAM using fluorescent microscopy. We confirmed that we were able to effectively detect

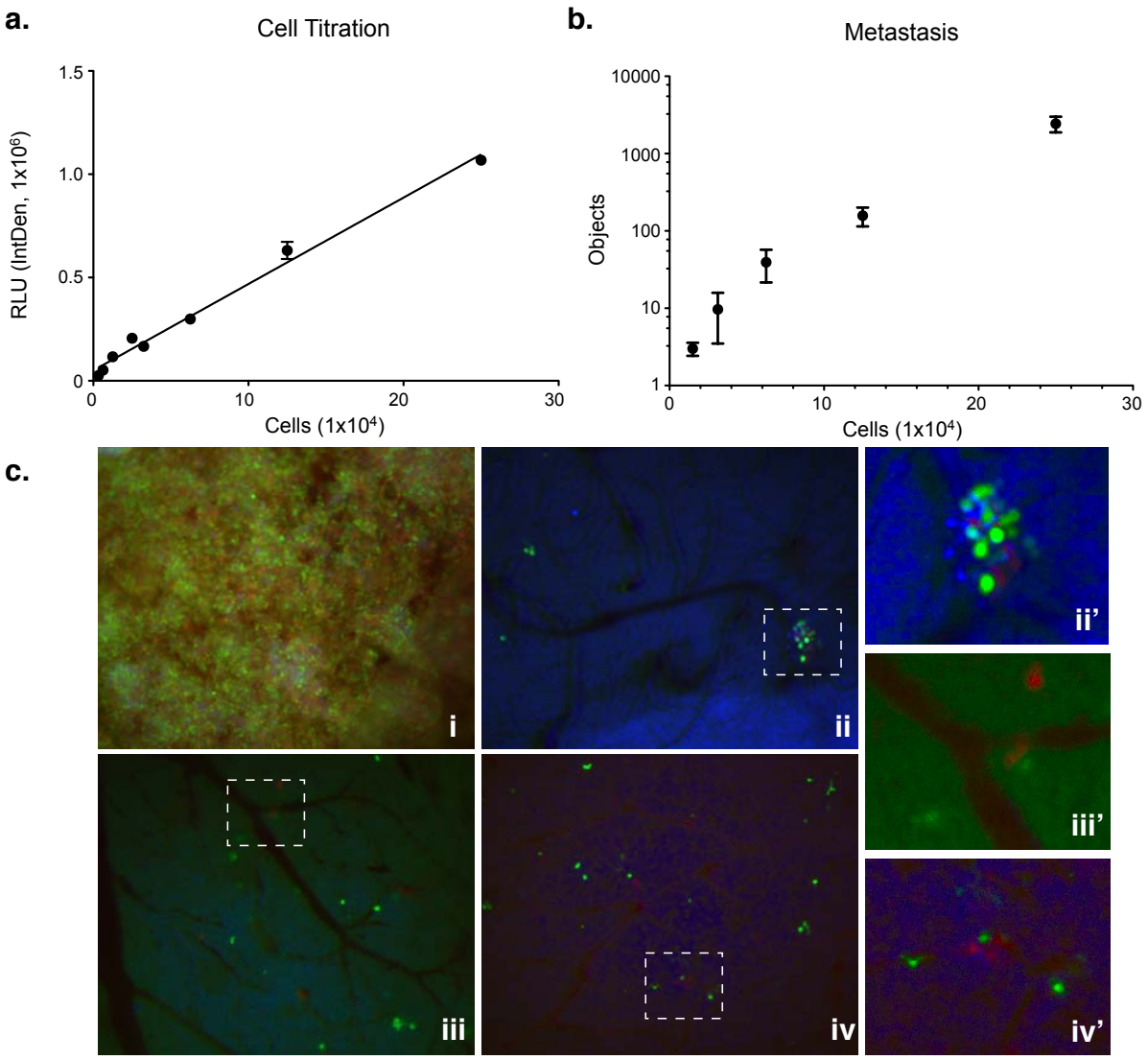

Figure 35. Metastasis in the avian embryo model is efficiently and simply quantifiable using cells expressing pRBow vectors. (**a**) Quantification of experimental metastasis of HT1080 cells stably expressing pRBow-RFP vector using luciferase activity. (**b**) Quantification of luciferase activity in HT1080 cells stably expressing pRBow-RFP ectopically placed on dissected avian embryo CAM. (**c**) Fluorescent imaging of primary tumor (i) and spontaneous metastases (ii-iv) using avian embryo model of spontaneous metastasis with HT1080 cells stably expressing pRBow-BFP, pRBow-Citrine, or pRBow-RFP. Higher magnification image corresponds with dashed outline.

metastatic colonies by epifluorescence (Fig. 35C, ii-iv). Interestingly, we also observed several multi-colored metastatic colonies (Fig. 35c, ii'-iv'), suggesting that these colonies were seeded by multiple tumor cells, in other words, were polyclonal. Therefore, we then investigated the clonality of metastasis using the full panel of pRBow MDA-MB-231 cells in a nude mouse model of skeletal metastasis.

Breast cancer metastasis to bone is a polyclonal process

To examine the clonality of breast cancer metastasis, equal portions of each MDA-MB-213 pRBow cell line were combined and injected into nude mice via intracardiac injection (Fig. 36a). Tumor burden was monitored longitudinally by bioluminescence. At end point, soft tissue and bone were analyzed by *ex vivo* spectral imaging. Representative images showing colocalization of several distinct pRBow populations within the same lesions are displayed (Fig. 36b). Similarly, single cell analysis by flow cytometry (Fig. 37) detected more than one pRBow label in the majority of tissues collected (Fig. 36c). Across all mice, 75% of samples collected contained cells from more than one pRBow cell line, as detected by flow cytometry. Furthermore, nearly 50% of all samples contained three or more pRBow cell lines (Fig. 36d).

Of note, we also demonstrate that proper processing of bone metastases is required for complete detection of all tumor cell subpopulations (Fig. 38a). The standard protocol to examine tumor burden in long bong tissue samples is by bone marrow flush. However, we demonstrate that this technique inefficiently extracts long bone metastases (Fig. 38b). Extracting bone metastases by whole bone digest provides a more accurate representation of the tumor heterogeneity of bone metastasis (Fig. 38c). Together, these data indicate that breast cancer metastases are often polyclonal, as demonstrated by the presence of more than one pRBow label in the majority of analyzed samples.

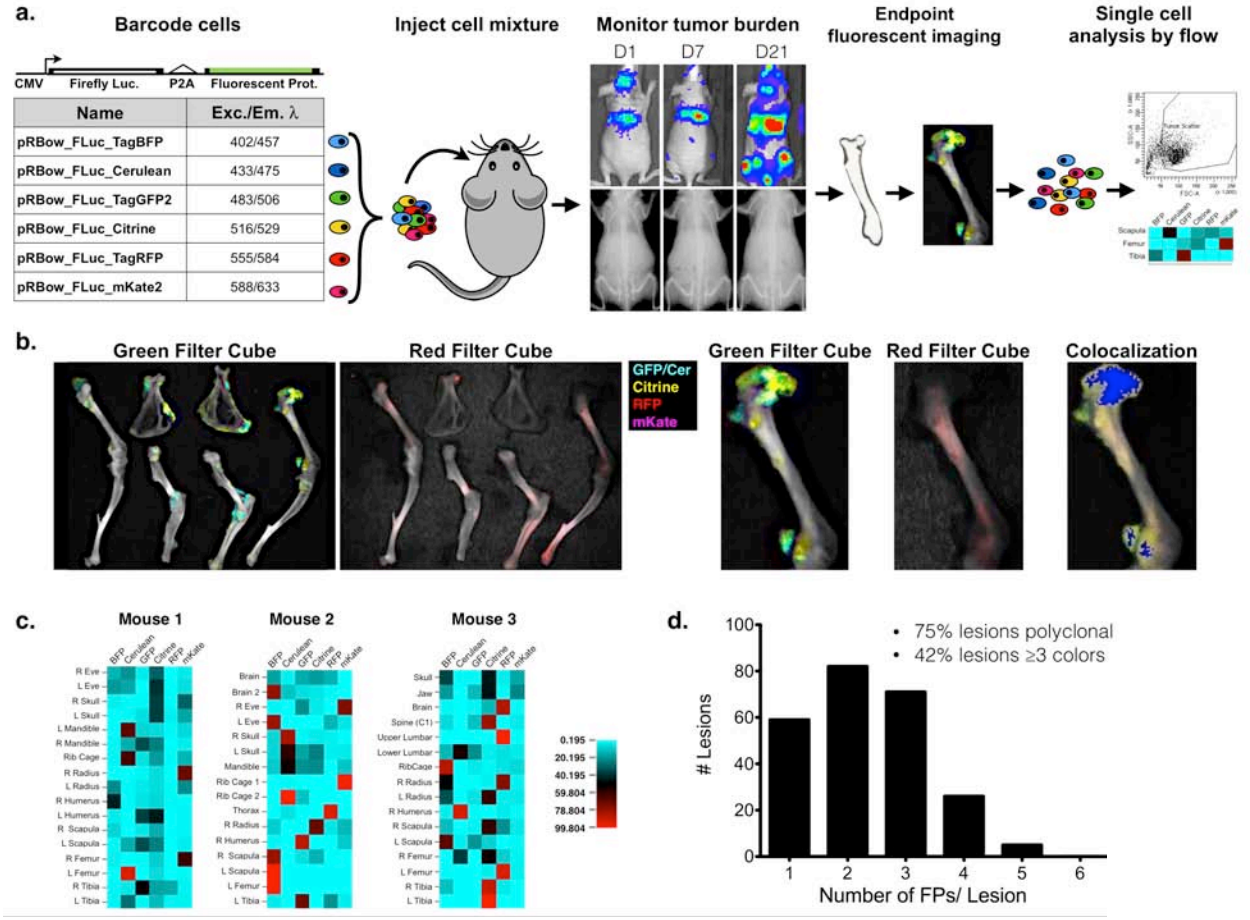

Figure 36. Breast cancer metastasis to bone is a polyclonal process. (**a**) Schematic depicting experimental design. (**b**) *Ex vivo* spectral imaging of bones from representative mouse. Insets show examples of polyclonal, multicolored metastases. Signal colocalization is indicated by blue shading. (**c**) Representative heat maps of color distribution in indicated sample. (**d**) Distribution of clonality across all samples in all mice. Samples containing cells from two or more pRBow populations were considered polyclonal. Only pRBow populations contributing 10% or more of the total sample population were considered for determination of clonality.

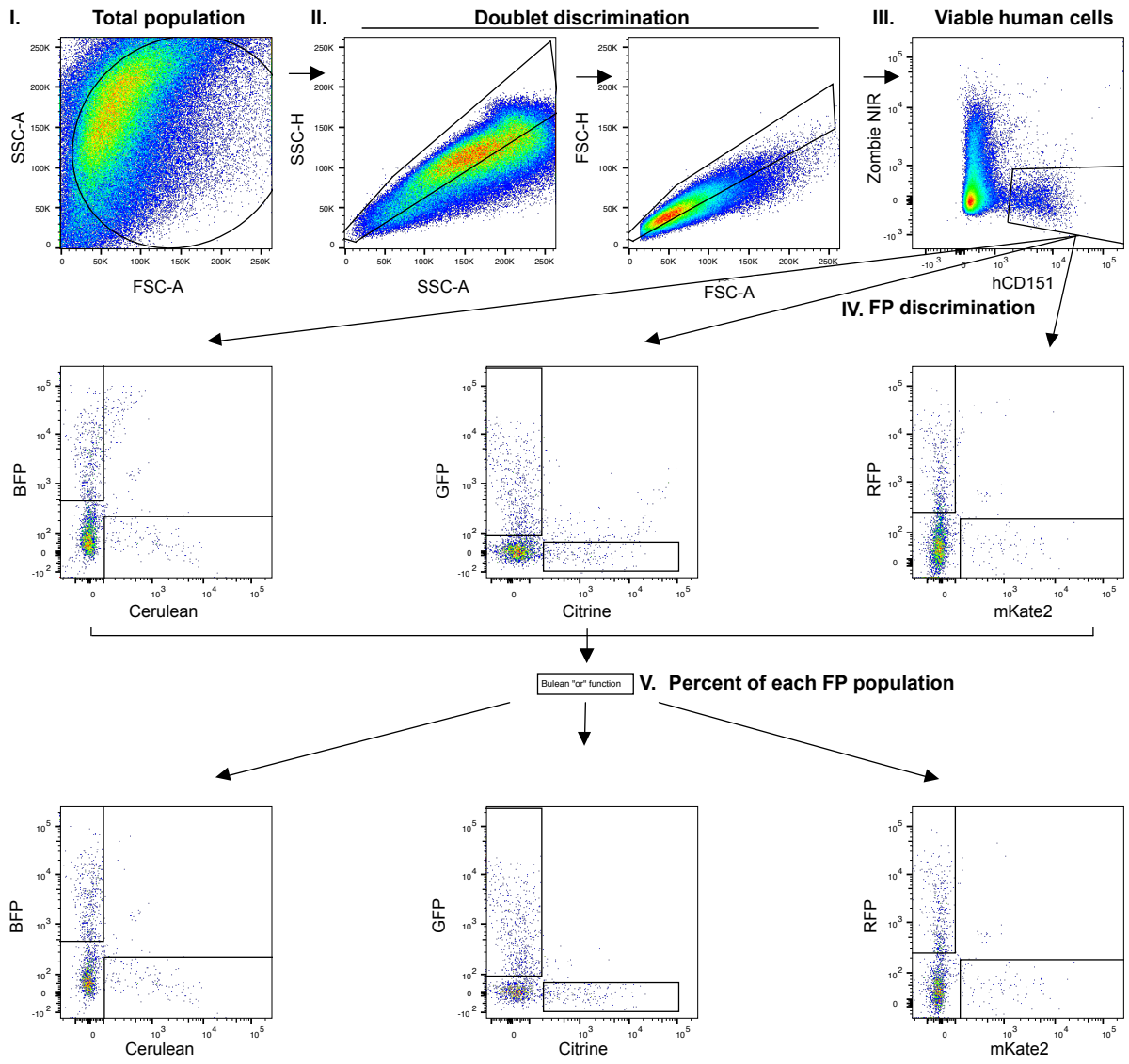

Figure 37. Gating schematic for flow cytometry protocol. pRBow labeled tumor cells were identified by flow cytometry as follows: (I.) Cells were discriminated from debris by forward (FSC-A) and side (SSC-A) laser scatter properties, (II.) single cells were identified by doublet discrimination-based gating, (III.) human cells were identified with Alexa 647-conjugated anti-hCD151 antibody and viable cells discriminated using Zombie NIR viability dye, (IV.) pRbow label of live human tumor cells was identified, (V.) percent of each pRBow population was calculated for each sample.

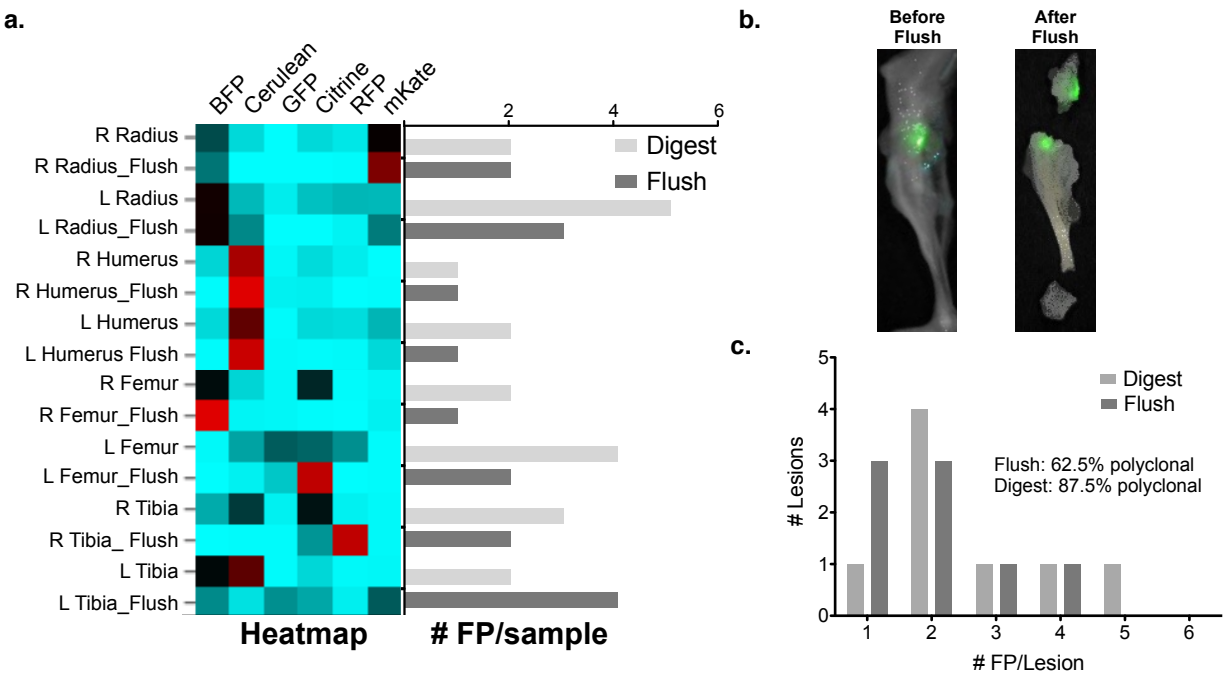

Figure 38. Whole bone digest extracts subpopulations more completely than bone marrow flush. (**a**) Heat map of color distribution for samples comparing bone marrow flush (_Flush) to subsequent whole bone digest. (**b**) *Ex vivo* spectral imaging of long bones before and after bone marrow flush. (**c**) Distribution of clonality for bone marrow flush alone versus subsequent whole bone digest. Samples containing cells from two or more pRBow populations were considered polyclonal. Only pRBow populations contributing 10% or more of the total sample population were considered for determination of clonality.

Discussion

Here, we describe a novel tool for labeling, tracking and quantifying multiple cell populations *in vitro* and *in vivo*. We demonstrate the usefulness of pRBow in several commonly used models with several accessible analytical instruments. Finally, we use pRBow to demonstrate that metastasis commonly occurs in a polyclonal fashion, whereby multiple cells seed a single metastasis, in two separate animal models.

In our breast cancer model, our conclusion that breast cancer metastasis to bone is polyclonal process would be supported by microscopic in situ analysis of individual lesion composition, rather than the whole bone analysis presented here. mportantly, however, our data confirm the conclusions of Ewald, *et al.* (34), that breast cancer metastasis is a polyclonal process. Additionally, our data raise the questions 1) Is spontaneous breast cancer metastasis similarly polyclonal? 2) Is polyclonality of metastasis increased over time by reseeding of established metastases?

These data show that the pRBow barcoding system is an accessible tool for tracking and analyzing multiple cell populations *in vivo*. These data also present a base on which pRBow can be expanded and developed to investigate more complex questions of metastasis. For example, multiphoton microscopy, when available, can be utilized for both realtime, intravital tracking as well as end-point quantification of pRBow labeled cell populations. Moreover, because investigators can sort cell populations by the pRBow fluorescent tag, each subpopulation can then be further analyzed for gene expression using techniques such as mass cytometry (239) for single cell analysis, or quantitative polymerase chain reaction, for population level analysis.

In conclusion, pRainbow is a dynamic and useful tool for the investigation of heterogeneous processes such as metastasis. Utilization and expansion of this tool has the potential to address previously unanswerable questions in the field of metastasis.

REFERENCES

1. Seyfried TN, Huysentruyt LC. On the origin of cancer metastasis. Crit Rev Oncog. 2013;18(1-2):43–73.

2. Siegel RL, Miller KD, Jemal A. Cancer statistics, 2017. CA A Cancer Journal for Clinicians. 3rd ed. 2017 Jan 5;67(1):7–30.

3. Chaffer CL, Weinberg RA. A perspective on cancer cell metastasis. Science. American Association for the Advancement of Science; 2011 Mar 25;331(6024):1559–64.

4. Friedl P, Wolf K. Tumour-cell invasion and migration: diversity and escape mechanisms. Nat Rev Cancer [Internet]. 2003 May;3(5):362–74. Available from: http://www.nature.com/doifinder/10.1038/nrc1075

5. Palmer TD, Ashby WJ, Lewis JD, Zijlstra A. Targeting tumor cell motility to prevent metastasis. Advanced Drug Delivery Reviews. Elsevier B.V; 2011 Jul 18;63(8):568–81.

6. Welch HG, Albertsen PC. Prostate Cancer Diagnosis and Treatment After the Introduction of Prostate-Specific Antigen Screening: 1986-2005. J Natl Cancer Inst. 2009 Oct 6;101(19):1325–9.

7. Thompson IM, Ankerst DP, Chi C, Lucia MS, Goodman PJ, Crowley JJ, et al. Operating Characteristics of Prostate-Specific Antigen in Men With an Initial PSA Level of 3.0 ng/mL or Lower. JAMA. American Medical Association; 2005 Jul 6;294(1):66–70.

8. Valkenburg KC, Amend SR, Verdone JE, van der Toom EE, Hernandez JR, Gorin MA, et al. A simple selection-free method for detecting disseminated tumor cells (DTCs) in murine bone marrow. Oncotarget. Impact Journals; 2016 Sep 13;7(43):69794–803.

9. Chambers AF, Groom AC, MacDonald IC. Metastasis: Dissemination and growth of cancer cells in metastatic sites. 2002 Aug;2(8):563–72. Available from: http://www.nature.com/doifinder/10.1038/nrc865

10. Klein CA. Cancer. The metastasis cascade. Science. 2008 Sep 26;321(5897):1785–7.

11. Klein CA. Parallel progression of primary tumours and metastases. Nat Rev Cancer. Nature Publishing Group; 2009 Apr;9(4):302–12.

12. Folkman J. Role of angiogenesis in tumor growth and metastasis. Seminars in Oncology. 2002 Dec;29(6Q):15–8.

13. Condeelis J, Segall JE. Intravital imaging of cell movement in tumours. Nat Rev Cancer. 2003 Dec;3(12):921–30.

14. Clark AG, Vignjevic DM. ScienceDirect Modes of cancer cell invasion and the role of the microenvironment. Current Opinion in Cell Biology. Elsevier Ltd; 2015 Oct 1;36(C):13–22.

15. Friedl P, Wolf K. Plasticity of cell migration: a multiscale tuning model. J Cell Biol. 2010 Jan 11;188(1):11–9.

16. Polyak K, Weinberg RA. Transitions between epithelial and mesenchymal states: acquisition of malignant and stem cell traits. Nat Rev Cancer. 2009 Mar 5;9(4):265–73.

17. Friedl P, Wolf K. Tube Travel: The Role of Proteases in Individual and Collective Cancer Cell Invasion. Cancer Res. 2008 Sep 15;68(18):7247–9.

18. Xing F. Cancer associated fibroblasts (CAFs) in tumor microenvironment. Frontiers in Bioscience. 2010;15(1):166.

19. Gaggioli C, Hooper S, Hidalgo-Carcedo C, Grosse R, Marshall JF, Harrington K, et al. Fibroblast-led collective invasion of carcinoma cells with differing roles for RhoGTPases in leading and following cells. Nature Cell Biology. 2007 Nov 25;9(12):1392–400.

20. Massagué J. TGFβ in Cancer. Cell. 2008 Jul;134(2):215–30.

21. Friedl P, Mayor R. Tuning Collective Cell Migration by Cell-Cell Junction Regulation. Cold Spring Harb Perspect Biol [Internet]. Cold Spring Harbor Lab; 2017 Apr 3;9(4):a029199. Available from: http://eutils.ncbi.nlm.nih.gov/entrez/eutils/elink.fcgi?dbfrom=pubmed&id=28096261&retmode=ref&cmd=prlinks

22. Wai Wong C, Dye DE, Coombe DR. The Role of Immunoglobulin Superfamily Cell Adhesion Molecules in Cancer Metastasis. International Journal of Cell Biology [Internet]. Hindawi Publishing Corporation; 2012;2012(5):1–9. Available from: http://www.hindawi.com/journals/ijcb/2012/340296/

23. Paduch R. The role of lymphangiogenesis and angiogenesis in tumor metastasis. Cellular Oncology. Cellular Oncology; 2016 Oct 3;:1–14.

24. Cho J-K, Hyun SH, Choi N, Kim M-J, Padera TP, Choi JY, et al. Significance of Lymph Node Metastasis in Cancer Dissemination of Head and Neck Cancer. TRANON. The Authors; 2015 Apr 1;8(2):119–25.

25. Bockhorn M, Jain RK, Munn LL. Active versus passive mechanisms in metastasis: do cancer cells crawl into vessels, or are they pushed? The Lancet Oncology. 2007 May;8(5):444–8.

26. Wong CW, Song C, Grimes MM, Fu W, Dewhirst MW, Muschel RJ, et al. Intravascular location of breast cancer cells after spontaneous metastasis to the lung. Am J Pathol. 2002 Sep;161(3):749–53.

27. Wyckoff JB, Jones JG, Condeelis JS, Segall JE. A critical step in metastasis: in vivo analysis of intravasation at the primary tumor. Cancer Res. 2000 May 1;60(9):2504–11.

28. Bockhorn M, Roberge S, Sousa C, Jain RK, Munn LL. Differential gene expression in metastasizing cells shed from kidney tumors. Cancer Res. 2004 Apr 1;64(7):2469–73.

29. Labelle M, Hynes RO. The Initial Hours of Metastasis: The Importance of Cooperative Host-Tumor Cell Interactions during Hematogenous Dissemination. Cancer Discovery. 2012 Dec 9;2(12):1091–9.

30. Egan K, Cooke N, Kenny D. Living in shear: platelets protect cancer cells from shear induced damage. Clin Exp Metastasis. 2014 Jun 19;31(6):697–704.

31. Nieswandt B, Hafner M, Echtenacher B, Männel DN. Lysis of tumor cells by natural killer cells in mice is impeded by platelets. Cancer Res. 1999 Mar 15;59(6):1295–300.

32. Pearlstein E, Salk PL, Yogeeswaran G, Karpatkin S. Correlation between spontaneous metastatic potential, platelet-aggregating activity of cell surface extracts, and cell surface sialylation in 10 metastatic-variant derivatives of a rat renal sarcoma cell line. Proc Natl Acad Sci USA. National Academy of Sciences; 1980 Jul;77(7):4336–9.

33. Aceto N, Bardia A, Miyamoto DT, Donaldson MC, Ben S Wittner, Spencer JA, et al. Circulating Tumor Cell Clusters Are Oligoclonal Precursors of Breast Cancer Metastasis. 2014 Aug 28;158(5):1110–22. Available from: http://dx.doi.org/10.1016/j.cell.2014.07.013

34. Cheung KJ, Padmanaban V, Silvestri V, Schipper K, Cohen JD, Fairchild AN, et al. Polyclonal breast cancer metastases arise from collective dissemination of keratin 14-expressing tumor cell clusters. Proc Natl Acad Sci USA. 2016 Feb 16;113(7):E854–63.

35. Hou J-M, Krebs MG, Lancashire L, Sloane R, Backen A, Swain RK, et al. Clinical Significance and Molecular Characteristics of Circulating Tumor Cells and Circulating Tumor Microemboli in Patients With Small-Cell Lung Cancer. JCO. 2012 Feb 10;30(5):525–32.

36. Sahai E. Illuminating the metastatic process. Nat Rev Cancer. 2007 Oct;7(10):737–49.

37. Shea DJ, Li YW, Stebe KJ, Konstantopoulos K. E-selectin-mediated rolling

facilitates pancreatic cancer cell adhesion to hyaluronic acid. FASEB J. 2017 Nov;31(11):5078–86.

38. Ito S, Nakanishi H, Ikehara Y, Kato T, Kasai Y, Ito K, et al. Real-time observation of micrometastasis formation in the living mouse liver using a green fluorescent protein gene-tagged rat tongue carcinoma cell line. Int J Cancer. Wiley Subscription Services, Inc., A Wiley Company; 2001 Jul 15;93(2):212–7.

39. Miles FL, Pruitt FL, van Golen KL, Cooper CR. Stepping out of the flow: capillary extravasation in cancer metastasis. Clin Exp Metastasis. Springer Netherlands; 2008;25(4):305–24.

40. Liang S, Hoskins M, Dong C. Tumor cell extravasation mediated by leukocyte adhesion is shear rate dependent on IL-8 signaling. Mol Cell Biomech. NIH Public Access; 2010 Jun;7(2):77–91.

41. Fidler IJ. Metastasis: quantitative analysis of distribution and fate of tumor emboli labeled with 125 I-5-iodo-2'-deoxyuridine. J Natl Cancer Inst. 1970 Oct;45(4):773–82.

42. Kim J-W, Wong CW, Goldsmith JD, Song C, Fu W, Allion M-B, et al. Rapid apoptosis in the pulmonary vasculature distinguishes non-metastatic from metastatic melanoma cells. Cancer Letters. 2004 Sep;213(2):203–12.

43. Paget S. The distribution of secondary growths in cancer of the breast. 1889. Vol. 8, Cancer metastasis reviews. 1989. 4 p.

44. EWING J. NEOPLASTIC DISEASES. A TREATISE ON TUMORS. The American Journal of the Medical Sciences. 1928 Aug;176(2):278.

45. Fidler IJ, Nicolson GL. Organ selectivity for implantation survival and growth of B16 melanoma variant tumor lines. J Natl Cancer Inst. 1976 Nov;57(5):1199–202.

46. Peinado H, Zhang H, Matei IR, Costa-Silva B, Hoshino A, Rodrigues G, et al. Pre-metastatic niches: organ-specific homes for metastases. Nat Rev Cancer. Nature Publishing Group; 2017 Mar 17;17(5):302–17.

47. van Zijl F, Krupitza G, Mikulits W. Initial steps of metastasis: Cell invasion and endothelial transmigration. Mutation Research-Reviews in Mutation Research. Elsevier B.V; 2011 Aug 5;728(1-2):23–34.

48. Hoshino A, Costa-Silva B, Shen T-L, Rodrigues G, Hashimoto A, Mark MT, et al. Tumour exosome integrins determine organotropic metastasis. Nature. Nature Publishing Group; 2015 Nov 19;527(7578):329–35.

49. Kraning-Rush CM, Califano JP, Reinhart-King CA. Cellular Traction Stresses Increase with Increasing Metastatic Potential. Laird EG, editor. PLoS ONE. 2012

Feb 28;7(2):e32572–10.

50. Lu P, Weaver VM, Werb Z. The extracellular matrix: A dynamic niche in cancer progression. J Cell Biol. 2012 Feb 20;196(4):395–406.

51. Høye AM, Erler JT. Structural ECM components in the premetastatic and metastatic niche. Am J Physiol Cell Physiol. 2016 Jun 15;310(11):C955–67.

52. Duda DG, Duyverman AMMJ, Kohno M, Snuderl M, Steller EJA, Fukumura D, et al. Malignant cells facilitate lung metastasis by bringing their own soil. Proc Natl Acad Sci USA. National Acad Sciences; 2010 Dec 14;107(50):21677–82.

53. Sosa MS, Bragado P, Aguirre-Ghiso JA. Mechanisms of disseminated cancer cell dormancy: an awakening field. Nat Rev Cancer. Nature Publishing Group; 2014 Sep;14(9):611–22.

54. Gomis RR, Gawrzak S. Tumor cell dormancy. Mol Oncol. 2016 Oct 7;11(1):62–78.

55. He Z, Jin Y. Intrinsic Control of Axon Regeneration. Neuron. Cell Press; 2016 May 4;90(3):437–51.

56. Shamir ER, Ewald AJ. Adhesion in mammary development: novel roles for E-cadherin in individual and collective cell migration. Curr Top Dev Biol. Elsevier; 2015;112:353–82.

57. Takeichi M. Cadherin cell adhesion receptors as a morphogenetic regulator. Science. 1991 Mar 22;251(5000):1451–5.

58. Tepass U. Genetic analysis of cadherin function in animal morphogenesis. Current Opinion in Cell Biology. 1999 Oct;11(5):540–8.

59. Shapiro L, Weis WI. Structure and biochemistry of cadherins and catenins. Cold Spring Harb Perspect Biol. 2009 Sep;1(3):a003053–3.

60. Gumbiner BM. Regulation of cadherin-mediated adhesion in morphogenesis. Nat Rev Mol Cell Biol. Nature Publishing Group; 2005 Aug;6(8):622–34.

61. Gumbiner BM. Cell adhesion: the molecular basis of tissue architecture and morphogenesis. Cell. 1996 Feb 9;84(3):345–57.

62. Shapiro L, Fannon AM, Kwong PD, Thompson A, Lehmann MS, Grübel G, et al. Structural basis of cell-cell adhesion by cadherins. Nature. Nature Publishing Group; 1995 Mar 23;374(6520):327–37.

63. Overduin M, Harvey TS, Bagby S, Tong KI, Yau P, Takeichi M, et al. Solution structure of the epithelial cadherin domain responsible for selective cell adhesion. Science. 1995 Jan 20;267(5196):386–9.

64. Nagar B, Overduin M, Ikura M, Rini JM. Structural basis of calcium-induced E-cadherin rigidification and dimerization. Nature. 1996 Mar 28;380(6572):360–4.

65. Yap AS, Niessen CM, Gumbiner BM. The juxtamembrane region of the cadherin cytoplasmic tail supports lateral clustering, adhesive strengthening, and interaction with p120ctn. J Cell Biol. The Rockefeller University Press; 1998 May 4;141(3):779–89.

66. Boggon TJ, Murray J, Chappuis-Flament S, Wong E, Gumbiner BM, Shapiro L. C-cadherin ectodomain structure and implications for cell adhesion mechanisms. Science. 2002 May 17;296(5571):1308–13.

67. Harris TJC, Tepass U. Adherens junctions: from molecules to morphogenesis. Nat Rev Mol Cell Biol. Nature Publishing Group; 2010 Jul;11(7):502–14.

68. Birchmeier W, Behrens J. Cadherin expression in carcinomas: role in the formation of cell junctions and the prevention of invasiveness. Biochim Biophys Acta. 1994 May 27;1198(1):11–26.

69. Berx G, Cleton-Jansen AM, Nollet F, de Leeuw WJ, van de Vijver M, Cornelisse C, et al. E-cadherin is a tumour/invasion suppressor gene mutated in human lobular breast cancers. EMBO J. European Molecular Biology Organization; 1995 Dec 15;14(24):6107–15.

70. Vleminckx K, Vakaet L, Mareel M, Fiers W, van Roy F. Genetic manipulation of E-cadherin expression by epithelial tumor cells reveals an invasion suppressor role. Cell. 1991 Jul 12;66(1):107–19.

71. Derksen PWB, Liu X, Saridin F, van der Gulden H, Zevenhoven J, Evers B, et al. Somatic inactivation of E-cadherin and p53 in mice leads to metastatic lobular mammary carcinoma through induction of anoikis resistance and angiogenesis. Cancer Cell. 2006 Nov;10(5):437–49.

72. Perl AK, Wilgenbus P, Dahl U, Semb H, Christofori G. A causal role for E-cadherin in the transition from adenoma to carcinoma. Nature. Nature Publishing Group; 1998 Mar 12;392(6672):190–3.

73. Thiery JP. Epithelial–mesenchymal transitions in tumour progression. Nat Rev Cancer. Nature Publishing Group; 2002 Jun;2(6):442–54.

74. Yang J, Weinberg RA. Epithelial-mesenchymal transition: at the crossroads of development and tumor metastasis. Dev Cell. 2008 Jun;14(6):818–29.

75. Cadigan KM, Nusse R. Wnt signaling: a common theme in animal development. Genes Dev. 1997 Dec 15;11(24):3286–305.

76. Fung YK, Shackleford GM, Brown AM, Sanders GS, Varmus HE. Nucleotide sequence and expression in vitro of cDNA derived from mRNA of int-1, a

provirally activated mouse mammary oncogene. Mol Cell Biol. American Society for Microbiology (ASM); 1985 Dec;5(12):3337–44.

77. Brown AM, Wildin RS, Prendergast TJ, Varmus HE. A retrovirus vector expressing the putative mammary oncogene int-1 causes partial transformation of a mammary epithelial cell line. Cell. 1986 Sep 26;46(7):1001–9.

78. Fodde R, Brabletz T. Wnt/beta-catenin signaling in cancer stemness and malignant behavior. Current Opinion in Cell Biology. 2007 Apr;19(2):150–8.

79. Heasman J, Crawford A, Goldstone K, Garner-Hamrick P, Gumbiner B, McCrea P, et al. Overexpression of cadherins and underexpression of beta-catenin inhibit dorsal mesoderm induction in early Xenopus embryos. Cell. 1994 Dec 2;79(5):791–803.

80. Caca K, Kolligs FT, Ji X, Hayes M, Qian J, Yahanda A, et al. Beta- and gamma-catenin mutations, but not E-cadherin inactivation, underlie T-cell factor/lymphoid enhancer factor transcriptional deregulation in gastric and pancreatic cancer. Cell Growth Differ. 1999 Jun;10(6):369–76.

81. Cox RT, Pai LM, Kirkpatrick C, Stein J, Peifer M. Roles of the C terminus of Armadillo in Wingless signaling in Drosophila. Genetics. Genetics Society of America; 1999 Sep;153(1):319–32.

82. Qian X, Karpova T, Sheppard AM, McNally J, Lowy DR. E-cadherin-mediated adhesion inhibits ligand-dependent activation of diverse receptor tyrosine kinases. EMBO J. EMBO Press; 2004 Apr 21;23(8):1739–48.

83. Lampugnani MG, Orsenigo F, Gagliani MC, Tacchetti C, Dejana E. Vascular endothelial cadherin controls VEGFR-2 internalization and signaling from intracellular compartments. J Cell Biol. 2006 Aug 14;174(4):593–604.

84. Ruoslahti E. Integrins. Journal of Clinical Investigation. American Society for Clinical Investigation; 1991 Jan;87(1):1–5.

85. Hynes RO. Integrins: versatility, modulation, and signaling in cell adhesion. Cell. 1992 Apr 3;69(1):11–25.

86. Hynes RO. Integrins. Cell. 2002 Sep;110(6):673–87.

87. Calderwood DA, Zent R, Grant R, Rees DJG, Hynes RO, Ginsberg MH. The Talin Head Domain Binds to Integrin β Subunit Cytoplasmic Tails and Regulates Integrin Activation. American Society for Biochemistry and Molecular Biology; 1999 Oct 1;274(40):28071–4.

88. Calderwood DA. Talin controls integrin activation. Biochemical Society Transactions. Portland Press Limited; 2004 Jun 1;32(3):434–7.

89. Yeh C-H, Peng H-C, Huang T-F. Cytokines Modulate Integrin αvβ3-Mediated Human Endothelial Cell Adhesion and Calcium Signaling. Experimental Cell Research. 1999 Aug;251(1):57–66.

90. Zaidel-Bar R, Itzkovitz S, Ma'ayan A, Iyengar R, Geiger B. Functional atlas of the integrin adhesome. Nature Cell Biology. Nature Publishing Group; 2007 Aug;9(8):858–67.

91. Plantefaber LC, Hynes RO. Changes in integrin receptors on oncogenically transformed cells. Cell. 1989 Jan;56(2):281–90.

92. Hsu M-Y, Shih D-T, Meier FE, Van Belle P, Hsu J-Y, Elder DE, et al. Adenoviral Gene Transfer of β3 Integrin Subunit Induces Conversion from Radial to Vertical Growth Phase in Primary Human Melanoma. Am J Pathol. 1998 Nov;153(5):1435–42.

93. Sugiura T, Berditchevski F. Function of α3β1–Tetraspanin Protein Complexes in Tumor Cell Invasion. Evidence for the Role of the Complexes in Production of Matrix Metalloproteinase 2 (Mmp-2). J Cell Biol. 1999 Sep 20;146(6):1375–89.

94. Zutter MM, Mazoujian G, Santoro SA. Decreased expression of integrin adhesive protein receptors in adenocarcinoma of the breast. Am J Pathol. American Society for Investigative Pathology; 1990 Oct;137(4):863–70.

95. Dedhar S, Saulnier R, Nagle R, Overall CM. Specific alterations in the expression of alpha 3 beta 1 and alpha 6 beta 4 integrins in highly invasive and metastatic variants of human prostate carcinoma cells selected by in vitro invasion through reconstituted basement membrane. Clin Exp Metastasis. 1993 Sep;11(5):391–400.

96. Barclay AN. Membrane proteins with immunoglobulin-like domains--a master superfamily of interaction molecules. Semin Immunol. 2003 Aug;15(4):215–23.

97. Rougon G, Hobert O. New insights into the diversity and function of neuronal immunoglobulin superfamily molecules. Annu Rev Neurosci. 2003;26(1):207–38.

98. Williams AF, Barclay AN. The immunoglobulin superfamily--domains for cell surface recognition. Annu Rev Immunol. Annual Reviews 4139 El Camino Way, P.O. Box 10139, Palo Alto, CA 94303-0139, USA; 1988;6(1):381–405.

99. Ohto U, Ishida H, Krayukhina E, Uchiyama S, Inoue N, Shimizu T. Structure of IZUMO1-JUNO reveals sperm-oocyte recognition during mammalian fertilization. Nature. Nature Publishing Group; 2016 Jun 23;534(7608):566–9.

100. Maruyama K, Matsubara S, Natori R, Nonomura Y, Kimura S. Connectin, an elastic protein of muscle. Characterization and Function. J Biochem. 1977 Aug;82(2):317–37.

101. Cavallaro U, Dejana E. Adhesion molecule signalling: not always a sticky business. 2011 Mar 1;12(3):189–97. Available from: http://dx.doi.org/10.1038/nrm3068

102. Francavilla C, Cattaneo P, Berezin V, Bock E, Ami D, de Marco A, et al. The binding of NCAM to FGFR1 induces a specific cellular response mediated by receptor trafficking. J Cell Biol. 2009 Dec 28;187(7):1101–16.

103. Stoletov K, Bond D, Hebron K, Raha S, Zijlstra A, Lewis JD. Metastasis as a therapeutic target in prostate cancer: a conceptual framework. Am J Clin Exp Urol. e-Century Publishing Corporation; 2014 Apr;2(1):45–56.

104. Craig SEL, Brady-Kalnay SM. Cancer cells cut homophilic cell adhesion molecules and run. Cancer Res. 2011 Jan 15;71(2):303–9.

105. van Kempen LC, Nelissen JM, Degen WG, Torensma R, Weidle UH, Bloemers HP, et al. Molecular basis for the homophilic activated leukocyte cell adhesion molecule (ALCAM)-ALCAM interaction. 2001 Jul 13;276(28):25783–90.

106. Bowen MA, Patel DD, Li X, Modrell B, Malacko AR, Wang WC, et al. Cloning, mapping, and characterization of activated leukocyte-cell adhesion molecule (ALCAM), a CD6 ligand. J Exp Med. The Rockefeller University Press; 1995 Jun 1;181(6):2213–20.

107. Masedunskas A, King JA, Tan F, Cochran R, Stevens T, Sviridov D, et al. Activated leukocyte cell adhesion molecule is a component of the endothelial junction involved in transendothelial monocyte migration. FEBS Lett. 2006 May 15;580(11):2637–45.

108. Lécuyer M-A, Saint-Laurent O, Bourbonnière L, Larouche S, Larochelle C, Michel L, et al. Dual role of ALCAM in neuroinflammation and blood–brain barrier homeostasis. Proc Natl Acad Sci USA. 2017 Jan 24;114(4):E524–33.

109. Zimmerman AW, Ben Joosten, Torensma R, Parnes JR, van Leeuwen FN, Figdor CG. Long-term engagement of CD6 and ALCAM is essential for T-cell proliferation induced by dendritic cells. Blood. American Society of Hematology; 2006 Apr 15;107(8):3212–20.

110. Weiner JA, Koo SJ, Nicolas S, Fraboulet S, Pfaff SL, Pourquié O, et al. Axon fasciculation defects and retinal dysplasias in mice lacking the immunoglobulin superfamily adhesion molecule BEN/ALCAM/SC1. Mol Cell Neurosci. 2004 Sep;27(1):59–69.

111. Lunter PC, van Kilsdonk JWJ, van Beek H, Cornelissen IMHA, Bergers M, Willems PHGM, et al. Activated leukocyte cell adhesion molecule (ALCAM/CD166/MEMD), a novel actor in invasive growth, controls matrix metalloproteinase activity. Cancer Res. 2005 Oct 1;65(19):8801–8.

112. Ma L, Wang J, Lin J, Pan Q, Yu Y, Sun F. Cluster of Differentiation 166 (CD166) Regulated by Phosphatidylinositide 3-Kinase (PI3K)/AKT Signaling to Exert Its Anti-apoptotic Role via Yes-associated Protein (YAP) in Liver Cancer. 2014 Mar 6;289(10):6921–33.

113. Hansen AG, Freeman TJ, Arnold SA, Starchenko A, Jones-Paris CR, Gilger MA, et al. Elevated ALCAM shedding in colorectal cancer correlates with poor patient outcome. Cancer Res. 2013 May 15;73(10):2955–64.

114. Arnold Egloff SA, Du L, Loomans HA, Starchenko A, Su P-F, Ketova T, et al. Shed urinary ALCAM is an independent prognostic biomarker of three-year overall survival after cystectomy in patients with bladder cancer. Oncotarget. Impact Journals; 2016 Nov 24;8(1):722–41.

115. Bowen MA, Bajorath J, D'Egidio M, Whitney GS, Palmer D, Kobarg J, et al. Characterization of mouse ALCAM (CD166): the CD6-binding domain is conserved in different homologs and mediates cross-species binding. Eur J Immunol. WILEY-VCH Verlag GmbH; 1997 Jun;27(6):1469–78.

116. King JA, Tan F, Mbeunkui F, Chambers Z, Cantrell S, Chen H, et al. Mechanisms of transcriptional regulation and prognostic significance of activated leukocyte cell adhesion molecule in cancer. Mol Cancer. BioMed Central; 2010 Oct 7;9(1):266.

117. Tan F, Ghosh S, Mbeunkui F, Thomas R, Weiner JA, Ofori-Acquah SF. Essential role for ALCAM gene silencing in megakaryocytic differentiation of K562 cells. BMC Mol Biol. BioMed Central; 2010 Dec 2;11(1):91.

118. Wang J, Gu Z, Ni P, Qiao Y, Chen C, Liu X, et al. NF-kappaB P50/P65 hetero-dimer mediates differential regulation of CD166/ALCAM expression via interaction with micoRNA-9 after serum deprivation, providing evidence for a novel negative auto-regulatory loop. Nucleic Acids Research. 2011 Aug;39(15):6440–55.

119. Jin Z, Selaru FM, Cheng Y, Kan T, Agarwal R, Mori Y, et al. MicroRNA-192 and -215 are upregulated in human gastric cancer in vivo and suppress ALCAM expression in vitro. Oncogene. Nature Publishing Group; 2010 Nov 29;30(13):1577–85.

120. Arai F, Ohneda O, Miyamoto T, Zhang XQ, Suda T. Mesenchymal stem cells in perichondrium express activated leukocyte cell adhesion molecule and participate in bone marrow formation. J Exp Med. The Rockefeller University Press; 2002 Jun 17;195(12):1549–63.

121. Levin TG, Powell AE, Davies PS, Silk AD, Dismuke AD, Anderson EC, et al. Characterization of the intestinal cancer stem cell marker CD166 in the human and mouse gastrointestinal tract. Gastroenterology. 2010 Dec;139(6):2072–5.

122. van Kilsdonk JWJ, Wilting RH, Bergers M, van Muijen GNP, Schalkwijk J, van Kempen LCLT, et al. Attenuation of melanoma invasion by a secreted variant of activated leukocyte cell adhesion molecule. Cancer Res. 2008 May 15;68(10):3671–9.

123. Tudor C, Riet te J, Eich C, Harkes R, Smisdom N, Bouhuijzen Wenger J, et al. Syntenin-1 and ezrin proteins link activated leukocyte cell adhesion molecule to the actin cytoskeleton. American Society for Biochemistry and Molecular Biology; 2014 May 9;289(19):13445–60. Available from: http://www.jbc.org/cgi/doi/10.1074/jbc.M113.546754

124. Riet te J, Helenius J, Strohmeyer N, Cambi A, Figdor CG, Muller DJ. Dynamic coupling of ALCAM to the actin cortex strengthens cell adhesion to CD6. Journal of Cell Science. 2014 Mar 31;127(7):1595–606.

125. Gilsanz A, Sánchez-Martín L, Gutiérrez-López MD, Ovalle S, Machado-Pineda Y, Reyes R, et al. ALCAM/CD166 adhesive function is regulated by the tetraspanin CD9. Cell Mol Life Sci. 2013 Feb;70(3):475–93.

126. Delgado VMC, Nugnes LG, Colombo LL, Troncoso MF, Fernández MM, Malchiodi EL, et al. Modulation of endothelial cell migration and angiogenesis: a novel function for the “tandem-repeat” lectin galectin-8. FASEB J. Federation of American Societies for Experimental Biology; 2011 Jan;25(1):242–54.

127. Iolyeva M, Karaman S, Willrodt A-H, Weingartner S, Vigl B, Halin C. Novel role for ALCAM in lymphatic network formation and function. FASEB J. Federation of American Societies for Experimental Biology; 2013 Mar;27(3):978–90.

128. Choudhry P, Joshi D, Funke B, Trede N. Alcama mediates Edn1 signaling during zebrafish cartilage morphogenesis. Dev Biol. 2011 Jan 15;349(2):483–93.

129. Wagner M, Bilinska M, Pokryszko-Dragan A, Sobczynski M, Cyrul M, Kusnierczyk P, et al. ALCAM and CD6 — multiple sclerosis risk factors. Journal of Neuroimmunology. Elsevier B.V; 2014 Nov 15;276(1-2):98–103.

130. Jezierska A, Matysiak W, Motyl T. ALCAM/CD166 protects breast cancer cells against apoptosis and autophagy. Med Sci Monit. 2006 Aug;12(8):BR263–73.

131. Chen M-J, Cheng Y-M, Chen C-C, Chen Y-C, Shen C-J. MiR-148a and miR-152 reduce tamoxifen resistance in ER+ breast cancer via downregulating ALCAM. Biochem Biophys Res Commun. 2017 Jan 4;483(2):840–6.

132. Xu L, Mohammad KS, Wu H, Crean C, Poteat B, Cheng Y, et al. Cell Adhesion Molecule CD166 Drives Malignant Progression and Osteolytic Disease in Multiple Myeloma. Cancer Res. 2016 Nov 30;76(23):6901–10.

133. Willrodt A-H, Beffinger M, Vranova M, Protsyuk D, Schuler K, Jadhav M, et al.

Stromal Expression of Activated Leukocyte Cell Adhesion Molecule Promotes Lung Tumor Growth and Metastasis. Am J Pathol. American Society for Investigative Pathology; 2017 Sep 14;:1–13.

134. Burkhardt M. Cytoplasmic overexpression of ALCAM is prognostic of disease progression in breast cancer. 2006 Apr 1;59(4):403–9. Available from: http://jcp.bmj.com/cgi/doi/10.1136/jcp.2005.028209

135. Kristiansen G, Pilarsky C, Wissmann C, Stephan C, Weissbach L, Loy V, et al. ALCAM/CD166 is up-regulated in low-grade prostate cancer and progressively lost in high-grade lesions. 2002 Dec 12;54(1):34–43. Available from: http://doi.wiley.com/10.1002/pros.10161

136. Hong X, Michalski CW, Kong B, Zhang W, Raggi MC, Sauliunaite D, et al. ALCAM is associated with chemoresistance and tumor cell adhesion in pancreatic cancer. J Surg Oncol. Wiley Subscription Services, Inc., A Wiley Company; 2010 Jun 1;101(7):564–9.

137. Devis L, Moiola CP, Masia N, Martinez-Garcia E, Santacana M, Stirbat TV, et al. Activated leukocyte cell adhesion molecule (ALCAM) is a marker of recurrence and promotes cell migration, invasion and metastasis in early stage endometrioid endometrial cancer. 2016 Nov 22.

138. Wiiger MT, Gehrken HB, Fodstad Ø, Maelandsmo GM, Andersson Y. A novel human recombinant single-chain antibody targeting CD166/ALCAM inhibits cancer cell invasion in vitro and in vivo tumour growth. Cancer Immunol Immunother. 2010 Nov;59(11):1665–74.

139. Piazza T, Cha E, Bongarzone I, Canevari S, Bolognesi A, Polito L, et al. Internalization and recycling of ALCAM/CD166 detected by a fully human single-chain recombinant antibody. Journal of Cell Science. 2005 Apr 1;118(Pt 7):1515–25.

140. Fernández MM, Ferragut F, Cárdenas Delgado VM, Bracalente C, Bravo AI, Cagnoni AJ, et al. Glycosylation-dependent binding of galectin-8 to activated leukocyte cell adhesion molecule (ALCAM/CD166) promotes its surface segregation on breast cancer cells. Biochim Biophys Acta. 2016 Oct;1860(10):2255–68.

141. Tomita K, van Bokhoven A, Jansen CF, Bussemakers MJ, Schalken JA. Coordinate recruitment of E-cadherin and ALCAM to cell-cell contacts by alpha-catenin. Biochem Biophys Res Commun. 2000 Jan 27;267(3):870–4.

142. Ofori-Acquah SF, King J, Voelkel N, Schaphorst KL, Stevens T. Heterogeneity of barrier function in the lung reflects diversity in endothelial cell junctions. Microvascular Research. 2008 Apr;75(3):391–402.

143. Xiao M, Yan M, Zhang J, Xu Q, Qi S, Wang X, et al. Cancer stem-like cell

related protein CD166 degrades through E3 ubiquitin ligase CHIP in head and neck cancer. 2017 Mar 6.

144. Bartee E, McCormack A, Früh K. Quantitative Membrane Proteomics Reveals New Cellular Targets of Viral Immune Modulators. PLoS Pathog. 2006;2(10):e107–14.

145. Thelen K, Georg T, Bertuch S, Zelina P, Pollerberg GE. Ubiquitination and Endocytosis of Cell Adhesion Molecule DM-GRASP Regulate Its Cell Surface Presence and Affect Its Role for Axon Navigation. American Society for Biochemistry and Molecular Biology; 2008 Nov 21;283(47):32792–801.

146. Rosso O, Piazza T, Bongarzone I, Rossello A, Mezzanzanica D, Canevari S, et al. The ALCAM shedding by the metalloprotease ADAM17/TACE is involved in motility of ovarian carcinoma cells. Mol Cancer Res. 2007 Dec;5(12):1246–53.

147. Miccichè F, Da Riva L, Fabbi M, Pilotti S, Mondellini P, Ferrini S, et al. Activated leukocyte cell adhesion molecule expression and shedding in thyroid tumors. Langsley G, editor. PLoS ONE. 2011 Feb 22;6(2):e17141.

148. Ikeda K, Quertermous T. Molecular isolation and characterization of a soluble isoform of activated leukocyte cell adhesion molecule that modulates endothelial cell function. 2004 Dec 31;279(53):55315–23.

149. Carbotti G, Orengo AM, Mezzanzanica D, Bagnoli M, Brizzolara A, Emionite L, et al. Activated leukocyte cell adhesion molecule soluble form: a potential biomarker of epithelial ovarian cancer is increased in type II tumors. Int J Cancer. Wiley Subscription Services, Inc., A Wiley Company; 2013 Jun 1;132(11):2597–605.

150. Müller U. Cell Adhesion Molecules and Human Disorders. eLS. 2005.

151. Nakajima S, Doi R, Toyoda E, Tsuji S, Wada M, Koizumi M, et al. N-cadherin expression and epithelial-mesenchymal transition in pancreatic carcinoma. Clin Cancer Res. American Association for Cancer Research; 2004 Jun 15;10(12 Pt 1):4125–33.

152. Yilmaz M, Christofori G. EMT, the cytoskeleton, and cancer cell invasion. Cancer Metastasis Rev. 2009 Jan 24;28(1-2):15–33.

153. Zutter MM, Santoro SA, Staatz WD, Tsung YL. Re-expression of the alpha 2 beta 1 integrin abrogates the malignant phenotype of breast carcinoma cells. Proc Natl Acad Sci USA. National Acad Sciences; 1995 Aug 1;92(16):7411–5.

154. Desgrosellier JS, Cheresh DA. Integrins in cancer: biological implications and therapeutic opportunities. Nat Rev Cancer. 2010 Jan;10(1):9–22.

155. Madamanchi A, Zijlstra A, Zutter MM. Flipping the switch: integrin switching

provides metastatic competence. Sci Signal. 2014 Mar 25;7(318):pe9–pe9.

156. Xie S, Luca M, Huang S, Gutman M, Reich R, Johnson JP, et al. Expression of MCAM/MUC18 by human melanoma cells leads to increased tumor growth and metastasis. Cancer Res. 1997 Jun 1;57(11):2295–303.

157. Swart GWM. Activated leukocyte cell adhesion molecule (CD166/ALCAM): developmental and mechanistic aspects of cell clustering and cell migration. Eur J Cell Biol [Internet]. 2002 Jun;81(6):313–21. Available from: http://linkinghub.elsevier.com/retrieve/pii/S0171933504702344

158. Diekmann H, Stuermer CAO. Zebrafish neurolin-a and -b, orthologs of ALCAM, are involved in retinal ganglion cell differentiation and retinal axon pathfinding. J Comp Neurol. Wiley Subscription Services, Inc., A Wiley Company; 2009 Mar 1;513(1):38–50.

159. Lyck R, Lécuyer M-A, Abadier M, Wyss CB, Matti C, Rosito M, et al. ALCAM (CD166) is involved in extravasation of monocytes rather than T cells across the blood-brain barrier. J Cereb Blood Flow Metab. SAGE PublicationsSage UK: London, England; 2017 Aug;37(8):2894–909.

160. Kristiansen G, Pilarsky C, Wissmann C, Stephan C, Weissbach L, Loy V, et al. ALCAM/CD166 is up-regulated in low-grade prostate cancer and progressively lost in high-grade lesions. Prostate. Wiley Subscription Services, Inc., A Wiley Company; 2003 Jan 1;54(1):34–43.

161. van Kempen LC, van den Oord JJ, van Muijen GN, Weidle UH, Bloemers HP, Swart GW. Activated leukocyte cell adhesion molecule/CD166, a marker of tumor progression in primary malignant melanoma of the skin. Am J Pathol. 2000 Mar;156(3):769–74.

162. Fujiwara K, Ohuchida K, Sada M, Horioka K, Ulrich CD, Shindo K, et al. CD166/ALCAM Expression Is Characteristic of Tumorigenicity and Invasive and Migratory Activities of Pancreatic Cancer Cells. Chandra D, editor. 2014 Sep 15;9(9):e107247–11. Available from: http://dx.plos.org/10.1371/journal.pone.0107247

163. Li Q, Xu F. Association between two polymorphisms of CD166/ALCAM gene and breast cancer risk in Chinese women. Breast Cancer Res Treat. Springer US; 2011 Sep;129(2):645–6–authorreply647.

164. Smith JR, Chipps TJ, Ilias H, Pan Y, Appukuttan B. Expression and regulation of activated leukocyte cell adhesion molecule in human retinal vascular endothelial cells. Exp Eye Res. 2012 Nov;104:89–93.

165. Hansen AG, Arnold SA, Jiang M, Palmer TD, Ketova T, Merkel A, et al. ALCAM/CD166 is a TGF-β-responsive marker and functional regulator of prostate cancer metastasis to bone. Cancer Res. 2014 Mar 1;74(5):1404–15.

166. Cunningham F, Amode MR, Barrell D, Beal K, Billis K, Brent S, et al. Ensembl 2015. Nucleic Acids Research. 2014 Oct 28;43(D1):D662–9.

167. Zijlstra A, Mellor R, Panzarella G, Aimes RT, Hooper JD, Marchenko ND, et al. A quantitative analysis of rate-limiting steps in the metastatic cascade using human-specific real-time polymerase chain reaction. Cancer Res. 2002 Dec 1;62(23):7083–92.

168. Palmer TD, Lewis J, Zijlstra A. Quantitative Analysis of Cancer Metastasis using an Avian Embryo Model. JoVE. 2011;(51):1–7.

169. Berthold MR, Cebron N, Dill F, Gabriel TR, Kötter T, Meinl T, et al. KNIME - the Konstanz information miner. ACM SIGKDD Explorations Newsletter. ACM; 2009 Nov 16;11(1):26–31.

170. Schindelin J, Arganda-Carreras I, Frise E, Kaynig V, Longair M, Pietzsch T, et al. Fiji: an open-source platform for biological-image analysis. Nat Meth. Nature Research; 2012 Jul 1;9(7):676–82.

171. Arganda-Carreras I, Kaynig V, Rueden C, Eliceiri KW, Schindelin J, Cardona A, et al. Trainable Weka Segmentation: a machine learning tool for microscopy pixel classification. Bioinformatics. 2017 Mar 29;:1–2.

172. Lonsdale J, Thomas J, Salvatore M, Phillips R, Lo E, Shad S, et al. The Genotype-Tissue Expression (GTEx) project. Nature Publishing Group. Nature Publishing Group; 2013 Jun 1;45(6):580–5.

173. Network TCGAR. Comprehensive molecular characterization of urothelial bladder carcinoma. Nature. Nature Publishing Group; 2014 Mar 11;507(7492):315–22.

174. Wang X, He K, Gerhart M, Huang Y, Jiang J, Paxton RJ, et al. Metalloprotease-mediated GH Receptor Proteolysis and GHBP Shedding. 2002 Dec 20;277(52):50510–9. Available from: http://www.jbc.org/lookup/doi/10.1074/jbc.M208738200

175. Hinkle CL, Sunnarborg SW, Loiselle D, Parker CE, Stevenson M, Russell WE, et al. Selective Roles for Tumor Necrosis Factor α-converting Enzyme/ADAM17 in the Shedding of the Epidermal Growth Factor Receptor Ligand Family. 2004 May 28;279(23):24179–88.

176. Schlöndorff J, Blobel CP. Metalloprotease-disintegrins: modular proteins capable of promoting cell-cell interactions and triggering signals by protein-ectodomain shedding. Journal of Cell Science. 1999 Nov;112 (Pt 21):3603–17.

177. The UniProt Consortium. UniProt: the universal protein knowledgebase. Nucleic Acids Research. 2017 Jan 3;45(D1):D158–69.

178. Zijlstra A, Lewis J, DeGryse B, Stuhlmann H, Quigley JP. The Inhibition of Tumor Cell Intravasation and Subsequent Metastasis via Regulation of In Vivo Tumor Cell Motility by the Tetraspanin CD151. Cancer Cell. 2008 Mar;13(3):221–34.

179. Reher D. Cell adhesion heterogeneity reinforces tumour cell dissemination: novel insights from a mathematical model. Biology Direct; 2017 Aug 9;:1–17.

180. Caescu CI, Jeschke GR, Turk BE. Active-site determinants of substrate recognition by the metalloproteinases TACE and ADAM10. Biochem J. 2009 Nov 15;424(1):79–88.

181. Miller MA, Meyer AS, Beste MT, Lasisi Z, Reddy S, Jeng KW, et al. ADAM-10 and -17 regulate endometriotic cell migration via concerted ligand and receptor shedding feedback on kinase signaling. Proc Natl Acad Sci USA. 2013 May 28;110(22):E2074–83.

182. Shirakabe K, Omura T, Shibagaki Y, Mihara E, Homma K, Kato Y, et al. Mechanistic insights into ectodomain shedding: susceptibility of CADM1 adhesion molecule is determined by alternative splicing and O-glycosylation. Sci Rep. Nature Publishing Group; 2017 Apr 10;7:46174.

183. Elenius K, Corfas G, Paul S, Choi CJ, Rio C, Plowman GD, et al. A novel juxtamembrane domain isoform of HER4/ErbB4. Isoform-specific tissue distribution and differential processing in response to phorbol ester. 1997 Oct 17;272(42):26761–8.

184. Song X, Zeng Z, Wei H, Wang Z. Alternative splicing in cancers: From aberrant regulation to new therapeutics. Seminars in Cell and Developmental Biology. Elsevier Ltd; 2017 Sep 25;:1–10.

185. Corrias MV, Gambini C, Gregorio A, Croce M, Barisione G, Cossu C, et al. Different subcellular localization of ALCAM molecules in neuroblastoma: Association with relapse. Cell Oncol. IOS Press; 2010;32(1-2):77–86.

186. Longo N. Regulatory role of tetraspanin CD9 in tumor-endothelial cell interaction during transendothelial invasion of melanoma cells. Blood. American Society of Hematology; 2001 Dec 15;98(13):3717–26.

187. Ikeyama S, Koyama M, Yamaoko M, Sasada R, Miyake M. Suppression of cell motility and metastasis by transfection with human motility-related protein (MRP-1/CD9) DNA. J Exp Med. The Rockefeller University Press; 1993 May 1;177(5):1231–7.

188. Radford KJ, Thorne RF, Hersey P. Regulation of tumor cell motility and migration by CD63 in a human melanoma cell line. J Immunol. 1997 Apr 1;158(7):3353–8.

189. Palmer TD, Martínez CH, Vasquez C, Hebron KE, Jones-Paris C, Arnold SA, et al. Integrin-free tetraspanin CD151 can inhibit tumor cell motility upon clustering and is a clinical indicator of prostate cancer progression. Cancer Res. 2014 Jan 1;74(1):173–87.

190. Hemler ME. Tetraspanin functions and associated microdomains. Nat Rev Mol Cell Biol. 2005 Oct;6(10):801–11.

191. Yáñez-Mó M, Barreiro O, Gordon-Alonso M, Sala-Valdés M, Sánchez-Madrid F. Tetraspanin-enriched microdomains: a functional unit in cell plasma membranes. Trends in Cell Biology. 2009 Sep;19(9):434–46.

192. Hemler ME. Tetraspanin proteins promote multiple cancer stages. Nat Rev Cancer. 2014 Jan;14(1):49–60.

193. Karamatic Crew V. CD151, the first member of the tetraspanin (TM4) superfamily detected on erythrocytes, is essential for the correct assembly of human basement membranes in kidney and skin. Blood. 2004 Jun 29;104(8):2217–23.

194. Wright MD, Geary SM, Fitter S, Moseley GW, Lau LM, Sheng KC, et al. Characterization of Mice Lacking the Tetraspanin Superfamily Member CD151. Mol Cell Biol. 2004 Jun 15;24(13):5978–88.

195. Cowin AJ, Adams D, Geary SM, Wright MD, Jones JCR, Ashman LK. Wound Healing Is Defective in Mice Lacking Tetraspanin CD151. Elsevier Masson SAS; 2006 Jan 1;126(3):680–9.

196. Nishiuchi R, Sanzen N, Nada S, Sumida Y, Wada Y, Okada M, et al. Potentiation of the ligand-binding activity of integrin alpha3beta1 via association with tetraspanin CD151. Proc Natl Acad Sci USA. National Acad Sciences; 2005 Feb 8;102(6):1939–44.

197. Lammerding J, Kazarov AR, Huang H, Lee RT, Hemler ME. Tetraspanin CD151 regulates alpha6beta1 integrin adhesion strengthening. Proc Natl Acad Sci USA. 2003 Jun 24;100(13):7616–21.

198. Copeland BT, Bowman MJ, Ashman LK. Genetic ablation of the tetraspanin CD151 reduces spontaneous metastatic spread of prostate cancer in the TRAMP model. Mol Cancer Res. 2013 Jan;11(1):95–105.

199. Takeda Y, Li Q, Kazarov AR, Epardaud M, Elpek K, Turley SJ, et al. Diminished metastasis in tetraspanin CD151-knockout mice. Blood. American Society of Hematology; 2011 Jul 14;118(2):464–72.

200. Yang Y-M, Zhang Z-W, Liu Q-M, Sun Y-F, Yu J-R, Xu W-X. Overexpression of CD151 predicts prognosis in patients with resected gastric cancer. St-Pierre Y, editor. PLoS ONE. Public Library of Science; 2013;8(3):e58990.

201. Testa JE, Brooks PC, Lin JM, Quigley JP. Eukaryotic expression cloning with an antimetastatic monoclonal antibody identifies a tetraspanin (PETA-3/CD151) as an effector of human tumor cell migration and metastasis. Cancer Res. 1999 Aug 1;59(15):3812–20.

202. Kapust RB, Tözsér J, Fox JD, Anderson DE, Cherry S, Copeland TD, et al. Tobacco etch virus protease: mechanism of autolysis and rational design of stable mutants with wild-type catalytic proficiency. Protein Eng. 2001 Dec;14(12):993–1000.

203. Delaglio F, Grzesiek S, Vuister GW, Zhu G, Pfeifer J, Bax A. NMRPipe: a multidimensional spectral processing system based on UNIX pipes. J Biomol NMR. 1995 Nov;6(3):277–93.

204. Johnson BA. Using NMRView to visualize and analyze the NMR spectra of macromolecules. Methods Mol Biol. New Jersey: Humana Press; 2004;278:313–52.

205. Zijlstra A. Tetraspanins in Cancer. In: Cell-Extracellular Matrix Interactions in Cancer. New York, NY: Springer New York; 2009. pp. 217–43.

206. Golub TR. Molecular Classification of Cancer: Class Discovery and Class Prediction by Gene Expression Monitoring. Science. American Association for the Advancement of Science; 1999 Oct 15;286(5439):531–7.

207. Beekman JM, Coffer PJ. The ins and outs of syntenin, a multifunctional intracellular adaptor protein. Journal of Cell Science. 2008 May 1;121(Pt 9):1349–55.

208. Ashby WJ, Zijlstra A. Established and novel methods of interrogating two-dimensional cell migration. Integr Biol (Camb). The Royal Society of Chemistry; 2012 Nov;4(11):1338–50.

209. Hemler ME. Targeting of tetraspanin proteins--potential benefits and strategies. Nat Rev Drug Discov. Nature Publishing Group; 2008 Sep;7(9):747–58.

210. Zöller M. Tetraspanins and Cancer Metastasis. In: The Tumor Microenvironment. New York, NY: Springer New York; 2010. pp. 555–98.

211. Winterwood NE, Varzavand A, Meland MN, Ashman LK, Stipp CS. A critical role for tetraspanin CD151 in alpha3beta1 and alpha6beta4 integrin-dependent tumor cell functions on laminin-5. Mol Biol Cell. American Society for Cell Biology; 2006 Jun;17(6):2707–21.

212. Hansen AG, Swart GW, Zijlstra A. ALCAM: Basis Sequence: Mouse. AFCS Nat Mol Pages [Internet]. 2011;2011. Available from: http://www.signaling-gateway.org/molecule/query?afcsid=A004126&mpv=1

213. Buhusi M, Demyanenko GP, Jannie KM, Dalal J, Darnell EPB, Weiner JA, et al. ALCAM regulates mediolateral retinotopic mapping in the superior colliculus. J Neurosci. Society for Neuroscience; 2009 Dec 16;29(50):15630–41.

214. Zimmerman AW, Nelissen JMDT, van Emst-de Vries SE, Willems PHGM, de Lange F, Collard JG, et al. Cytoskeletal restraints regulate homotypic ALCAM-mediated adhesion through PKCalpha independently of Rho-like GTPases. Journal of Cell Science. 2004 Jun 1;117(Pt 13):2841–52.

215. Zhang XA, Bontrager AL, Hemler ME. Transmembrane-4 superfamily proteins associate with activated protein kinase C (PKC) and link PKC to specific beta(1) integrins. American Society for Biochemistry and Molecular Biology; 2001 Jul 6;276(27):25005–13.

216. Yang W, Li P, Lin J, Zuo H, Zuo P, Zou Y, et al. CD151 promotes proliferation and migration of PC3 cells via the formation of CD151-integrin α3/α6 complex. J Huazhong Univ Sci Technol Med Sci. 2012 Jun;32(3):383–8.

217. Wang F, Flanagan J, Su N, Wang L-C, Bui S, Nielson A, et al. RNAscope: a novel in situ RNA analysis platform for formalin-fixed, paraffin-embedded tissues. J Mol Diagn. 2012 Jan;14(1):22–9.

218. Jezierska A, Matysiak W, Motyl T. ALCAM/CD166 protects breast cancer cells against apoptosis and autophagy. Med Sci Monit. 2006 Aug;12(8):BR263–73.

219. Corbel C, Pourquié O, Cormier F, Vaigot P, Le Douarin NM. BEN/SC1/DM-GRASP, a homophilic adhesion molecule, is required for in vitro myeloid colony formation by avian hemopoietic progenitors. Proc Natl Acad Sci USA. National Academy of Sciences; 1996 Apr 2;93(7):2844–9.

220. Scheele CLGJ, Maynard C, van Rheenen J. Intravital Insights into Heterogeneity, Metastasis, and Therapy Responses. Trends Cancer. 2016 Apr;2(4):205–16.

221. Caswell DR, Swanton C. The role of tumour heterogeneity and clonal cooperativity in metastasis, immune evasion and clinical outcome. BMC Med. BioMed Central; 2017 Jul 18;15(1):133.

222. Jenkins DE, Oei Y, Hornig YS, Yu S-F, Dusich J, Purchio T, et al. Bioluminescent imaging (BLI) to improve and refine traditional murine models of tumor growth and metastasis. Clin Exp Metastasis. 2003;20(8):733–44.

223. O'Farrell AC, Shnyder SD, Marston G, Coletta PL, Gill JH. Non-invasive molecular imaging for preclinical cancer therapeutic development. Br J Pharmacol. 2013 May 27;169(4):719–35.

224. Prasher DC, Eckenrode VK, Ward WW, Prendergast FG, Cormier MJ. Primary structure of the Aequorea victoria green-fluorescent protein. Gene. 1992 Feb

15;111(2):229–33.

225. Kain SR, Adams M, Kondepudi A, Yang TT, Ward WW, Kitts P. Green fluorescent protein as a reporter of gene expression and protein localization. BioTechniques. 1995 Oct;19(4):650–5.

226. Weber K, Thomaschewski M, Warlich M, Volz T, Cornils K, Niebuhr B, et al. RGB marking facilitates multicolor clonal cell tracking. Nature Medicine. Nature Publishing Group; 2011 Mar 27;:1–7.

227. Livet J, Weissman TA, Kang H, Draft RW, Lu J, Bennis RA, et al. Transgenic strategies for combinatorial expression of fluorescent proteins in the nervous system. Nature. Nature Publishing Group; 2007 Nov 1;450(7166):56–62.

228. Schepers AG, Snippert HJ, Stange DE, van den Born M, van Es JH, van de Wetering M, et al. Lineage tracing reveals Lgr5+ stem cell activity in mouse intestinal adenomas. Science. 2012 Aug 10;337(6095):730–5.

229. Thomaschewski M, Riecken K, Unrau L, Volz T, Cornils K, Ittrich H, et al. Multi-color RGB marking enables clonality assessment of liver tumors in a murine xenograft model. Oncotarget. 2017 Dec 29;8(70):115582–95.

230. Cornils K, Thielecke L, Huser S, Forgber M, Thomaschewski M, Kleist N, et al. Multiplexing clonality: combining RGB marking and genetic barcoding. Nucleic Acids Research. 2014 Apr 14;42(7):e56–6.

231. Subach OM, Gundorov IS, Yoshimura M, Subach FV, Zhang J, Grüenwald D, et al. Conversion of red fluorescent protein into a bright blue probe. Chem Biol. 2008 Oct 20;15(10):1116–24.

232. Rizzo MA, Springer GH, Granada B, Piston DW. An improved cyan fluorescent protein variant useful for FRET. Nat Biotechnol. Nature Publishing Group; 2004 Apr;22(4):445–9.

233. Griesbeck O, Baird GS, Campbell RE, Zacharias DA, Tsien RY. Reducing the environmental sensitivity of yellow fluorescent protein. Mechanism and applications. J Biol Chem. 2001 Aug 3;276(31):29188–94.

234. Shaner NC, Lin MZ, McKeown MR, Steinbach PA, Hazelwood KL, Davidson MW, et al. Improving the photostability of bright monomeric orange and red fluorescent proteins. Nat Meth. Nature Publishing Group; 2008 Jun;5(6):545–51.

235. Shcherbo D, Murphy CS, Ermakova GV, Solovieva EA, Chepurnykh TV, Shcheglov AS, et al. Far-red fluorescent tags for protein imaging in living tissues. Biochem J. Portland Press Limited; 2009 Mar 15;418(3):567–74.

236. de Felipe P, Luke GA, Hughes LE, Gani D, Halpin C, Ryan MD. E unum pluribus: multiple proteins from a self-processing polyprotein. Trends Biotechnol.

2006 Feb;24(2):68–75.

237. Luke GA, de Felipe P, Lukashev A, Kallioinen SE, Bruno EA, Ryan MD. Occurrence, function and evolutionary origins of “2A-like” sequences in virus genomes. J Gen Virol. Microbiology Society; 2008 Apr;89(Pt 4):1036–42.

238. Kain KH, Miller JWI, Jones-Paris CR, Thomason RT, Lewis JD, Bader DM, et al. The chick embryo as an expanding experimental model for cancer and cardiovascular research. Dev Dyn. 2nd ed. 2014 Feb;243(2):216–28.

239. Lamble AJ, Dietz M, Laderas T, McWeeney S, Lind EF. Integrated functional and mass spectrometry-based flow cytometric phenotyping to describe the immune microenvironment in acute myeloid leukemia. J Immunol Methods. 2018 Feb;453:44–52.